STUDIES ON FLUORESCENT MOLECULAR ROTORS AS ENVIRONMENT-SENSITIVE PROBES

by

Marlius Castillo

Bachelor of Science, Chemistry 2008
University of Carabobo
Venezuela

Submitted to the Graduate Faculty of the
College of Science and Engineering
Texas Christian University
in partial fulfillment of the requirements
for the degree of

Doctor of Philosophy

May 2019

ACKNOWLEDGEMENTS

I want to thank God for the many blessings he has given me, especially for my family and the opportunity to continue my studies. To my parents Maria and Luis: gracias por la hermosa crianza que me dieron y por todo su apoyo.

I am extremely grateful to my advisor Sergei for his kindness, patience and thoughtfulness, for always guide and encourage me to become a better scientist and make me dream with being a professor one day. His enthusiasm and leadership inspired me throughout all the good and bad moments. Being a mentor and a scientist is his true vocation.

I want to thank also to my committee Dr. Simanek, Dr. Montchamp and Dr. Annunziata for their advises and contributions to my projects and academic growth. Expressly, Dr. M. and Dr. A. whom I admire and had the pleasure to interact the most with, for all their patience, guidance and assistance, for fueling me with passion for science.

Special gratitude to Dr. Gryczynski, Dr. Naumov and their groups for supporting my research and welcome me with kindness to their labs.

I want to express thanks to my husband Pablo for his love and support, I could not have made it with him by my side. Also, thanks to my sister Vanessa and my brother in-law Luis for inspiring me to this adventure and giving me Sebastian and Julian.

Finally, many appreciations to the faculty, students and staff in the Departments of Chemistry and Physics that I interacted with and support me during these years. Thanks to TCU as well for funding my research and my residency in the graduate program.

-Dedicated to Samuel. You make me so proud every single day, I hope one day you look at this and be a little proud of me. I love you with all my heart.

TABLE OF CONTENT

LIST OF FIGURES

LIST OF TABLES

LIST OF SCHEMES

LIST OF ABBREVIATIONS

AIE	Aggregation-induced emission
ATP	Adenosine triphosphate
BSA	Bovine serum albumin
CF	Cystic fibrosis
DCE	1,2-dichloroethyl
DMF	N,N-dimethylformamide
DMPC	1,2-dimyristoyl-sn-glycerol-3-phosphocholine
DMSO	Dimethyl sulfoxide
DNA	Deoxyribonucleic acid
DSSC	Dye-sensitized solar cells
FLIM	Fluorescence lifetime image microscopy
FWHM	Full width half maxima
G	Gelator
GC	Gas chromatography
GC-VUV	Gas chromatography with vacuum ultraviolet detector
HAS	Human serum albumin
HPLC	High performance liquid chromatography
MOF	Metal-organic frameworks
NIR	Near infrared
NMR	Nuclear magnetic resonance
OSC	Organic solar cells
PD	Porphyrin dimer
PDT	Photodynamic therapy
QD	Quantum dot
RNA	Ribonucleic acid
ROS	Reactive oxygen species
TBHP	*Tert*-butyl hydroperoxide
THF	Tetrahydrofuran
TICT	Twisted Intramolecular charge transfer
TPE	Two-photon electron

CHAPTER I: INTRODUCTION TO MOLECULAR PROBES

Several chemical and physical changes of matter could be detected using various types of instrumentations. However, in many instances either *in situ* or non-destructive monitoring of the changes of physical properties of the matter might not be possible. In addition, some perturbation to the system could be introduced, which in turn might compromise the integrity of the results. In order to enhance the validity of evaluations of the media, especially those that are related to biological environments, the use non-invasive methods would be advantageous. Due to structural diversity, and versatility of synthetic approaches, small-molecule based probes are interesting, viable and useful tools that could be used for the assessment of changes of various properties of many types of environments. Numerous molecular probes have been used for the detection of changes on a molecular scale, and they are of great significance for many fields of modern science, engineering and medicine.

On the structural level, molecular probes need to have several characteristics, such as preference for the target motif, the capability to convert the events into measurable signals, good solubility in the required environment, and resistance to degradation. Molecular probes have found ample applications in biological sciences as they proved viable for an array of systems (Figure 1.1A). In addition, many biological processes, such as apoptosis, for example, are characterized by morphological changes that might be detected using molecular probes.[1] Since many small molecule probes are amenable to high-throughput screening techniques, great amount of information could be obtained in very short periods of time.[1,2] In addition, molecular probes are extensively used for characterization of chemical processes, including various types of polymerization that

provide materials that are utilized in various aspects of day-to-day life as well as research (Figure 1.1B). Studies on polymerization processes using molecular probes allowed for the determination of degree of cross-linking, functionalization as well as morphology.[3,4]

Even though many probes have been developed and explored, there is a continued need for novel constructs, which have higher selectivity and higher signal-to-noise ratio that can be used for monitoring real time events. In addition, a number of techniques have emerged to aid in better utilization of the novel probes. For example, molecular imaging, with the primary goal to characterize and quantify biological processes at the cellular and subcellular levels in living subjects. Overall, availability of non-invasive, reliable protocols to achieve early detection of disease, might aid in the development of more effective therapies.[4-8]

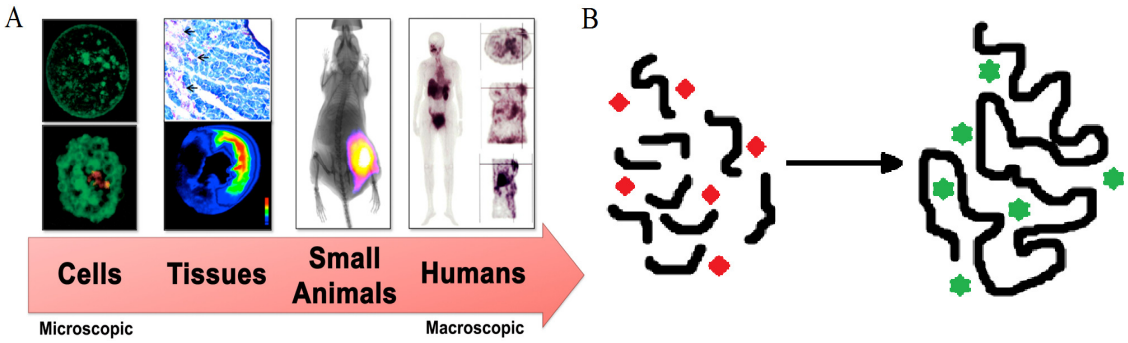

Figure 1.1. Molecular probes for: biological (A) and material science (B).
A – adapted from ref. 8

1.1 Fluorescent probes

Molecular probes that that could emit light upon excitation and change their emission characteristics in response to environmental factors or stimuli are known as fluorescent molecular probes. Despite wide utility of fluorescent based probes, and a relatively simple operational procedures of fluorescent-based spectroscopy, the underlying mechanisms of excitation and emission are complex, as a series of events can take place (Figure 1.2).[9,10] Such as, a molecule in the ground state (S_0) absorbs light and transitions to higher electronic levels (S_1) follows, in about 10^{-15} s. Subsequently, in case of fluorophores, an internal conversion or rapid relaxation to the lowest vibrational level (S_1) in about 10^{-12} s or less would take place, and generally after these events, emission takes place on about 10^{-8} s scale to return to the ground state (S_0). However, molecules in the S_1 could also undergo spin conversion to the triplet state (T_1) or intersystem crossing, with the subsequent relaxation to S_0, the process known as phosphorescence.[10]

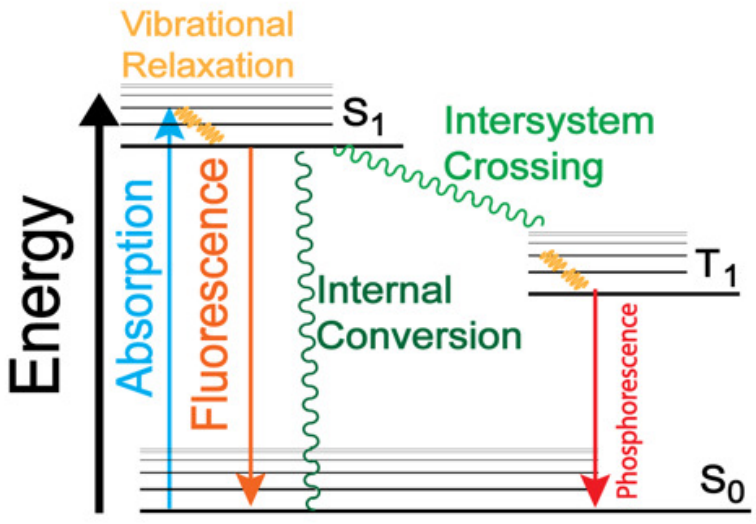

Figure 1.2. Simplified Jablonski diagram.[10]

When changes in the emission profile of fluorescent probes are coupled with changes in the environment, the photophysical characteristics of these compounds might be extremely sensitive to their environment, thus providing a possibility for monitoring molecular variations in a highly sensitive manner. For example, only pH sensitive probes can be used to determine pH values and only probes with long emission wavelengths, in the near infrared (NIR) range are practical to measure pH changes inside tissues.[10] Cell imaging using fluorescent probes is essential to study biological molecules, pathways and events in living cells. The currently available probes typically have high sensitivity, fast response time, and high selectivity toward specific types of cells, for example, which allows to observe perturbation only in the desired types of environments. There are two major classes of fluorescent probes that are used for cellular imaging: a) so-called on-off probes, where probes emit light under one set of conditions, while they become non-fluorescent under another set of conditions (or *vice versa*), and b) the probes that change their emission profiles (such as emission intensity, position of the emission maxima, etc) upon exposure to a stimulus. Fluorescent probes in general, but especially those that are to be used for imaging, need large extinction coefficients and quantum yields, in order to maximize the number of detectable photons per molecule, so that they would provide high contrast ratios.[11-14]

The library of fluorescent probes includes small organic molecules, metal-ligand complexes, polymers nanostructures, and nanoparticles. The necessity of continuing to expand the structural and functional diversity and to develop new fluorescent structures is due to the issues related to their non-ideal properties, such as water solubility, pH sensitivity, photostability, membrane permeability, aggregation and cytotoxicity in the

cases of biological employment.

Even though nano-size species, polymers and metal-ligand architectures are not part of this work, an illustrative, brief description has been added to highlight the use of fluorescence probes. Nanoparticles, as fluorescent probes composed of silica materials, used for the detection of hydrogen peroxide that possess chemical, biological, medical and environmental interest, being one of the most relevant reactive oxygen species (ROS) generated by living organisms.[15] Other constructs of silica nanoparticles have been also utilized for fluorescent tumor imaging *in vitro* and *in vivo* for cancer therapy.[16,17] However, more compositionally intricate nanoparticles containing a combination of polymers and platinum (II) complexes were also assembled and employed to create fluorescence fingerprint of various proteins.[18]

Other fluorescent structures that could have applications in molecular imaging are polymer nanoparticles (Figure 1.3). Some of these structures, such as **1.3.A**, exhibit interesting photophysical properties, such as room temperature phosphorescence with lifetimes in the range of 540 ms, (Figure 1.3),[19] very particular because phosphorescence is usually achieved by complexation with transition or noble metals.[20] **1.3.B** and other similar polymeric probes exhibit aggregation induced emission in the presence of various species, such as mercury and fluoride ions, which makes them viable environmental probes (Figure 1.3).[21,22]

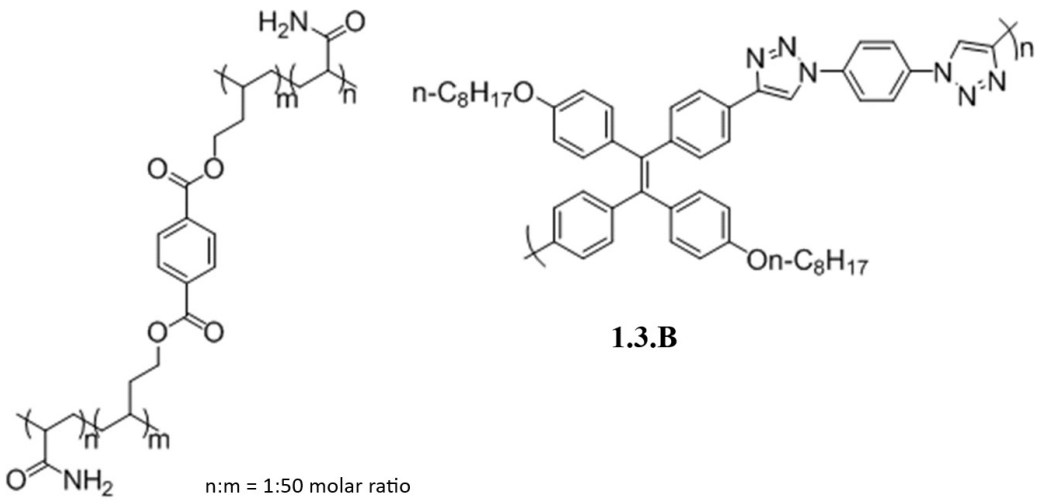

1.3.A **1.3.B**

Figure 1.3. Some polymer fluorescent probes.

In one of biologically relevant applications, a co-polymer, where each fragment contains unique fluorescent dye, was used as a fluorescent sensor for liver fibrosis with 60 % accuracy in blood serum.[23] Also, a spherical polymeric construct for photothermal dynamic therapy (PDT) with NIR fluorescence and afterglow tumor imaging was used *in vitro* and *in vivo* studies.[24] PDT treatment is minimally invasive and it is based on activation of a photosensitizer with light at specific wavelengths, which subsequently transfer energy to neighboring oxygen to produce cytotoxic ROS, that in turn will cause damage to specific (diseased) cells.[25] A unique photoactive polymer scaffold was used for cell imaging, drug delivery and photo-responsive drug release *in vitro.*[26]

On the other hand, metal-ligand fluorescence complexes, such as those that contain gallium (III), were studied as on-off switches upon interaction with ATP, and they were capable of mapping this phosphate compound in cells.[27] Fluorescence cell imaging was

also possible using imine-N-cyclic carbene iridium (III) complex **1.4.A**, which was also found to have antibacterial properties towards Gram positive *S. aureus* and anticancer activity *in vitro* in lung cancer cells (Figure 1.4).[28] *In vitro* imaging was successfully performed with other complexes, such as rhodium (I) and ruthenium (II) **1.4.B** as (Figure 1.4), as well as DNA binding was studied to access their ability to act as regulators in cancer cells.[29]

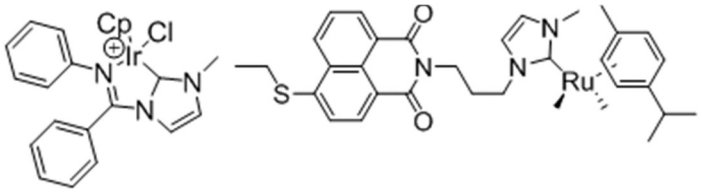

1.14.A **1.14.B**

Figure 1.4. Some metal-ligand complexes fluorescent probes.

1.2 Viscosity

Viscosity is a fundamental property of fluids. When a liquid flows, it has an internal resistance to flow, and viscosity is a measure of this resistance. This is known as, dynamic or absolute viscosity.[30] Many techniques have been used to measure viscosity, such as mechanical methods that measure the internal friction of liquids under shear stress. These methods allow for evaluation of the bulk viscosities. In addition, there are methods that measure viscosity on a microscopic scale, known as microviscosity. These methods are realized by the application of viscosity sensitive probes, which allow for the assessment of viscosity changes of the media in the immediate proximity to the probe.[31]

Microviscosity is a crucial factor that also imparts the diffusion-controlled

processes. It has been recognized to contribute to biochemical functions through interaction and transport of various species. As such, microviscosity is of paramount importance in a number of different fields, specifically those that are related to biological systems. The ability to determine and to monitor changes of cellular and subcellular viscosities is valuable for fundamental understanding of various processes that are related to biology, pathologies and disease diagnosis.

In addition, monitoring microviscosity is important during the synthesis of various materials. For example, during polymerization processes the microviscosity changes of the media affect the mobility, morphology, transport of additives, self-assembly and degree of polymerization, and monitoring these parameters is crucial for assuring the quality and structural integrity of the polymeric materials.[32,33]

Even though the significance of microviscosity is clear, there are many challenges associated with the measurement. One of the tools that has been recently emerging for measuring microviscosity is fluorescent molecular rotors. These are small molecules, whose fluorescence is sensitive to the media's microviscosity.[31,34]

Sensitivity towards viscosity of fluorescence molecular rotors originates from a conformational change that happens when the rotor is in the excited state before it is relaxed to the ground state. Specifically, an internal rotational motion may occur, which depends on the viscosity of the environment and leads to differentiation between distinct conformations of the excited rotors, which have distinct photophysical properties (Figure 1.5).[10,35]

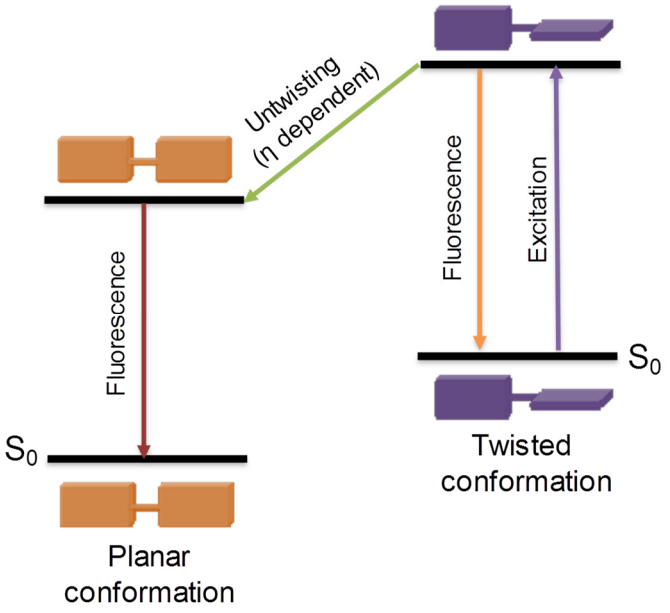

Figure 1.5. Simplified energy diagram of molecular rotor conformers. Refer to Figure 1.2.

A number of structurally diverse small molecule rotors have been used as molecular viscometers, including simple push-pull species **1.6.A**, cyanines **1.6.B** and **1.6.C**, BODIPYs **1.6.D** and **1.6.E** porphyrins, rhodamine, and coumarin-based scaffolds (Figure 1.6).[35-38]

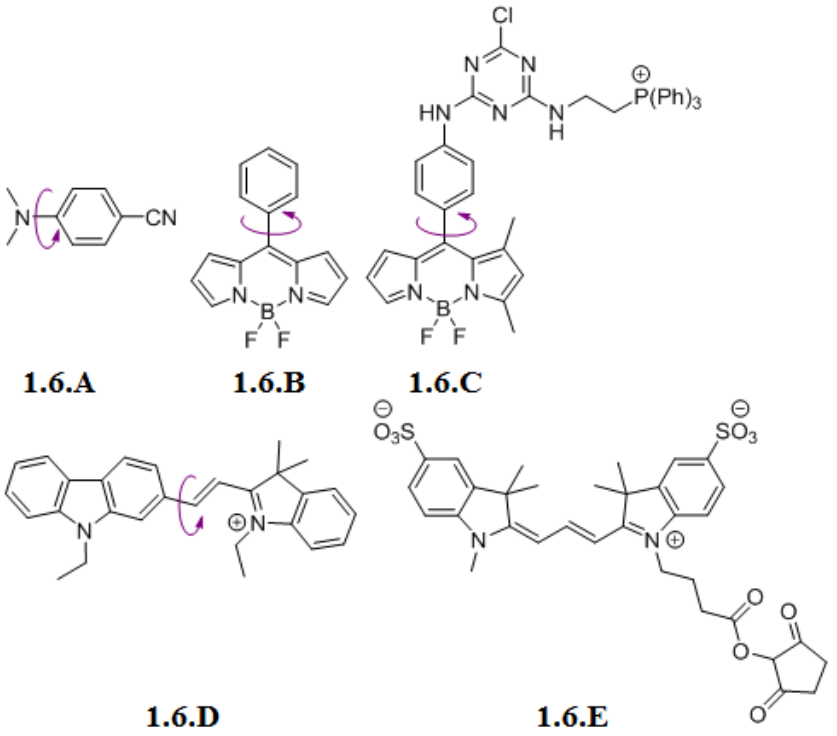

Figure 1.6. Some small molecule rotors that have been used for microviscosity measurements.

1.3 Fluorescent small molecules

Fluorescent dyes have found extensive applications in biological systems, specifically in cellular imaging, biomolecular labeling and as environmental sensors, due to their characteristics, such as small size, tunable cytotoxicity and permeability, high sensitivity and fast response times. Classical dyes include coumarin, porphyrin, fluorescein, BODIPY, or cyanine. Structural modifications of these scaffolds provide arrays of dyes that are among the most studied fluorescent small molecules.[39,40]

The range of applications of the fluorescent probes is extremely broad,[41] and thus, it cannot be covered within this dissertation. For illustrative purposes, a few interesting and/or unique applications as well as structural motifs will be given below.

For example, the detection *in vitro* and *in vivo* of hypobromous acid (an excessive generation and accumulation of this acid was related to several diseases, including rheumatoid arthritis, inflammatory tissue damage, neurodegenerative conditions, and cancer), with a biphenyl-containing fluorescent probe **1.7.A** (Figure 1.7) exhibited a high sensitivity by generating a structure with a red shifted emission of about 100 nm after reacting with hypobromous acid.[42]

Another characteristic species that are typically associated with various neurodegenerative diseases, known as amyloids, are misfolded and/or modified proteins that exhibit high propensity for aggregation. Many fluorescent probes have been synthesized to study amyloid aggregates however many challenges remain and an "ideal" probe that allows early detection is yet be developed. Towards this goal, a set of amino-aryl cyanoacrylate probes **1.7.B** (Figure 1.7), was synthetized, and they exhibited solvatochromic properties in the presence of various amyloid forming proteins. Thus, a possibility of not only detecting amyloids, but distinguishing among different amyloids was demonstrated.[43]

NIR fluorescent small molecules, such as **1.7.C**, have also been explored in biological imaging, because they allow for deeper tissue penetration as compared to probes that are active in the visible range (Figure 1.7).[44] Although penetration-depth of light through biological tissues is tissue dependent, it typically increases as the wavelength of light increases (Table 1.1).[45]

So-called *off-on probes*, *i.e.*, probes whose emission is triggered by or coupled to some event/stimulus, have also been explored. For example, a non-emissive prodrug that has an azobenzene moiety, **1.7.D**, susceptible to cellular reduction, which after hypoxia conditions inside tumor tissue releases a potent anticancer drug leading to "on" structure that possess strong fluorescence (Figure 1.7).[46]

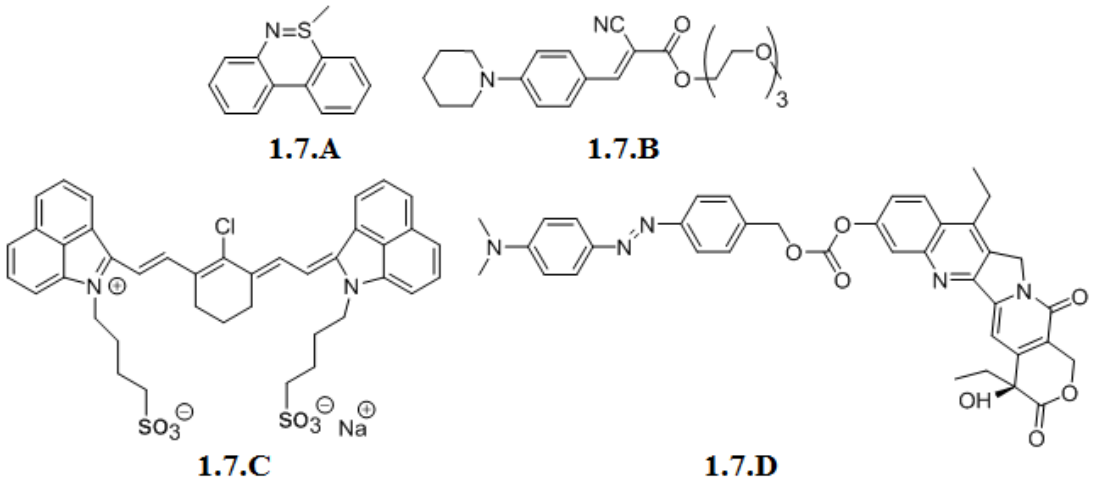

Figure 1.7. Some small molecule probes used for detection of analytes in biological systems (part 1).

wavelength / nm	**Tissue penetration / mm[a]**	
	rabbit muscle	rabbit liver
400	1.7	0.1
500	4.0	0.5
600	4.1	0.5
700	6.0	0.9
800	7.8	1.3

Table 1.1 Tissue penetration-depth as a function of wavelength.[45]

[a]-approximate values, for illustrative purposes.

Fluorescent small molecules for cell imaging *in vivo* and *in vitro* have become indispensable in biomedical sciences, which contributed to a constantly growing number of new structural motifs. For example, quinoline "core" scaffolds, **1.8.A** and **1.8.B (**which are ubiquitous in natural product motifs, while not been sufficiently utilized in dye-related research) represent a synthetically tunable core for pH and polarity sensors, with some additional applications as microscopy stains (Figure 1.8).[40,47]

The use of small molecules probes has evolved to provide a better recognition towards biomacromolecules as well as intracellular species. Since various specific activities of enzymes have been associated with the development or progression of certain diseases, the ability to track those activities by using fluorescent small molecules as enzymatic probes has become a vibrant area of modern research. These probes can image and detect abnormal levels of enzymes in cancer cells, for example, thus providing an early diagnosis as well as potentially aiding in the development of therapeutic approaches.[48]

In addition, since different forms of cancers could be studied by tracking various intracellular species, molecular probes that could report on the concentration changes and/or appearance of those species are of interest. For example, species that is known to regulate cancer cells is RNA. RNA is one of the most important and dominant biomacromolecules along with lipids, proteins, enzymes and carbohydrates. Imaging RNA using small molecule probe has been one of the interesting areas of modern research.[49] Specifically, a recent study utilized a dimethylamine vinyl linked benzimidazolium iodide probe **1.8.C** (Figure 1.8), which allowed for RNA imaging with great permeability in living cells, low cytotoxicity and good photostability.[50] In addition, this two-photon electron (TPE) sensitive fluorescent probe provided much brighter and more well-defined images.

In general it should be pointed out that TPE microscopy is more advantageous for performing biomolecular imaging studies, as compared to conventional techniques.[50] Specifically, this microscopy technique has been applied to identify and quantify endogenous species in vesicles, specifically lysosomal ATP, for real-time monitoring of lysosomal processes *in vitro*, by using a selective small molecule probe that can bind to lysosomal ATP through hydrogen bonds with an amine chain that links a modified rhodamine 6G dye (lysosome tracker) and BODIPY dye (signal probe, **1.8.D**) (Figure 1.8).[51]

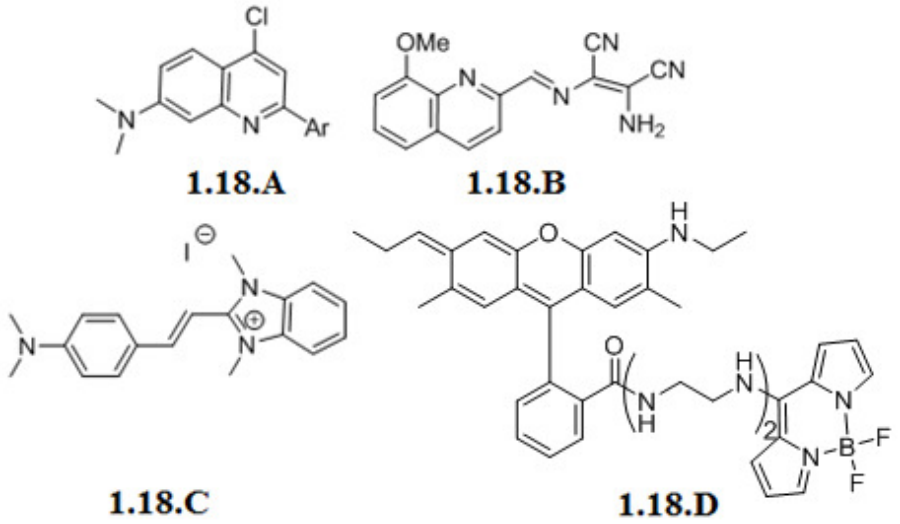

Figure 1.8. Some small molecule probes used for detection of analytes in biological systems (part 2).

In summary, virtually unlimited structural diversity provided by small molecule fluorescent probes is one of the major stimulating factors that fuels continuous explorations in synthesis, properties, response or their selectivity to different compounds.

1.4 Synthetic overview of BODIPY dyes

Fluorescent small molecule 4,4-difluoro-4-bora-3a,4a-diaza-s-indacene or boron dipyrromethene, known as BODIPY (Scheme 1.1), is one of the paramount chromophore cores, due to the unique photophysical characteristics, which include high quantum yields, large extinction coefficients (thus, bright fluorescence), relatively high photostability, sufficient chemical inertness under various conditions, which could be further tuned through chemical transformations. This type of dye was first reported five decades ago, yet the applications of this probe, especially those that are related to materials and biological sciences, have been emerging only recently.[52,53]

Conventional approaches towards the synthesis of BODIPY dyes rely on a multistep processes that are typically conduced in a one-pot manner, that include pyrrole condensation reaction with highly electrophilic carbonyl moieties, such as acid chlorides, anhydrides and aldehydes, followed by oxidation to induce conjugation of the dipyrromethane core, and subsequent complexation with BF_3 under basic conditions (Scheme 1.1).[41,54]

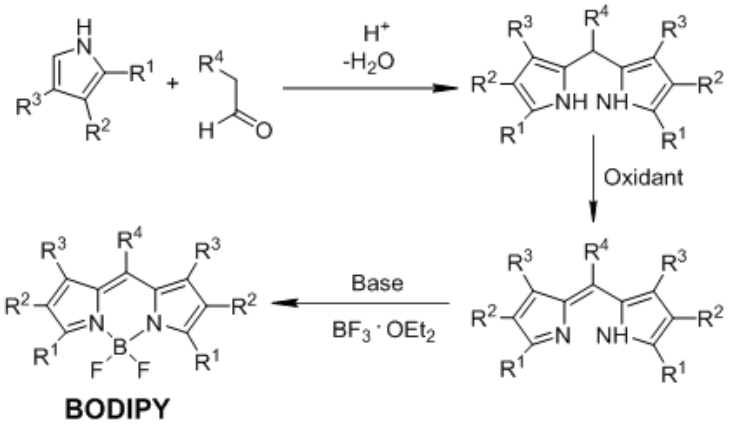

Scheme 1.1. Synthesis of BODIPY dyes. R_1, R_2, R_3, R_4 are H or alkyl, aryl, etc substituents.

Synthesis of more structurally and functionally elaborate BODIPY dyes is typically done using functionalized pyrroles (approach that is known as pre-derivatization) or *via* derivatization of the chromophore core (approach known as post-derivatization).[55] Overall, the construction of BODIPY scaffold and BODIPY dyes, in general, is robust, facile and modular, which favorably distinguishes BODIPY dyes from other types of fluorophores.[52]

Most BODIPY-based molecular rotors rely on a substituent in the *meso*-position (R_8) of the BODIPY scaffold (Figure 1.9), and the rotation of the substituent in the *meso*-position relative to BODIPY core has shown to produce distinct fluorescence lifetimes as a function of the viscosity of the environment.[56]

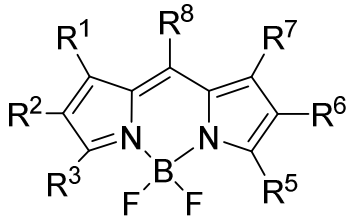

Figure 1.9. BODIPY core.

Notably, determination of viscosity in self-organized systems such as micelles or membranes is problematic using conventional methods, or a viscometer equipment. Therefore, incorporation of long alkyl chain or cholestanol moiety onto the aromatic substituent, *i.e.*, lipophilic groups, was explored (Scheme 1.2), and it allowed to selectively measure viscosity of lipid bilayers.[56,57] Specifically, the lipophilic groups were incorporated onto *para*-hydroxy benzaldehyde, followed by a one-pot, three step procedure to assemble the BODIPY core.[56,57]

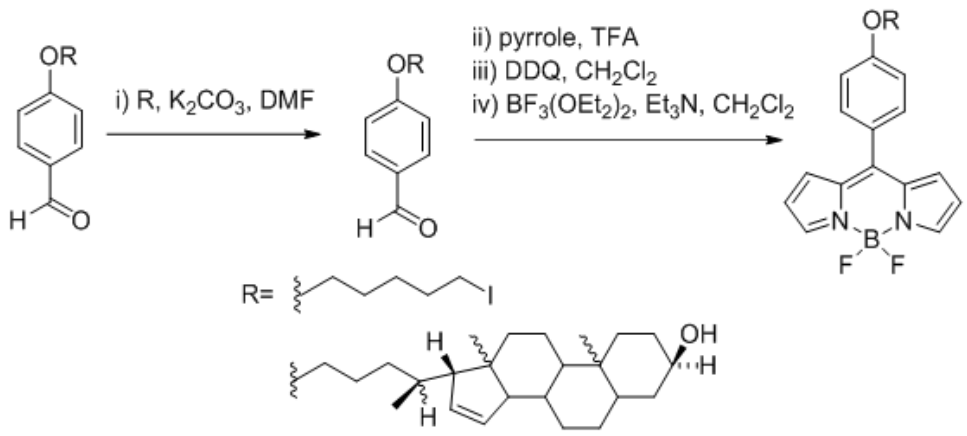

Scheme 1.2. Synthesis of BODIPY probes for determination of viscosity of lipid bilayers.

Another possible type of BODIPY-based rotors, which found applications as molecular viscometers, are featuring dimeric structures, which are either homodimeric, *i.e.*, comprising two identical BODIPY cores, **1.10.A** and **1.10.B** (Figure 1.10)[58,59] or heterodimeric, where the two rotating units are distinct such as a coumarin-based dye, which is linked to BODIPY, **1.10.C** (Figure 1.10, a triphenylphosphonium moiety is introduced to target mitochondria).[60]

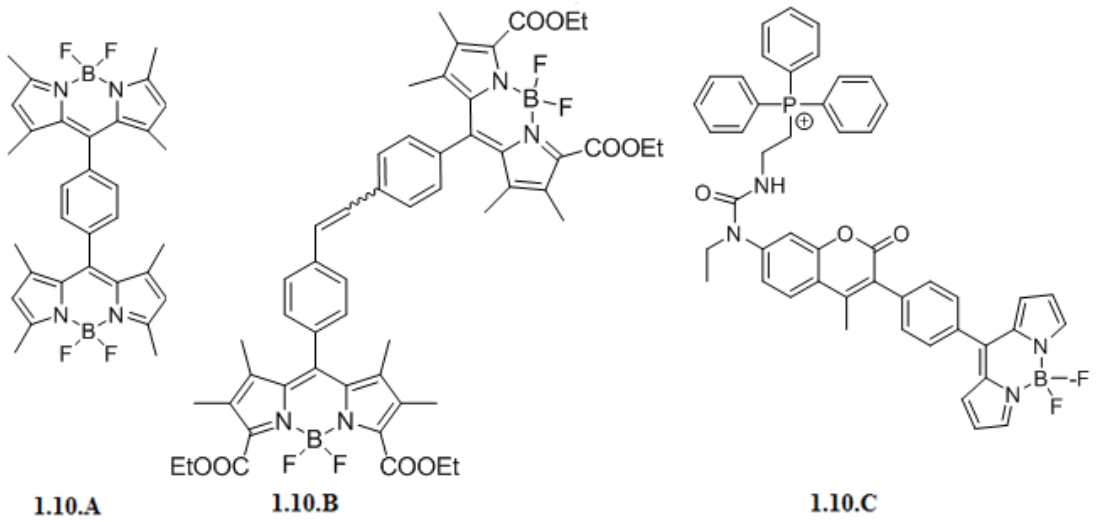

Figure 1.10. BODIPY dimers as microviscosity probes.

Furthermore, since many applications, such as biomedical and optical imaging, optoelectronics, require long wavelength (over 600 nm range) absorbing and emitting BODIPY species, several structures with aromatic rings fused at the β,β`- (1,2- or 7,6-) pyrrolic positions have been developed.[61] Specifically, benzo-fused BODIPY moieties **1.11.A** (Figure 1.11), where functionalization of the 3- and 5-positions (see Figure 1.9) with aromatic groups caused a red shifted absorption and emission spectra maintaining the same high fluorescence and quantum yield of the original tetrafluorobenzo-BODIPY.[62]

The addition of aromatic rings to the BODIPY core is attractive because it expands the π-system, and added rigidity reduces non-radiative decay, which might lead to increasing the quantum yield or brightness of the system. Naphtho-fused BODIPY (Figure 1.11.B) was synthesized in one-pot reaction platform and exhibited a NIR emission, which is appealing for biological imaging applications, as the background interference is virtually absent at this wavelength range.[63]

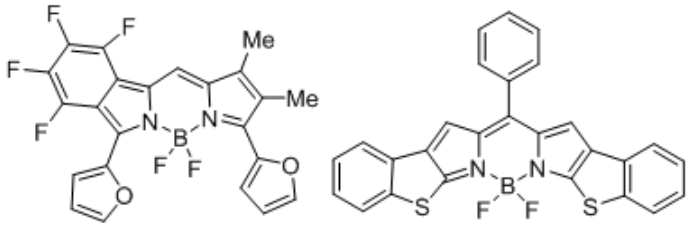

1.11.A **1.11.B**

Figure 1.11. Benzo-fused BODIPYs with NIR emission.

Systems that feature porphyrin-BODIPY constructs have attracted a lot of attention due to the possibility of exploring various energy transfer phenomena as well as possible applications for molecular devices.[64,65] For a description of porphyrin-based probes see sections 1.6 and 1.7. For example, a heterodimeric porphyrin-BODIPY conjugate was synthesized using copper-catalyzed alkyne-azide cycloaddition **1.12**A (Figure 1.12).[66] This construct exhibited a very efficient energy transfer, which produced deep-red lighting devices with great stabilities and efficiencies.

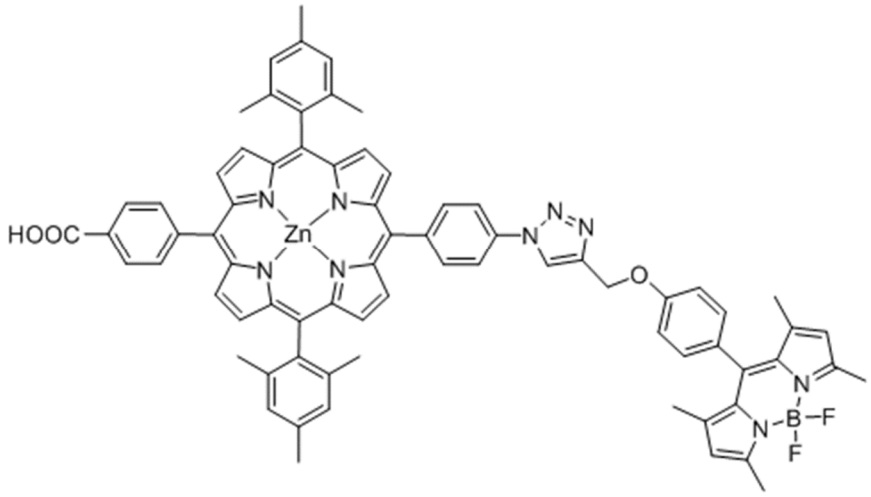

Figure 1.12. Porphyrin-BODIPY dyad.

BODIPY oligomers have been constructed for possible applications in organic photonics, as solar energy concentrators and for super-resolution microscopy. Synthetically these structures, with emission above 640 nm, were built from the monomeric BODIPY dyes either via oxidative dimerization of the α-methyl groups to form BODIPY-octamers **1.13.A**[67] or diyne formation **1.13.B**[68] (Figure1.13).

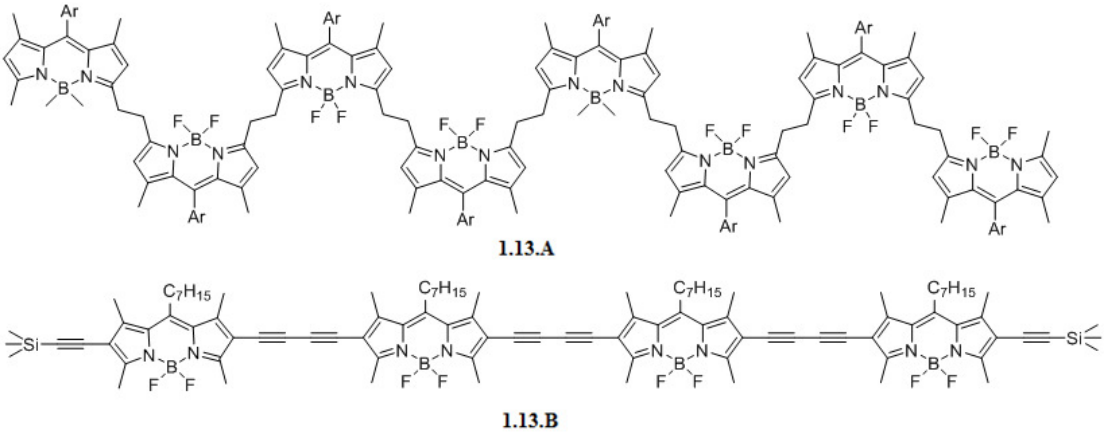

Figure 1.13. Some BODIPY oligomers.

Furthermore, BODIPYs have been modified using radical C-H arylation with regioselectivity of the 3- and 5-positions using ferrocene as catalyst (Figure1.14).[69] Recently, another radical coupling was performed using $Cu(OAc)_2$ as catalyst in the presence of *tert*-butyl hydroperoxide (TBHP) as oxidant which have been known to remove a hydrogen from toluene to form a benzylic radical for the benzylation of BODIPY with good selectivity (Figure1.14).[70] Functionalization of 2- and 6-positions (Figure 1.9) produced BODIPYs **1.14.C** and **1.14.D** that exhibit emission over 600nm (Figure1.14).[71,72]

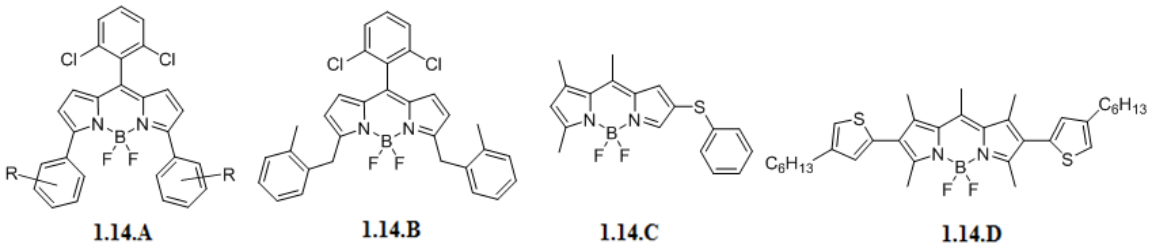

Figure 1.14. Some examples of functionalized BODIPY dyes.

Additionally, functionalization of the boron center by replacing one or both B-F bonds with B-O or B-C, in order to tune the properties to a new class of fluorescent dyes has also been explored. By reacting a typical, BF_2-containing BODIPY dye with various alcohols in the presence of $AlCl_3$ resulted in the desired substitution at the boron atom to give a set of B-O-containing BODIPYs, e.g. **1.15.A** (Figure 1.15).[73] Likewise, variation of the core, such as strapping or forming a ring could be made by forming a 6-membered ring through the use of $SnCl_4$ as catalyst to form a cyclic structure **1.15.B** at the boron center (Figure 1.15), This modification red shifted the emission to 587 nm.[74] Another option of core modification is via the addition of malonic acid in the presence of excess of trimethylsilyl

chloride, to form diacyloxyl bridge on the boron atom **1.15.C** (Figure 1.15).[75] It has been shown that these modifications significantly enhanced the quantum yield, photochemical stability and solubility of these B-O-containing dyes as compared to unstrapped BODIPY analogues.[76]

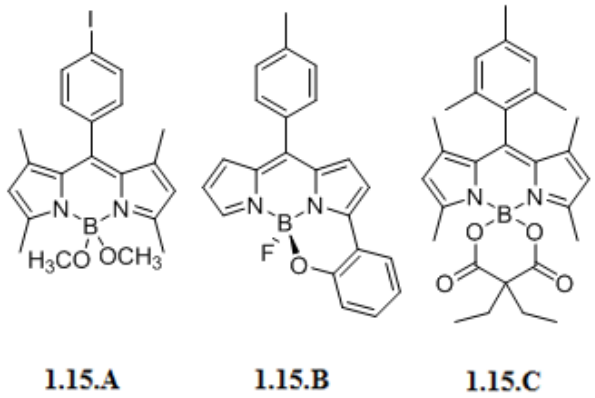

1.15.A **1.15.B** **1.15.C**

Figure 1.15. Some B-O containing BODIPY dyes.

In general, extensive, yet facile chemical modifications of BODIPY dyes is another property that makes this chromophore an attractive option for many different applications.

1.5 BODIPY dye applications

Application of BODIPY dyes for studying various biologically relevant processes has been one of the major areas of modern research, especially as it relates to monitoring of analytes and events in noninvasive manner.[77]

Due to ease of functionalization, various groups could be introduced onto BODIPY scaffold to allow for the detection of biologically interesting molecules. For example, incorporation of boronic ester moieties in the *meso*-position of the BODIPY core **1.16 A**

(Figure 1.16), allowed to detect hydrogen peroxide (H_2O_2), thus realizing bio-probes that are capable of detecting (ROS) *via* a "turn on" mechanism.[77] Furthermore, BODIPYs can be employed for recognition of enzymes such as tyrosine oxidase that catalyzes hydroxylation and oxidation of phenols to quinones in the presence of ROS.[70] It is of interest to note that the probe containing dopamine in the *meso*-position **1.16.B** (Figure 1.16) was found to be highly selective towards the recognition of tyrosine oxidase, as its spectroscopic profile changed from non-fluorescent turning into a bright moiety with an emission at 452 nm.[78]

Other areas where BODIPY dyes have been utilized are related to cancer therapy.[79] Molecular arrangements of the dye have been employed to sustain anticancer potency of capsaicin for the treatment of prostate tumors in mice, the therapy relayed on the formation of nanocluster aggregates of capsaicin-containing BODIPY **1.16.C** (Figure 1.16), showing viable antitumor activity with lower dosage compared to unmodified capsaicin.[80]

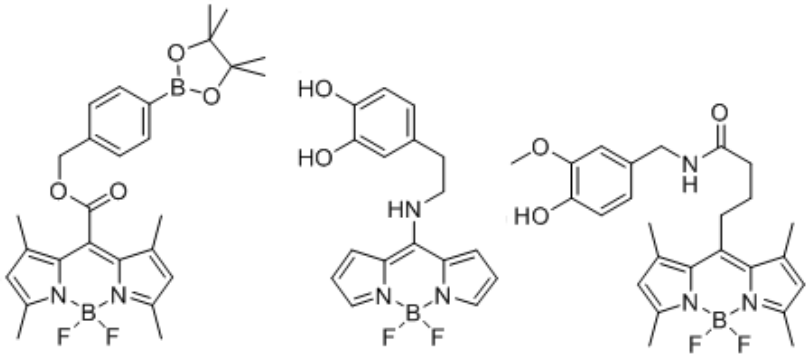

Figure 1.16. Some BODIPYs for detection of and interaction with biologically relevant species.

In addition, incorporation of groups that can form supramolecular assemblies have been explored. For instance, a combination of BODIPY dye (as an imaging agent) and Pt(II) containing species (as anticancer drug) produced a PDT construct that was highly active even in drug resistant cells.[80]

Another important area of utilization of BODIPYs is the recognition of oligomers of amyloid β-peptide (Aβ). Aβ aggregates are considered as one of the pathogenic hallmarks of Alzheimer's disease, producing amyloid (proto)fibrils or filamentous protein aggregates that ultimately lead to the the formation of extracellular neuritic plaques in the brain. The identification of these Aβ oligomeric species may lead to early diagnosis and treatment of the disease.[82-84] Numerous fluorescence-based probes have been used for the detection of Aβ aggregates.[85,86] NIR-based BODPIY dyes have been showing the most promise for imaging Aβ showed low background signal in *in vivo* studies, in mice, being a promising dye to identify early stages of Alzheimer's disease.[82]

Other applications of BODIPY dyes, which also have been of great interest, are related to their uses as molecular viscometers, where BODIPY dyes have been shown to report on microviscosity changes.[31] Specifically, BODIPY-based molecular rotors have been widely used due to the sensitivity of internal rotation to media's viscosity in the excited state, which could be measured using steady state or time-resolved fluorescence.[87] In addition, BODIPYs were shown to report on viscosity changes in plasma membranes induced by amyloids.[88]

Viscosity around proteins could be used to assess changes in protein conformation (and thus, function), therefore, determining microviscosity changes in the immediate proximity of the proteins is of great importance. By using BODIPY-labeled proteins, it was

possible to determine local viscosity around protein *in vitro* and the results suggested that the viscosity around proteins was different from macroviscosity of the solution. This study also demonstrated that viscosity in the close proximity of protein was protein dependent.[89]

In cells, lysosome is involved in several processes, such as protein degradation and secretion, plasma membrane repair, cell signaling and autophagy.[90] Autophagy is the recycling of defective or excess components into basic elements that cell can utilize. One of the important subcellular parameter in this process is lysosome viscosity, as a key indicator of the lysosomal function and status in cells.[91] Morpholine-BODIPY-based molecular rotors **1.17.A** and **1.17.B** (Figure 1.17) have been used for lysosomal viscosity measurements, and the real-time quantification of lysosomal viscosity changes *in vitro* could be beneficial for understanding fundamental aspects of cell biology and diagnosis of lysosome-related diseases.[92] The morpholine functional group on BODIPY (Figure 1.17) acts as a lysosome target, which causes a "turn on" fluorescence. In the case of **1.17.B** the hydrophilic polyethylene glycol groups were introduced to reduce cytotoxicity and increase biocompatibility, and the extended conjugation increased the TPE absorption, making this probe ideal for TPE fluorescence imaging thus yielding enhanced resolution (Figure 1.17). This probe successfully realized real-time detection of lysosomal viscosity and activity.[93,94]

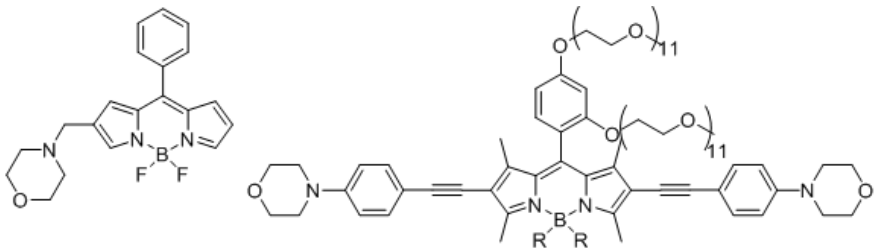

Figure 1.17. BODIPY probes for lysosome viscosity.

Other areas of the many applications have included BODIPY as energy harvesting materials for organic photovoltaics. BODIPYs can be good NIR electron donors, therefore their use in organic solar cells (OSC), shows decent energy conversion values.[95,96] BODIPY 1.18.A with extended conjugation due to addition of fused furan groups promoted electron transfer processes (Figure 1.18).[97] Further, the incorporation of thiophene groups, i.e., BODIPYs **1.18B** and **1.18.C**, was shown to have a similar effect (Figure 1.18).[98.99] Multi-chromophoric structures are also studied to improve conversion efficiency, either with more than one BODIPY or in conjunction with other types of dyes.[100,101]

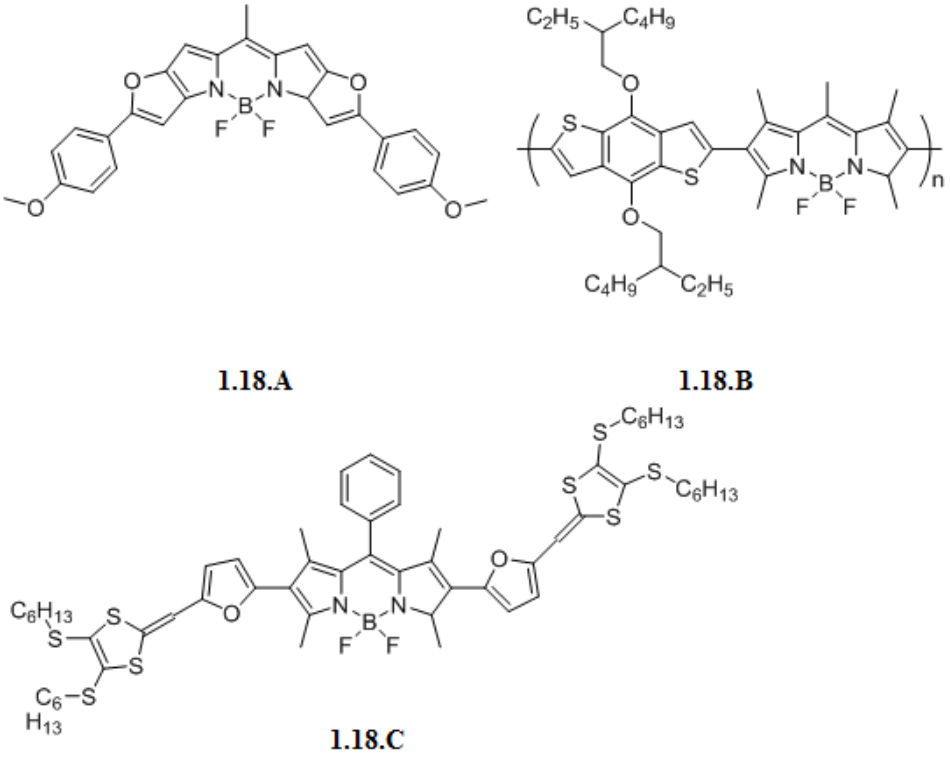

Figure 1.18. Some representative structures of BODIPY dyes in organic solar cells.

1.6 Some general comments on the synthesis of porphyrin dyes

Porphyrin is an aromatic macrocyclic compound than contains four pyrrole units and four bridging carbon atoms in a planar geometry and may have a large variety of functional groups in *meso*- an β-positions (Figure 1.19). The porphyrin macrocyclic cavity can also act as a tetradentate ligand of four pyrrole's nitrogen atoms having the ability to complex a wide range of transition metal ions.[102] In nature, the chemical structure of porphyrins is presented in various types of hemes and chlorophylls, and these compounds are vital to numerous processes. For example, hemes, as one of the key components for various biocatalytic processes as well as oxygen carriers in blood, whereas chlorophylls are playing critical roles in photosynthesis as light harvesting structures. These functions stimulated numerous studies on the synthesis and application of porphyrin-like structures, which span over various areas of natural sciences, including photosynthesis, biocatalysis, organic photovoltaics, photodynamic therapy, bioimaging probes, chemosensors, organic materials, light emitting materials.[103]

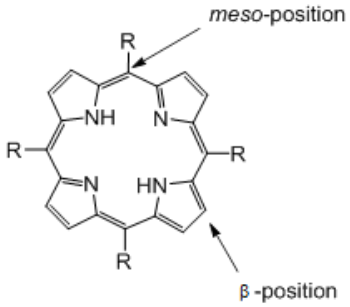

Figure 1.19. Porphyrin core.

Symmetric *meso*-aryl substituted porphyrins can be prepared using the Rothemund's method, which features condensation between aldehydes and pyrroles

(Scheme 1.3A). Non-symmetric porphyrins could be prepared according to Fisher's synthesis that features coupling of dipyrromethene salts under high temperatures in the presence organic acids (Scheme 1.3B). Furthermore, Macdonald's synthesis of non-symmetric porphyrins could be accomplished by using formyl-substituted dipyrromethenes in the presence of acid and oxidation agent (Scheme 1.3C). These methods are among the major approaches to make various porphyrin-like structures.[104,105]

Similarly to BODIPY dyes synthesis, numerous porphyrin syntheses have been reported. Typically, incorporation of functional groups on the porphyrin scaffold could be done through pre- or post-functionalization, or a combination of both methods.[104,106-108]

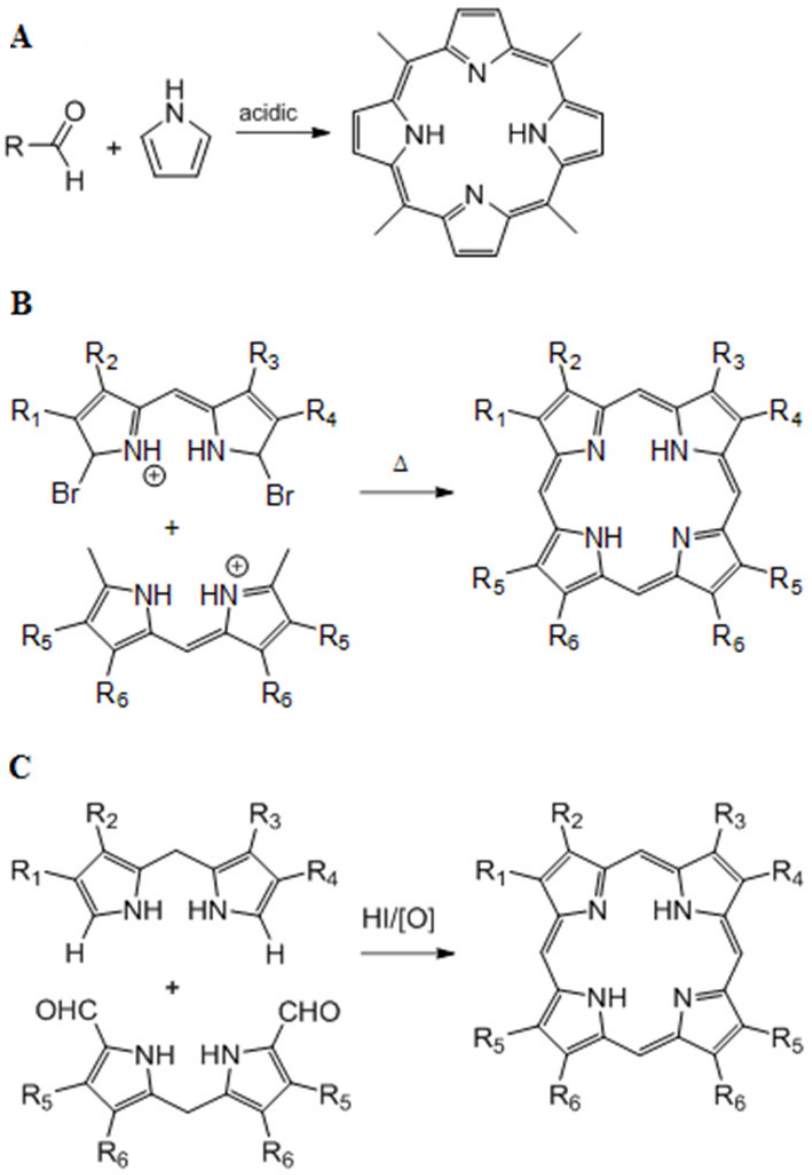

Scheme 1.3. Rothemund (A), Fisher (B), and MacDonald (C)

1.7 Some applications of porphyrin dyes

Constructs featuring porphyrin moieties are extensively used in various areas of modern research, specifically those that are related to (bio)spectroscopy and (bio)imaging due to their unique and interesting spectral properties. For example, the electronic

configuration of porphyrins featuring 18 π-electron conjugate system gives rise to electronic transitions that yield signatures that are active in both visible and NIR spectral regions. Below is a relatively brief account of the applications of porphyrins as they relate to studies in biological therapy.

Relatively long lifetimes of triplet state make it possible to explore porphyrin-like structures regarding their interaction with molecular oxygen, which upon photoactivation in cellular types of environments, makes them photosensitizers, PDT agents.[109,110]

Zinc (II) metallated porphyrins, such as **1.20.A** (Figure 1.20), have exhibited good results as photosensitizers in therapeutic experiments with cancer cells, by exhibiting low cytotoxicity in the dark and high toxicity under irradiation. Porphyrins were functionalized with morpholine as lysosome tracker and an aromatic moiety for TPE excitation through energy transfer for high-resolution cellular imaging.[111]

Some challenges have been presented on the use of monomeric porphyrins in PDT, such as self-aggregation, accumulation, drug resistant and treatment of hypoxic tumor cells, along others have been overcome using porphyrins within supramolecular assemblies.[109] Metal-organic frameworks (MOFs) composed of magnesium-porphyrins, such as **1.20.B**, have shown promising results for *in vivo* tumor reduction compared to regular chemotherapy (Figure 1.20).[112] Similar therapeutic effect was found using free-base porphyrin MOFs **1.20.C** (Figure 1.20).[113] Porphyrin nanoparticles and porphyrin micelles constructs showed good photosensitizer activity and valuable properties for optical imaging in mice.[114,115] The resulting nanoparticles assembly enhanced the delivery of the photosensitizer and radioisotopes into the cancerous area *in vivo* to allow radio-activated therapy inhibiting tumor growth.[116]

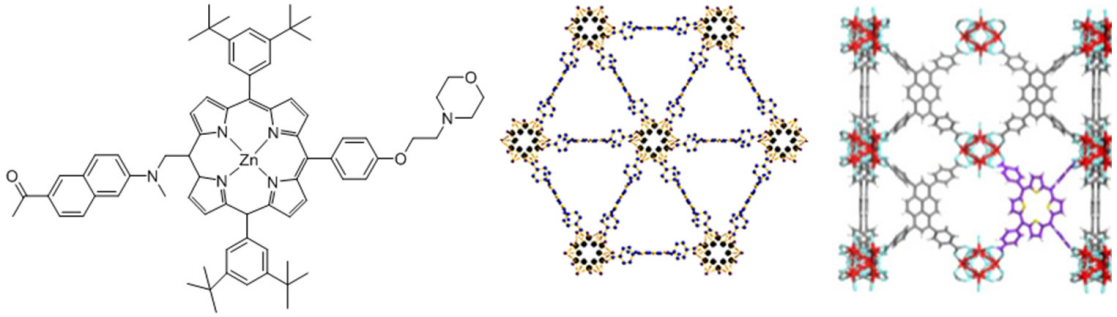

1.20.A **1.20.B** **1.20.C**

Figure 1.20. Some representative structures of porphyrins that have been used in biological applications.

Porphyrins can also be immobilized on carbon nanotubes through covalent or noncovalent approaches for applications in chemical catalysis, detection of various analytes as well as light harvesting materials for energy conversion.[11,118]

Due to tunability of porphyrins's structures and unique photophysical properties, porphyrins have been explored in organic light-conversion materials as sensitizers, electron donor or electron acceptor constituents. As sensitizers porphyrins have been widely explored for dye-sensitized solar cells (DSSC) where through optimization of porphyrin structure the optimization of conversion efficiencies was demonstrated.[119,120] As electron donors, porphyrins they have been combined with electron deficient small molecules to attain reasonable electron conversion efficiencies close to 9% inside the range of OSCs, **1.21.A** (Figure 1.21).[121] In view of the electron transport properties of porphyrins in natural systems, some examples of using porphyrins as potential electron acceptors, **1.21**.**B**, have also been shown (Figure 1.21).[122]

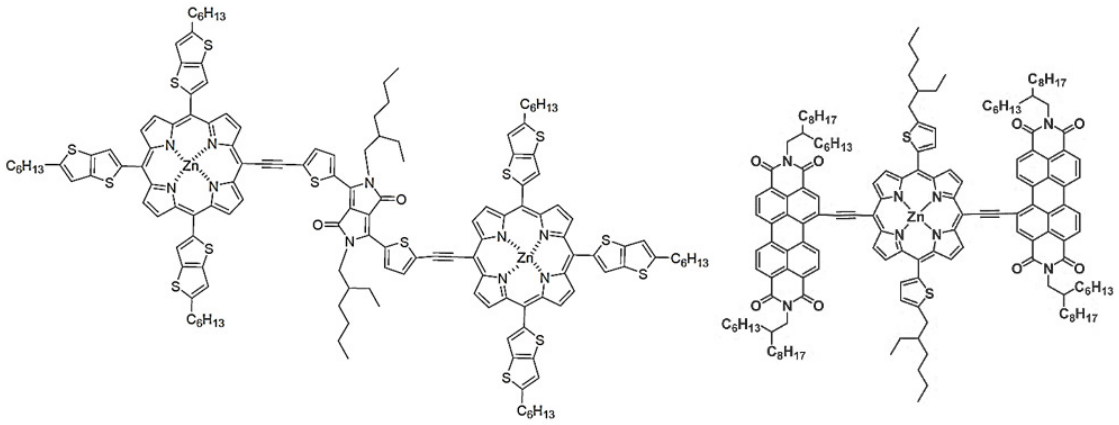

1.21.A **1.21.B**

Figure 1.21. Some representative structures of porphyrins that have been used as electron donors and acceptors in organic light-conversion materials.

CHAPTER 2: AGGREGATION OF BODIPY DYES

2.1 Introduction

Although BODIPY dyes have been studied over several decades, they continue to be a subject of interest due to ever-expanding applications. BODIPY dyes are known to have good thermal and photochemical stability, high fluorescence quantum yield, intense absorptions and good solubility in molecular solvents. The aggregation of organic small molecules chromophores has been explored in a range of application, included those related to optoelectronic sensors, because strong π-π interactions between spatially close conjugated motifs could lead to charge separation and transport, directional energy transfer, which result in changes of optical and photophysical properties.[41,123,124]

The spectroscopic changes that results from the dyes aggregation processes provide valuable information in regard to the orientation of adjacent molecules, *i.e.*, the structure of the aggregates. The most studied types of aggregates are known as J- and H-aggregates (Figure 2.1). In H-aggregates (Figure 2.1), the chromophores are oriented in a side-by-side fashion or one in front of the other, which results in blue-shifted emission profiles and suppressed excited state radiative decays. On the contrary, J-aggregates (Figure 2.1) display a head-to-tail alignment of the chromophores or one after the other and exhibit red-shifted and enhanced emission.[125-127] Supramolecular assemblies formed by these aggregates are widely explored as energy harvest materials, sensors, plasmonic antennas, and as building blocks of optical devices.[128] Introduction of amphiphilic groups on fluorescent scaffolds produces a variety of water-soluble functional supramolecular aggregates, thus expanding the range of applications to biological systems.[129]

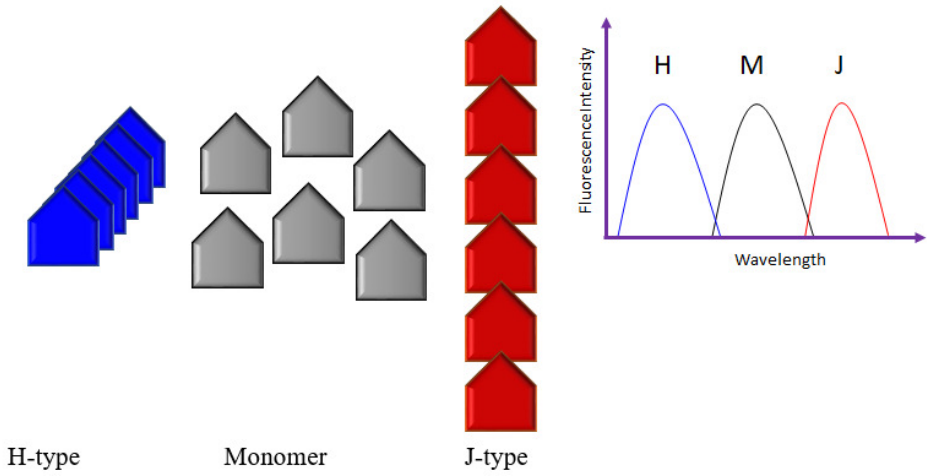

Figure 2.1 Types of aggregation of fluorophores.

In regard to biologically related processes, several applications of BODIPY aggregates are noteworthy. Conjugation of BODIPY dyes with biologically active moieties, such as **2.2.A** (Figure 2.2) formed various assemblies, which were shown to deliver medication in increased dosage to unhealthy tissues.[80] In addition, by incorporating BODIPY dyes, such as **2.2.B**, inside polymeric nanoparticles (Figure 2.2) long-term cellular imaging was explored, and it was shown to be a viable approach that allowed to detect various processes.[130] In material sciences, J-and H-aggregates of thiophene-BODIPY dyes, such as **2.2.C**, were used as a part of a quantum dot (QD) based systems (Figure 2.2) that led to enhance energy transfer and charge separation processes, which might lead to better solar energy conversions.[131]

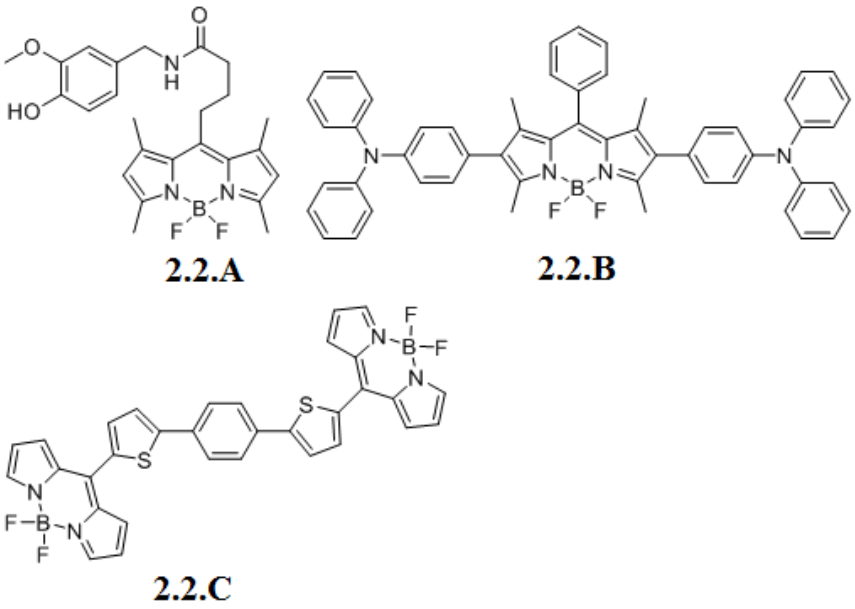

Figure 2.2 Some examples of BODIPYs used for supramolecular assemblies.

BODIPY self-assemblies haven been the subject of numerous studies,[132] even though many mechanistic details have not been thoroughly investigated. Many of these BODIPY self-assemblies have been also generated in confined environments, such as protein or gel-like type of environments. In addition, in some instances, aggregation of BODIPY dyes was found to produce specific fluorescent signals, which were more pronounced as those originating from the monomeric species. This process is known as aggregation-induced emission (AIE), and it was shown to be useful for a number of processes, including biological imaging.[133-135] Typical groups that could induce aggregation are long alkyl chain with ionic head, hydrogen bonding and protic moieties, planar aromatic systems, among others.

It is crucial to note that in molecular organic solvents, BODIPY dyes, at low concentrations (μM-range), are known to be present in a monomeric state. In general, the emission spectrum of a BODIPY is a mirror image of the absorption (or excitation) spectrum. Typically, a single emission maximum in 500 – 65 nm range is observed. This range depends on the type and position of the functional groups present on the BODIPY core, and it does not change within a certain concentration range (typically within a few μM). [52] However, our studies indicated that the aggregation of several BODIPYs in organic solvents does take place even at low μM-concentrations of BODIPY dyes.[136]

2.2 Synthesis

The vast majority of literature preparations of BODIPY dyes rely on solution-based synthesis, with condensation of a pyrrole with an aldehyde, in the presence of Lewis acids as catalysts, or an acid chloride as first step. Application of acid chlorides is limited, as compared to aldehydes, due to moisture sensitivity of this functional group, and lower degree of structural and functional diversity. Subsequently, oxidation of the dipyrromethane core is carried out to induce aromatization of scaffold, followed by installation of the BF_2-group by using BF_3-Et_2O in the presence of organic base, with Et_3N being the most widely used (Scheme 2.1).[41]

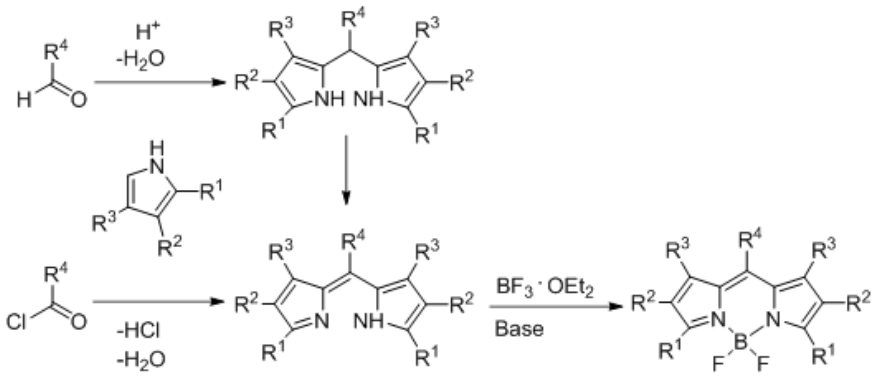

Scheme 2.1 Typical syntheses of symmetric BODIPY dyes.[41]

An alternative procedure was also developed, in which *meso*-functionalized BODIPY dyes were synthetized without the use of solvent.[54] Specifically, commercially available pyrrole and aldehyde were grinded in a mortar with pestle, followed by the addition of a catalytic amount of trifluoroacetic acid, subsequent addition of *p*-chloranil induced the oxidation of the core, and finally the addition of triethyl amine and $BF_3{\cdot}OEt_2$ furnished BODIPY dye in 5 minutes (Scheme 2.2).[54] Importantly, this process avoided the necessity of inert atmosphere, all steps performed in one pot, which arguably minimized the amounts of waste and time.[54] Thus prepared ethynyl-containing BODIPY was subjected to Glaser coupling to produce BODIPY dimer **1** using copper (I) iodide and a base in polar aprotic solvent (Scheme 2.2). The simple and facile nature of this two-step procedure towards this molecular rotor for the determination of viscosity, is in sharp contrast to typically employed multistep synthetic routes that are used to prepare molecular rotors.[45] A good correlation between viscosity of the environment and the steady-state fluorescence intensity (and/or fluorescence life-time) made this dimer a viable molecular viscometer.[92,137]

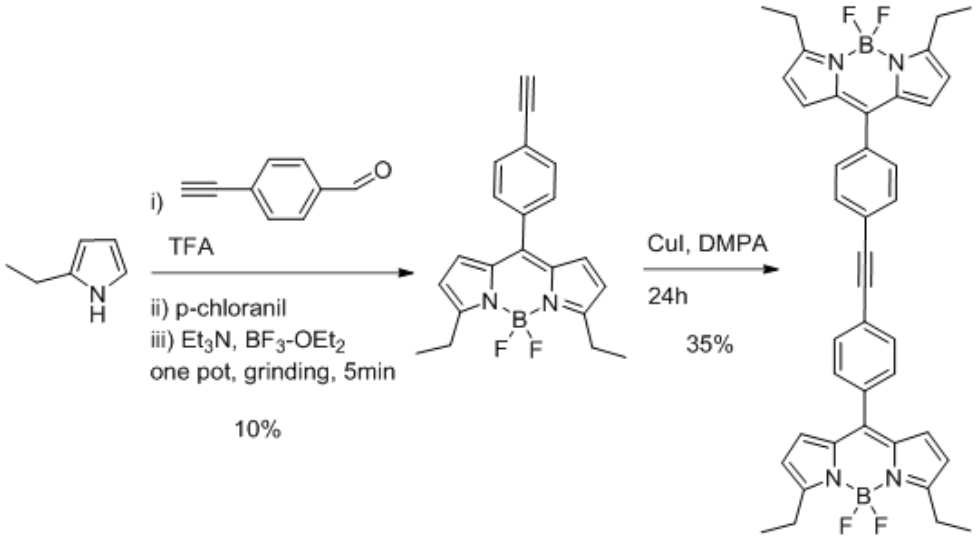

Scheme 2.2 Synthesis of BODIPY dimer **1**.[139]

Specifically, the BOPIDY dimer **1** was utilized to study microviscosity of molecular solvents as well as ionic liquids. **1** showed a unique viscosity/fluorescent lifetime correlation with each ionic liquid studied, most likely due to the unique nanostructural complexity of this type of media. **1** was further studied in amphiphilic environments, such as lipid vesicles. In addition, *in vitro* imaging and viscosity representation inside cells was possible using this probe.[138,139]

Because the limited number of molecular solvents were used in previous studies, [139] it was decided to expand the range of solvents, and include chlorinated (*e.g.* dichloromethane (CH_2Cl_2), chloroform ($CHCl_3$), 1,2-dichloroethane $(CH_2Cl)_2$, etc), polar aprotic (*e.g.* dimethyl sulfoxide (CH_3SOCH_3), acetonitrile (CH_3CN), tetrahydrofuran ($(CH_2)_4O$)), polar protic (*e.g.* ethanol (CH_3CH_2OH)), and non-polar (*e.g.* dioxane ($(C_2H_4O)_2$), hexane (n-C_6H_{14})) solvents.

Using the above-mentioned procedure (Scheme 2.2), a set of BODIPY monomers **2 - 6** were synthetized for the study of the BODIPYs in organic solvents (Figure 2.3). The monomers included rotors (possibility of rotation along the phenyl ring), i.e., dyes **5** and **6**, where the substituent in the *meso*-position has a free rotation relative to the BODIPY core, and non-rotors, i.e., **2** - **4** that possess methyl groups on the 1- and 7-positions to prevent the rotation of the substituent in the *meso*-position. Notably, neither aggregation inducing groups nor groups that could promote hydrogen bonding have been introduced.

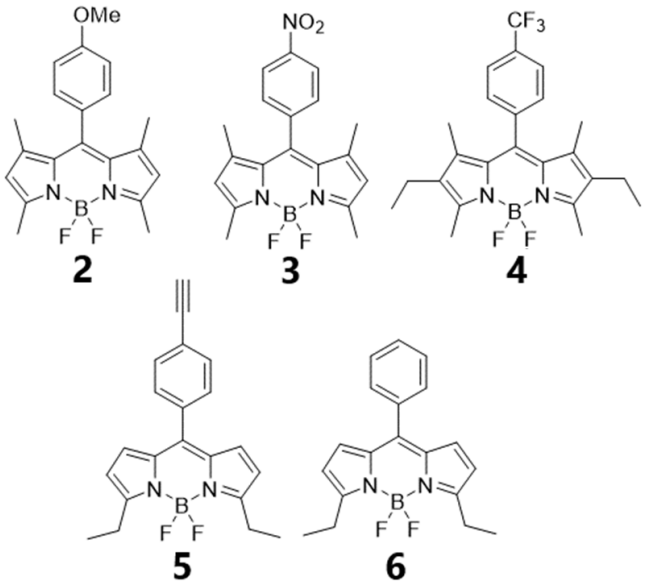

Figure 2.3 BODIPY monomers synthesized for the current study.

2.3 Results

In a quest to further establish dimeric BODIPY dye **1** as an environmental probe, with a high extinction coefficient, and hence a brighter fluorescent, as compared to monomeric BODIPY dyes, **1** was studied in a range of molecular solvents with different characteristics such as polar and non-polar, protic and aprotic, halogenated, aromatic and

aliphatic, (Table 2.1). To facilitate the evaluation process, 1 mM stock solution of **1** in DMSO was prepared, and it was added to different solvents to evaluate spectroscopic characteristics of the dye, such as UV/visible absorbance and steady-state fluorescence. Notably, the final concentration of DMSO in all solutions was 0.5 % v/v, which was similar to previous studies,[139] and this concentration was assumed to have a negligible effect on the overall properties of the solvents.

Solvent	Dipole moment / D
1,2-DCE	1.8
chloroform	1.0
acetonitrile	3.5
dioxane	0.4
DMSO	3.9
ethanol	1.7
n-hexane	0.0
THF	1.6

Table 2.1 Dipole moment of various molecular solvents.[141]

In the solvents tested, the absorbance maximum of **1** was found to be in the range of 512 – 518 nm, which was consistent with previous investigations.[139] In addition, this maximum appeared to be insensitive to viscosities of various types of media: molecular solvents, such as ethanol (η = 1.4 cP), propylene glycol (η = 70.0 cP) and glycerol (η = 1475.0 cP), as well as in ionic liquids, such as [C_4-mim]NTf_2 (η = 78.0 cP), [C_{12}-mim]NTf_2 (η = 248.0 cP) and [C_4-mim]PF_6 (η = 435.0 cP) (all values are at 20 ^oC).[139] However, in 1,2-dichloroethane (1,2-DCE), purchased from ACROS (from this point designated as:

ACROS/for spectroscopy), the absorption maximum appeared at 546 nm, *i.e.*, a red-shift of the maximum, in comparison with the other solvents (Figure 2.4A). Furthermore, a broadening of the absorption band, as judged by a full width half maxima (FWHM), from 29 nm to 42 nm indicated the presence of unique species in the ground state. In addition, the emission maximum was also red shifted: 535-542 nm detected in all solvents except 563 nm observed in 1,2-DCE (Figure 2.4B). Thus, the presence of unique species in 1,2-DCE in the excited state was also established.

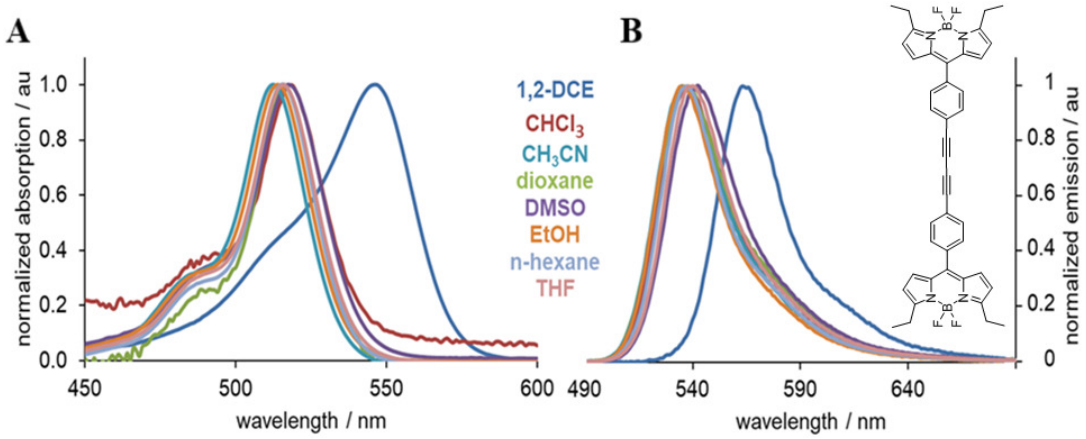

Figure 2.4 Normalized UV/visible absorbance (A) and emission (B) of **1** in molecular solvents
Conditions: [**1**] = 1 μM, λ_{ex} = 480 nm; DMSO = 0.1 % v/v

This novel, unique and interesting behavior forced us to further investigate the spectroscopic properties of **1** over a range of concentrations, *i.e.*, 0.5 to 10 μM (Figure 2.5). The wavelength of the absorbance maximum was found to strongly depend on the concentration of **1**. In addition, the absorbance maxima as a function of BODIPY **1** concentration at two wavelengths, *i.e.*, 517 and 546 nm, indicated the transition from one type of species to the other.

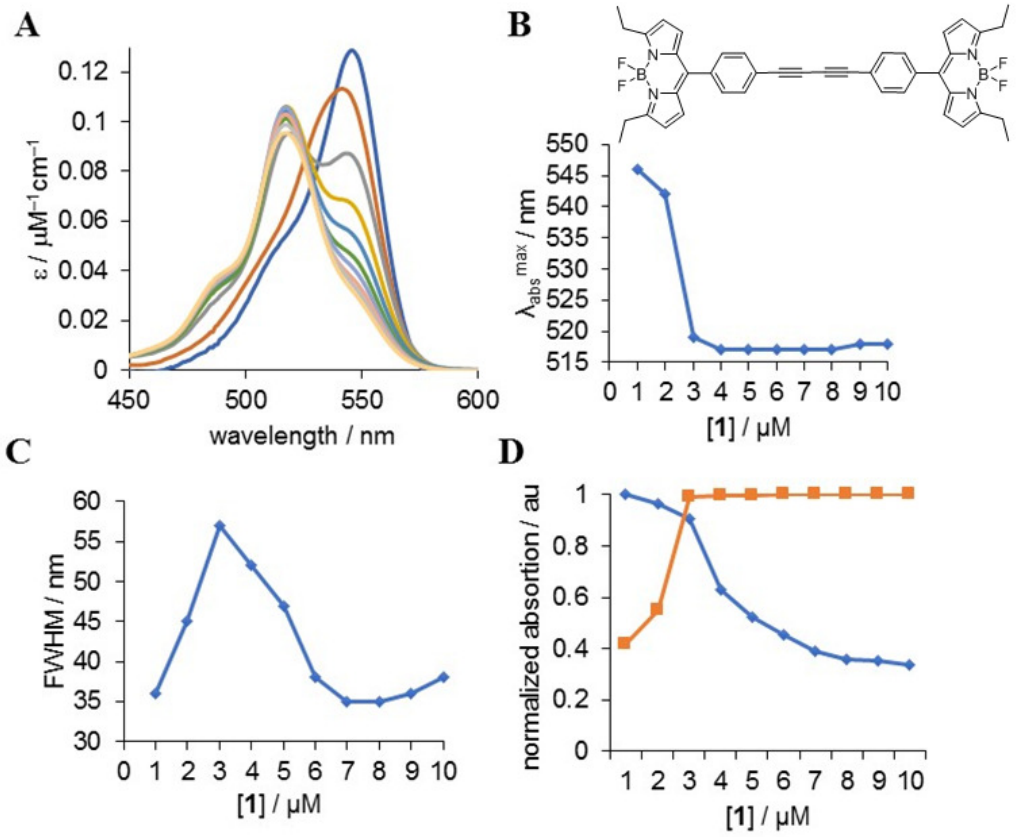

Figure 2.5 Absorbance profile of **1** in 1,2-DCE ACROS/for spectroscopy
A: UV/visible spectra of BODIPY **1** in 1,2-DCE ACROS/ spectroscopy while increasing the concentration 0.1 - 10 μM
B: changes of the absorption maxima as a function of dye's concentration;
C: changes of the absorption intensity as a function of dye's concentration at two maxima;
D: Changes of the FWHM as a function of dye's concentration
Conditions: DMSO = 0.1-1 % v/v

In the excited state, the presence of different types of species was also noted as change from 567 nm to 544 nm was observed with increasing concentration of dye **1** (Figure 2.6). The changes of the wavelength of the emission maximum as well as intensities at two distinct maxima, *i.e.*, 544 and 567 nm, were observed as a function of dye's concentration.

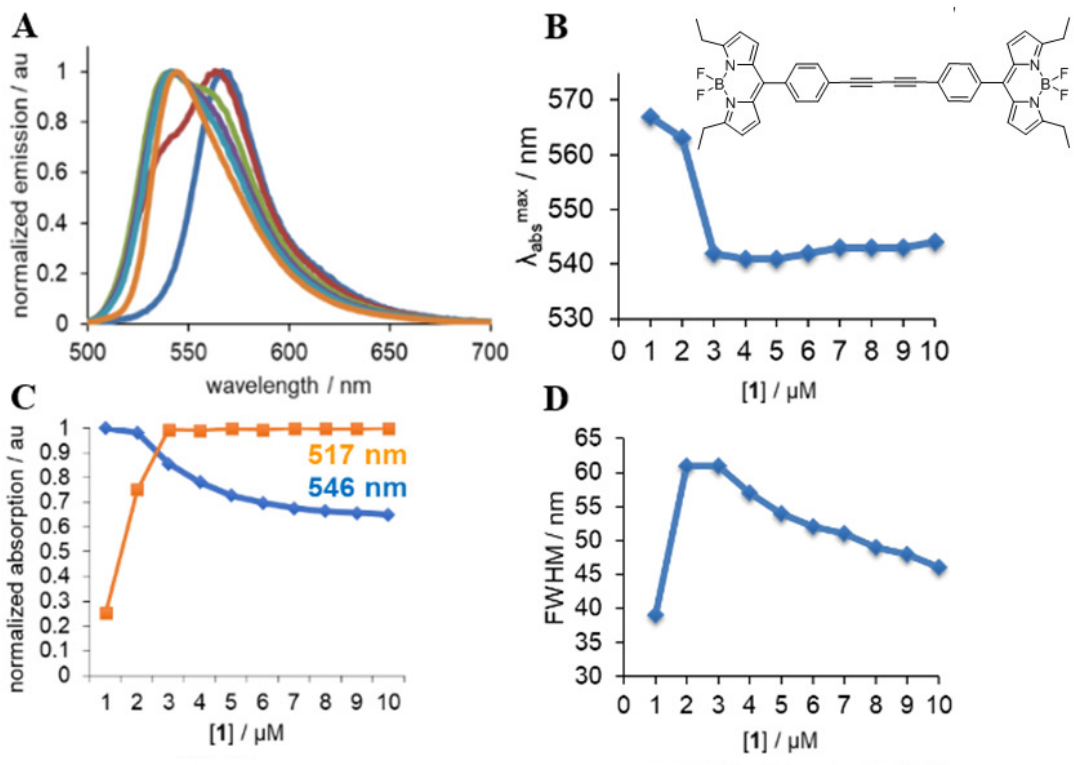

Figure 2.6 Concentration dependent emission profile of **1** in 1,2-DCE ACROS/for spectroscopy
A: normalized, concentration-dependent emission spectra of BODIPY **1**;
B: changes of the emission maxima as a function of **1**'s concentration;
C: changes of the emission intensity as a function of dye's concentration at two emission maxima;
D: Changes of the FWHM as a function of dye's concentration
Conditions: λ_{ex} = 480 nm; DMSO = 0.1-1 % v/v

Furthermore, fluorescence lifetime measurements were performed (Figure 2.7). Lifetime measurements represent the average time between excitation and return to the ground state of a chromophore, and more specifically it determines the time available for the excited state of the fluorophore to interact with the environment. Both amplitude and intensity measurements in a range of concentrations of **1** in 1,2-DCE, appeared to decrease as the concentration of the dye increased (Table 2.2). These measurements further

supported the notion that two different types of species (or two different types of aggregates) were present in this concentration range.[136]

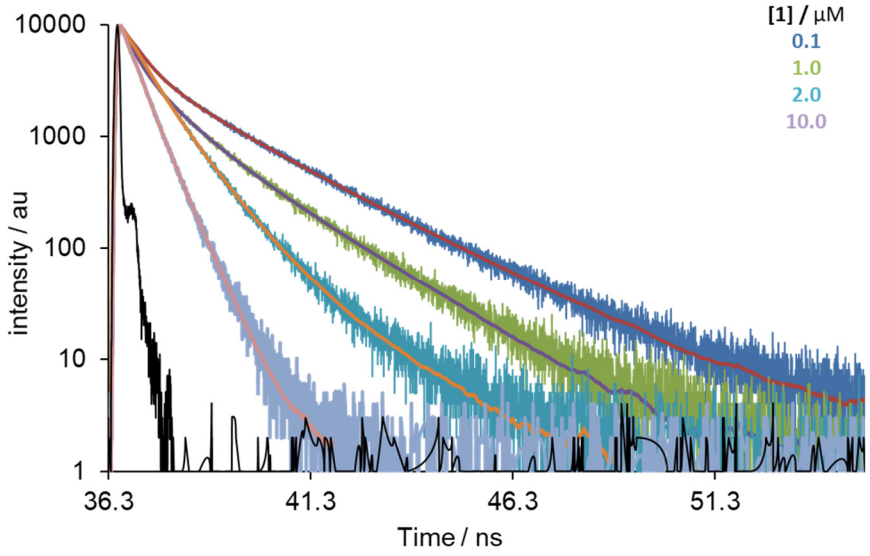

Figure 2.7 Fluorescence lifetimes of BODIPY **1** in 1,2-DCE ACROS/for spectroscopy.

2 / μM	Lifetime / ns
0.1	1.05 ± 0.03
0.2	1.04 ± 0.03
0.5	1.01 ± 0.02
1.0	0.70 ± 0.02
2.0	0.67 ± 0.02
5.0	0.41 ± 0.01
10.0	0.40 ± 0.01

Table 2.2 Fluorescence lifetime of BODIPY **2** in 1,2-DCE ACROS/spectroscopy as a function of dye's concentration.

Arguably, dimeric structures might be prone to aggregation or formation of supramolecular constructs at higher concentrations, which might persist even upon dilution into other environments. Thus, different concentrations of stock solutions of **1** in 1,2-DCE, *i.e.*, 0.1 mM and 100 mM, were prepared. However, no differences between these stock solutions and 1 mM stock were noted, when these newly prepared stocks were diluted to various types of liquids.

To gain further insight into this phenomenon, spectroscopic investigation of common BODIPY dyes, such as **2** – **6** (Figure 2.3) was performed in 1,2-DCE. Unlike **1**, dye **2** is a non-rotor due to the presence of the methyl groups in 1- and 7-positions that restrict the rotation of the group in the *meso*-position. This restriction prohibits a change of dye's geometry in the ground and excited states, and as a result, it might form different types of assemblies as compared to dimer **1**.

The absorption maximum of dye **2** was observed at 529 nm at 0.1 μM concentration (Figure 2.8). Increasing amounts of the dye led to a blue shift, with new absorption maximum at 501 nm before reaching 1 μM, plateauing to 10 μM. Also, the FWHM went from 29 nm, passing through broad bands with FWHM of 52 nm at 0.3 and 0.4 μM concentration (while the absorption maxima shifted to the shorter wavelength), and a 20 nm wide peak was observed at the higher concentrations. Overall, these changes indicated the presence of multiple assemblies.

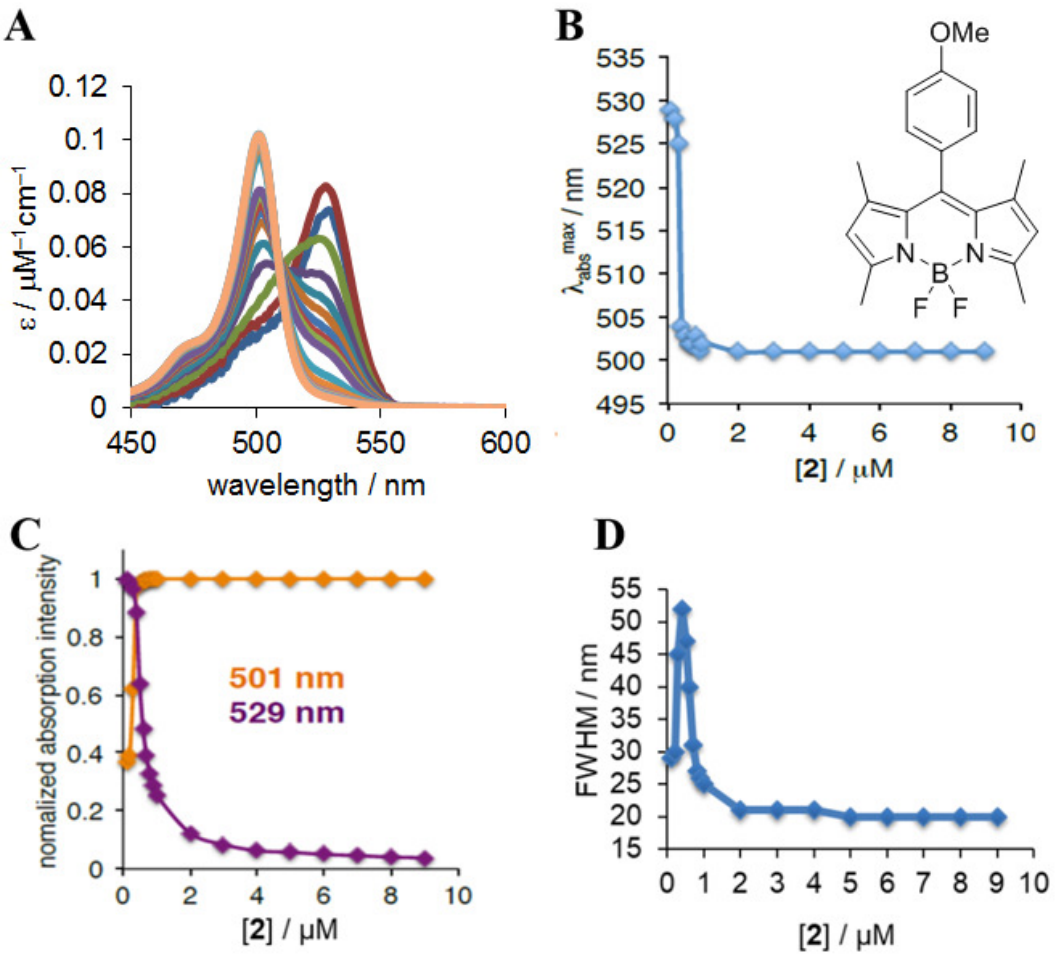

Figure 2.8 Concentration-dependent absorption characteristics of **2** in 1,2-DCE ACROS/for spectroscopy.
A: UV/visible spectra of BODIPY **2** in 1,2-DCE ACROS/ spectroscopy while increasing the concentration 0.1 - 10 μM
B: changes of the absorption maximum as a function of dye's concentration
C: changes of the absorbance intensity as a function of dye's concentration at two wavelengths
D: Changes of the FWHM as a function of dye's concentration
Conditions: [DMSO] = 0.1-1 % v/v

Upon increasing the concentration, the emission band of **2** (Figure 2.9) also had a broadening of the band, while exhibiting a blue shift from 540 to 510 nm at the low end of

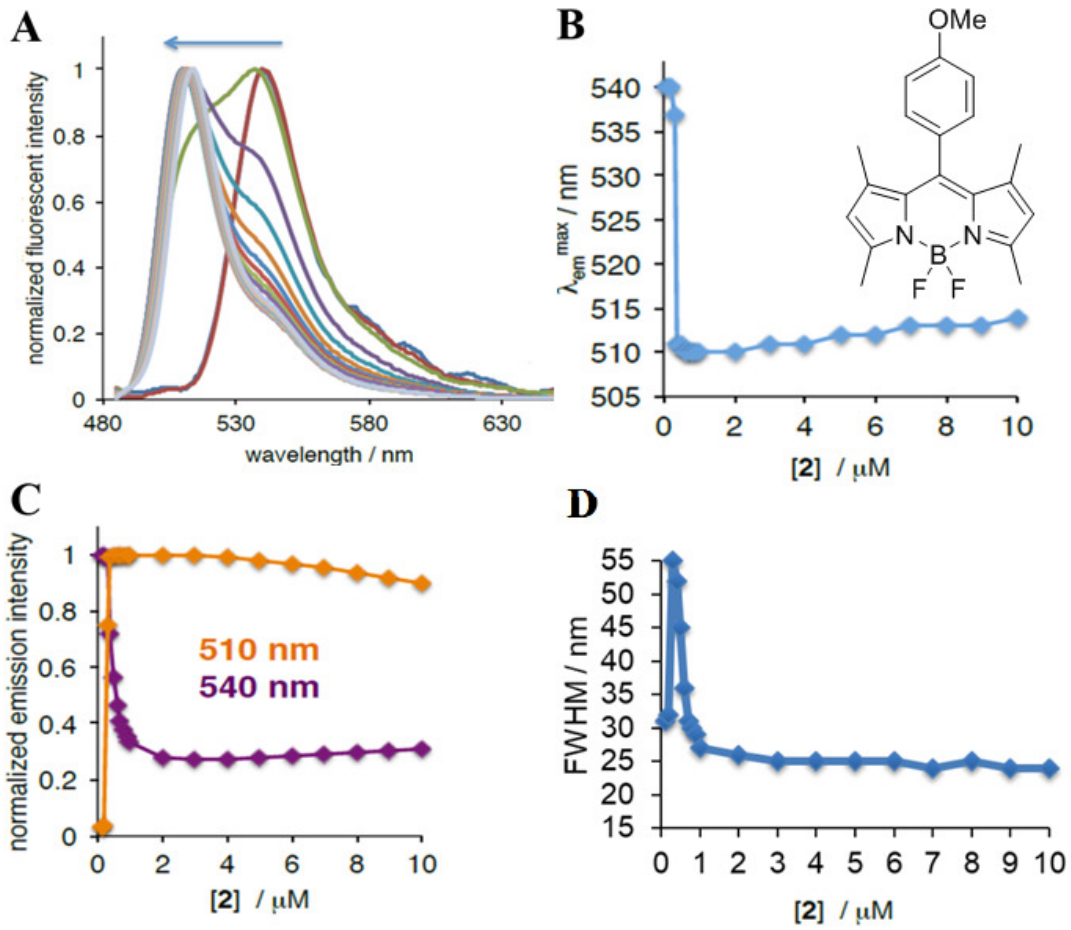

Figure 2.9 Concentration-dependent emission characteristics of **2** in 1,2-DCE ACROS/for spectroscopy,
A: normalized, concentration-depend emission intensity of **2**;
B: changes of the emission maximum as a function of dye's concentration;
C: changes of the emission intensity as a function of dye's concentration at two maxima;
D: Changes of the FWHM as a function of dye's concentration,
Conditions: λ_{ex} = 480 nm; [DMSO] = 0.1-1 % v/v

the concentrations. Thus, the presence of the different assemblies in the excited state was evident as well.

Next, concentration-dependent spectroscopic profiles of dye **3** were investigated (Figures 2.10 and 2.11). Based on the absorption spectra (Figure 2.10), a shift from 535

nm to 506 nm was obtained when the concentration of the dye varied from 0.05 µM to 10 µM. The switch between two distinct forms of this dye appeared to take place when concentration was 4 µM. Notably, a broad band (FWHM = 59 nm) at this concentration gradually became narrower, and at [**3**] = 9 µM, it reached the same value (*i.e.*, FWHM = 29 nm), observed at the low range of concentrations. Arguably, this might have indicated

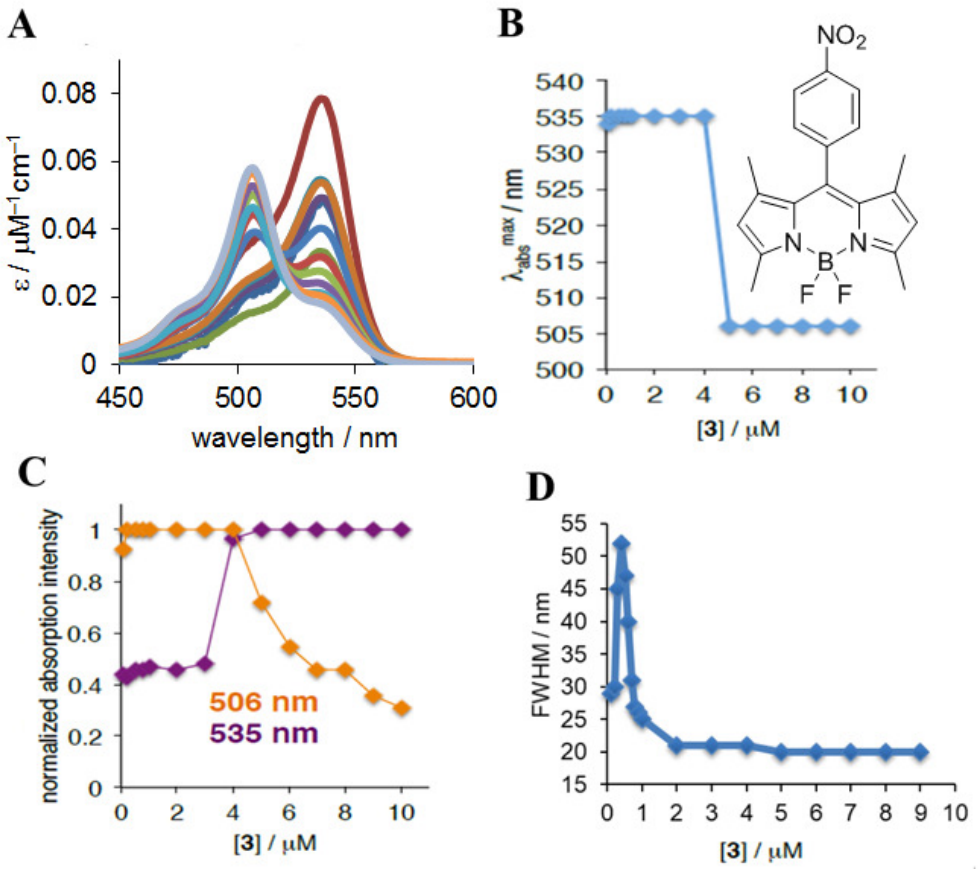

Figure 2.10 Concentration-dependent absorption characteristics of **3** in 1,2- DCE ACROS/for spectroscopy.
A: UV/visible spectra of BODIPY **3** in 1,2-DCE ACROS/ spectroscopy while increasing the concentration 0.1 - 10 µM
B: changes of the absorption maximum as a function of dye's concentration;
C: changes of the absorbance intensity as a function of dye's concentration at two wavelengths;
D: Changes of the FWHM as a function of dye's concentration.
Conditions: DMSO = 0.1-1 % v/v

that some sort of reorganizations of the dye's assemblies (or different types of aggregates) were taking place as a function of the dye's concentration.

The excited state characteristics of this dye appeared to be unique from previously described cases (Figure 2.11). A single emission maximum at 549 nm wavelength was observed for the entire concentration range, with a shoulder at 522 nm. However, the

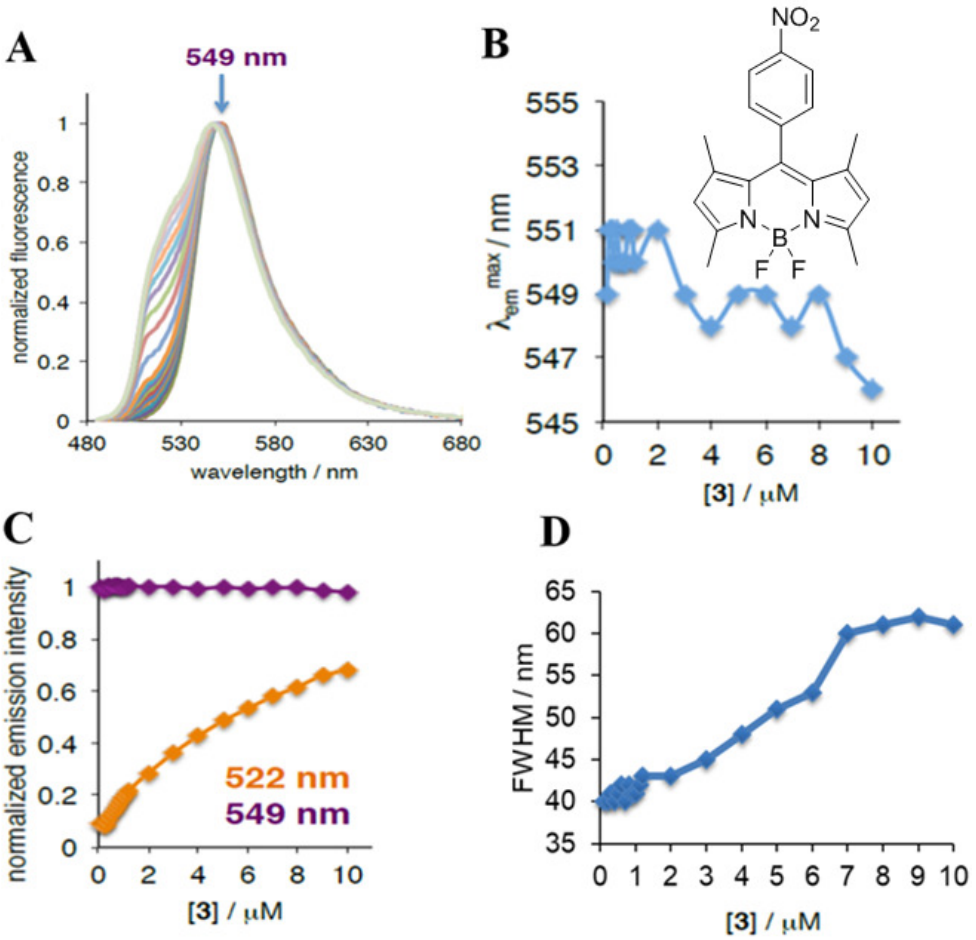

Figure 2.11 Concentration-dependent emission characteristics of **3** in 1,2-DCE ACROS/for spectroscopy.
A: normalized, concentration-depend emission intensity of **3**;
B: changes of the emission maximum as a function of dye's concentration;
C: changes of the emission intensity as a function of dye's concentration at two maxima;
D: Changes of the FWHM as a function of dye's concentration.
Conditions: λ_{ex} = 480 nm; DMSO = 0.1-1 % v/v

broadening of the emission bands from 40 to 61 nm FWHM was noted. This, in turn, confirmed that some distinct structural aggregates of the dye were present within the studies concentration range.

Dye **4** was selected for further evaluations because it has additional ethyl groups 3- and 6-positions that were expected to prevent any self-association processes. The absorption characteristics of dye **4** (Figure 2.12) revealed a 12 nm blue shift, which was

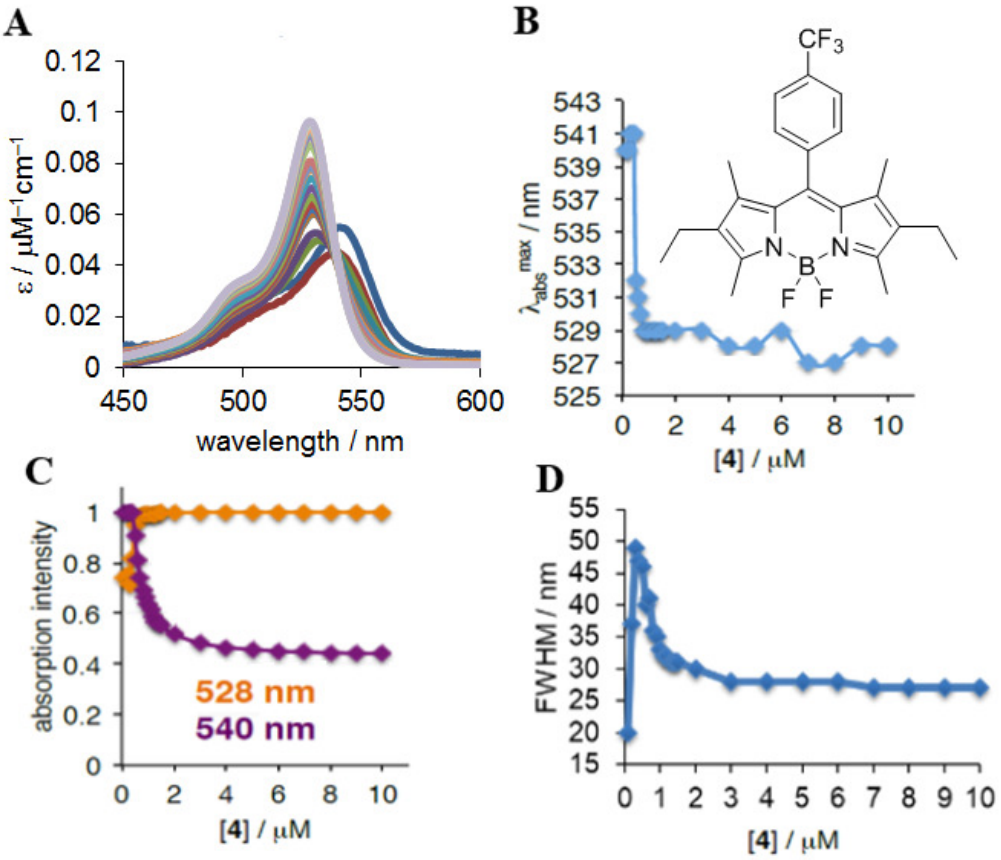

Figure 2.12 Concentration-dependent absorption characteristics of **4** in 1,2- DCE ACROS/for spectroscopy.
A: UV/visible spectra of BODIPY **4** in 1,2-DCE ACROS/ spectroscopy while increasing the concentration 0.1 - 10 μM
B: changes of the absorption maximum as a function of dye's concentration;
C: changes of the absorbance intensity as a function of dye's concentration at two wavelengths.
D: Changes of the FWHM as a function of dye's concentration
Conditions: DMSO = 0.1-1 % v/v

smaller as compared to previous BODIPY dyes **2** and **3** (where blue shifts as large as 29 nm were noted). In addition, the shift towards shorter wavelengths occurred at very low concentrations of the dye, *i.e.,* 0.5 μM. Additionally, as the concentration of the dye increased, a gradual change of FWHM from 49 to 27 nm was noted.

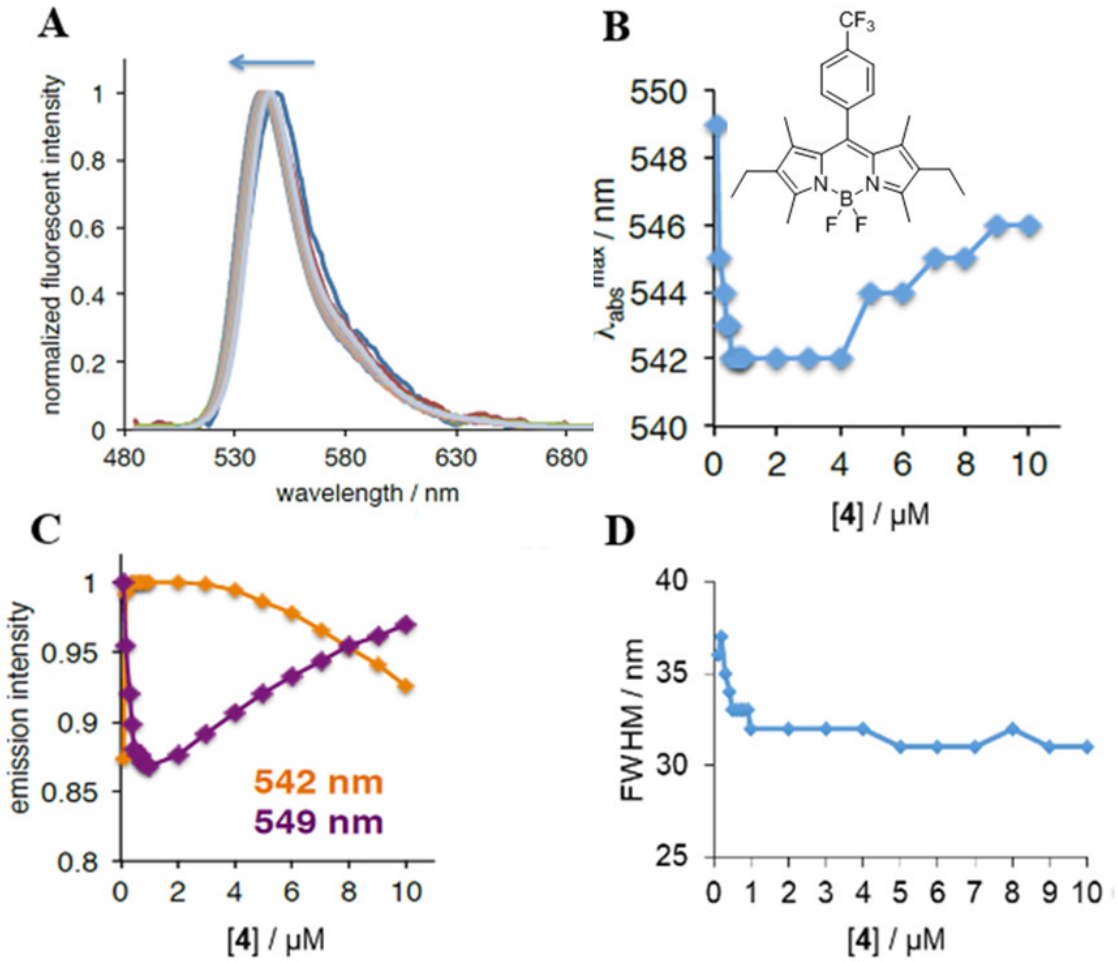

Figure 2.13 Concentration-dependent emission characteristics of **4** in 1,2-DCE ACROS/for spectroscopy.
A: normalized, concentration-depend emission intensity of **4**;
B: changes of the emission maximum as a function of dye's concentration;
C: changes of the emission intensity as a function of dye's concentration at two maxima;
D: Changes of the FWHM as a function of dye's concentration.
Conditions: λ_{ex} = 480 nm; DMSO = 0.1-1 % v/v

Emission characteristics of dye **4** (Figure 2.13) appeared to be somewhat distinct from those of the dyes **2** and **3**. A smaller shift to shorter wavelengths (*ca*. 7 nm) was observed over the range of studies concentrations. Furthermore, very similar FWHM values were obtained for all concentrations. Thus, it appears that rigidity of this structure as well as additional alkyl group on the BODIPY core suppressed the aggregation process to some extent.

The monomeric unit of rotor **1**, *i.e*., dye **5** was also studied (Figures 2.14 and 2.15). It should be noted that unlike dyes **2** – **4**, dye **5** is a rotor, due to a free rotation of the substituent at the *meso*-position around the BODIPY core. The absorption maxima values for dye **5** were found to be close to those observed for the dimer **1**. A blue shift from 544 to 516 nm was noted, with most changes occurring below 1 μM concentration (Figure 2.14). Interestingly, as the concentration increased from 0.1 to 0.5 μM, a broadening of the absorption band was noted (FWHM = 43 nm at 0.1 μM; FWHM = 51 nm at 0.5 μM), yet upon further increase of the concentration (*i.e*., to 10 μM), no changes of band width were noted (FWHM = 24 nm), which indicated that from 0.5 to 10 μM the nature of the aggregates of dye 5 remained the same.

The emission characteristics of dye **5** exhibited a blue shift of about 30 nm (Figure 2.15). Since no significant changes took place at concentrations above 2 μM (Figure 2.15.B and C) it could be assumed that the same type of aggregates was present at these concentrations, whereas different forms of this dye existed at concentrations below 2 μM.

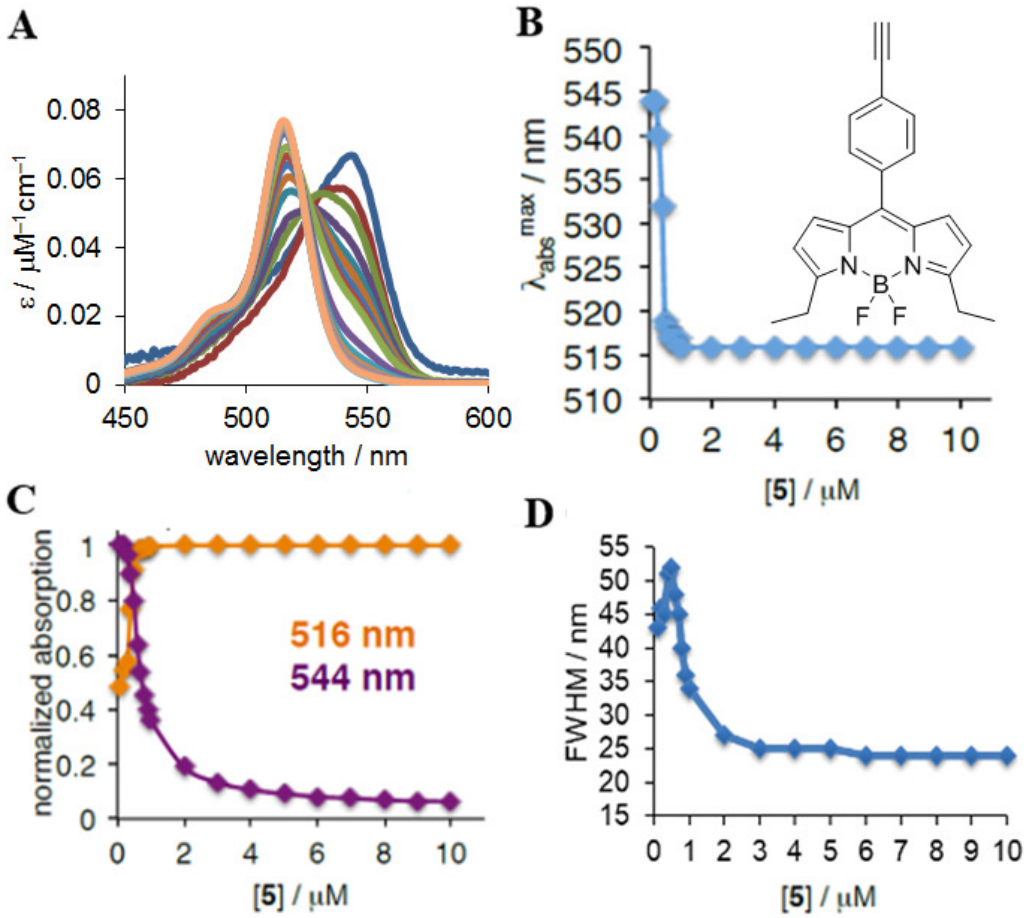

Figure 2.14 Concentration-dependent absorption characteristics of **5** in 1,2-DCE ACROS/for spectroscopy.
A: UV/visible spectra of BODIPY **5** in 1,2-DCE ACROS/ spectroscopy while increasing the concentration 0.1 - 10 μM
B: changes of the absorption maximum as a function of dye's concentration;
C: changes of the absorbance intensity as a function of dye's concentration at two wavelengths;
D: changes of the FWHM as a function of dye's concentration
Conditions: DMSO = 0.1-1 % v/v

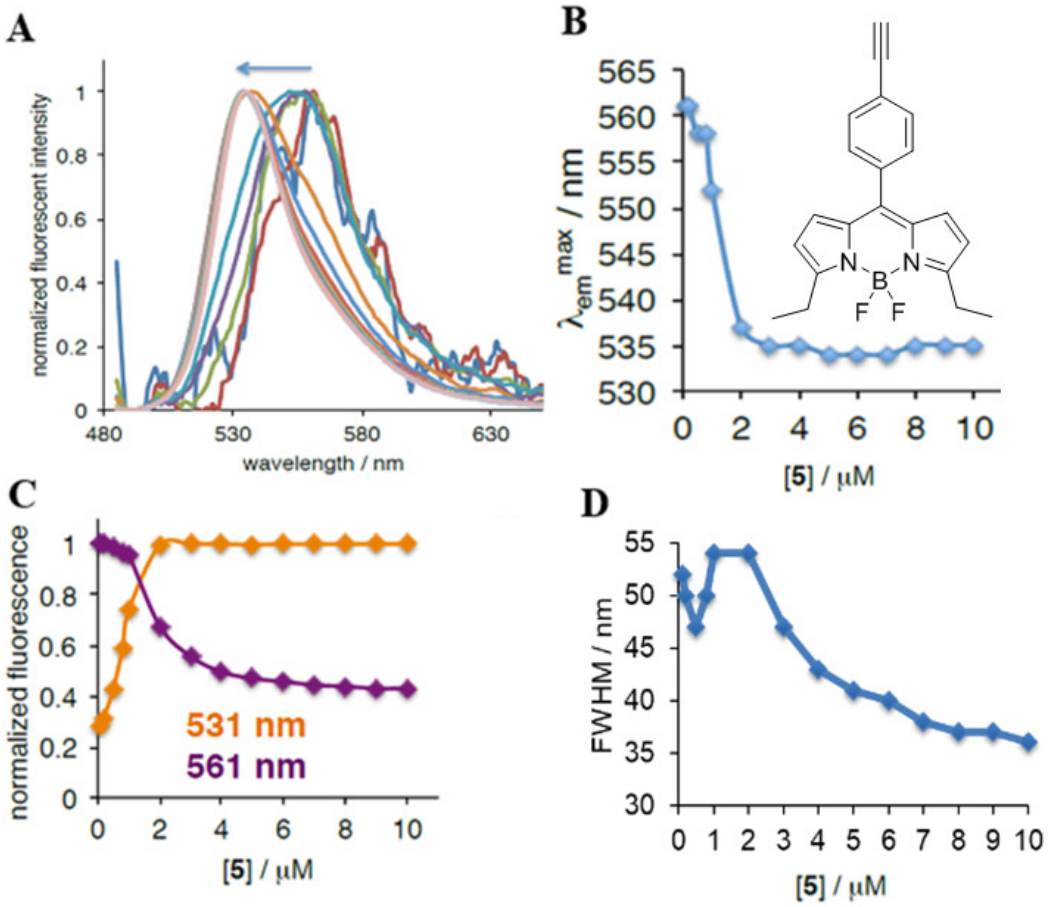

Figure 2.15 Concentration-dependent emission characteristics of **5** in 1,2-DCE ACROS/for spectroscopy.
A: normalized, concentration-depend emission intensity of **5**;
B: changes of the emission maximum as a function of dye's concentration;
C: changes of the emission intensity as a function of dye's concentration at two maxima;
D: changes of the FWHM as a function of dye's concentration.
Conditions: λ_{ex} = 480 nm; DMSO = 0.1-1 % v/v

Another molecular rotor, *i.e.,* dye **6,** was investigated as well, where the rotating element is a phenyl group in the *meso*-position (Figures 2.16 and 2.17). The dye displayed an absorption maximum at 542 nm at low micromolar concentrations, which underwent a

blue shift to 513 nm as the concentration of the dye in 1,2-DCE was gradually increased to 10 µM (Figure 2.16). It was found that a continuous increase of FWHM from 28 nm at 0.1 µM to 54 nm at 1.1 µM, was followed by a continuous decrease that reached 22 nm at 10 µM. This trend might have been indicative of multiple types of assemblies that were forming over the range of concentrations.

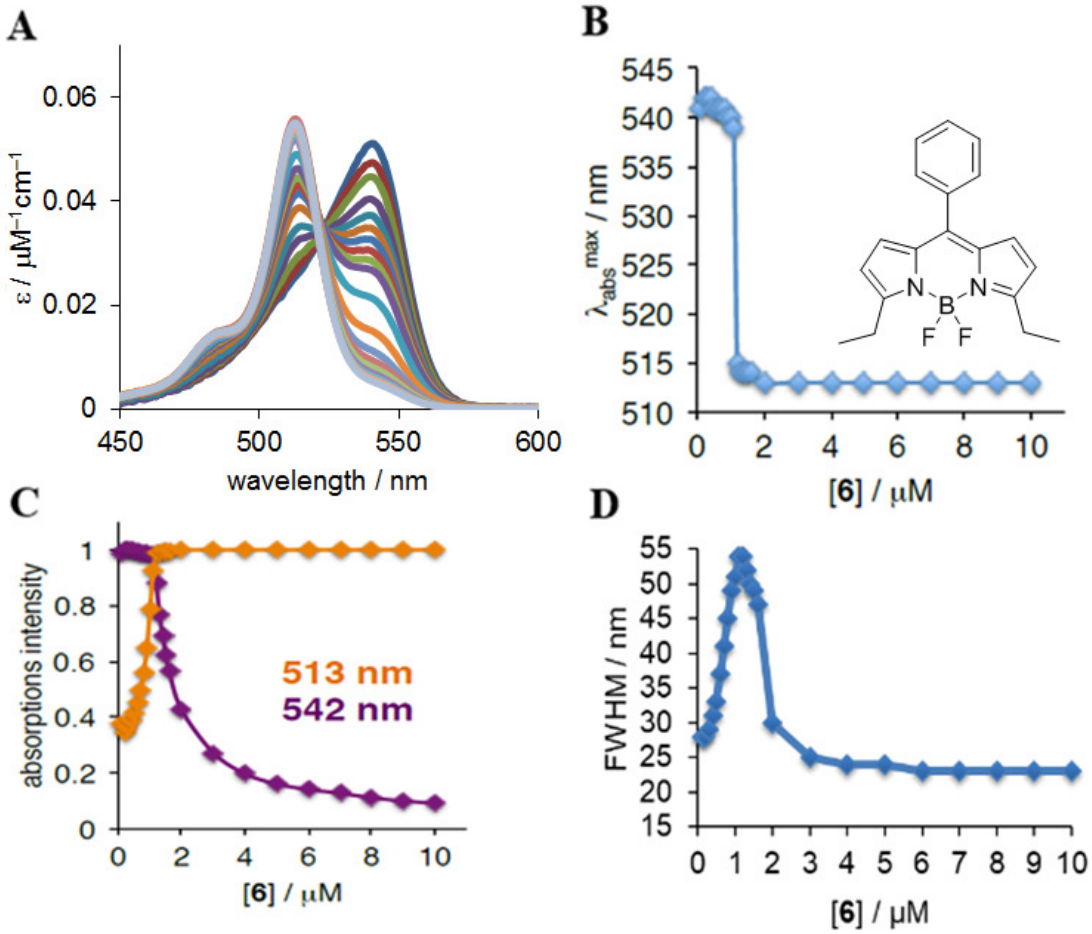

Figure 2.16 Concentration-dependent absorption characteristics of **6** in 1,2-DCE ACROS/for spectroscopy.
A: normalized UV/visible spectra of various concentrations of BODIPY **6;**
B: changes of the absorption maximum as a function of dye's concentration;
C: changes of the absorbance intensity as a function of dye's concentration at two wavelengths
D: changes of the FWHM as a function of dye's concentration.
Conditions: DMSO = 0.1-1 % v/v

The emission spectra of **6** also revealed a blue shift as the concentration of the dye increased, i.e., from 550 to 527 nm (Figure 2.17). Similar to the absorption data, a 40 nm FWHM at 0.1 μM increased to 59 nm at 1.0 μM before experiencing a decrease to 29 nm FWHM at 10 μM.

The spectral changes observed for dye **6** were found to be relatively consistent with other dyes studied here, *i.e.*, **1** – **5**. Since all dyes possess distinct structural elements, *i.e.*,

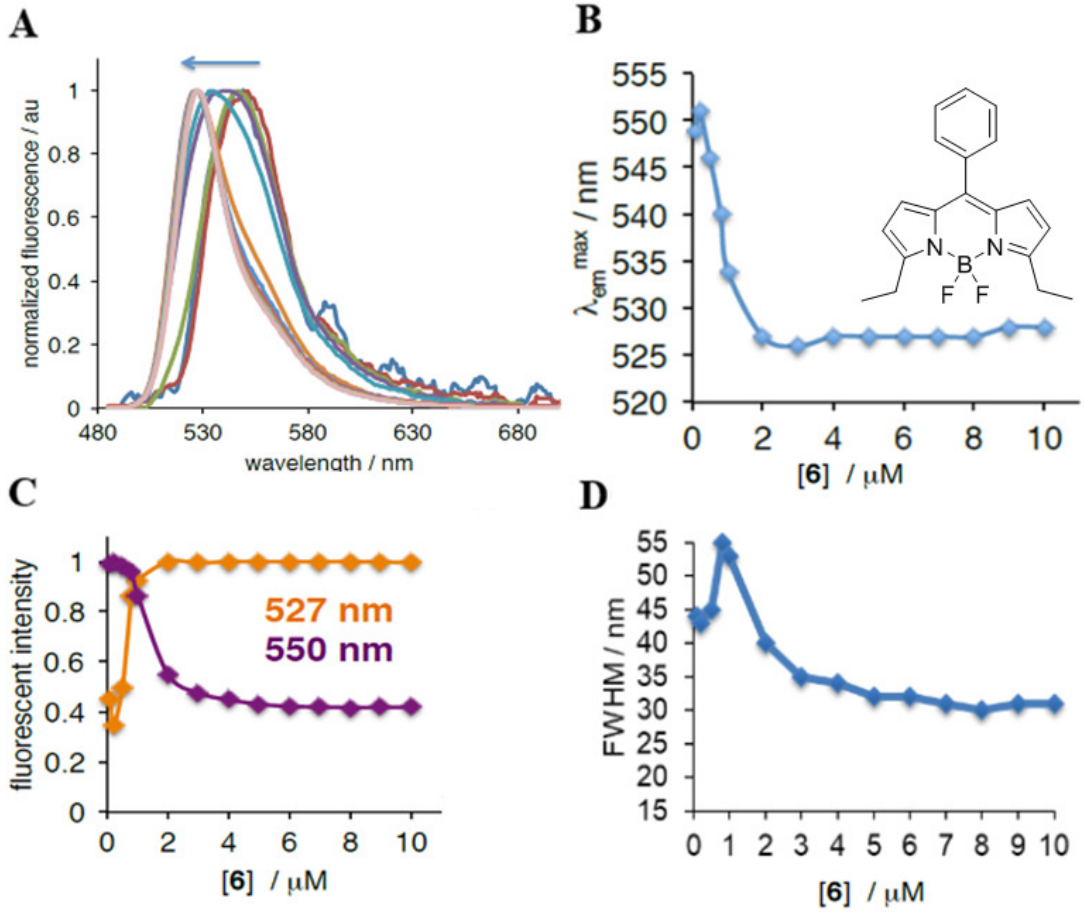

Figure 2.17 Concentration-dependent emission characteristics of **6** in 1,2-DCE ACROS/for spectroscopy
A: UV/visible spectra of BODIPY **6** in 1,2-DCE ACROS/ spectroscopy while increasing the concentration 0.1 - 10 μM
B: changes of the emission maximum as a function of dye's concentration;
C: changes of the emission intensity as a function of dye's concentration at two maxima;
D: changes of the FWHM as a function of dye's concentration
Conditions: λ_{ex} = 480 nm; DMSO = 0.1-1 % v/v

electron-donating and electron-withdrawing groups, rotors and rotors, monomeric and dimeric structures, it was plausible that a particular solvation ability and/or interaction of this chlorinated solvent with the dyes led to the formation of different aggregated species.

To further investigate solvent–BODIPY interactions, BODIPY **2** (Figure 2.18) was chosen, due to large and distinct changes in both absorption and emission characteristics. Photophysical properties of dye **2** were evaluated in a collection of chlorinated solvents, due to their relationship to 1,2-DCE (Figure 2.18). It appeared that in all chlorinated solvents, but 1,2-DCE, the absorption maxima of **2** was within 501 – 505 nm range, while in 1,2-DCE it was observed at 529 nm (Figure 2.18.A). In addition, a larger FWHM was observed in 1,2-DCE than in all other solvents, 30 nm and 18 nm, respectively. Furthermore, the emission of **2** in 1,2-DCE displayed a maximum at 542 nm with FWHM of 46 nm, while all other chlorinated solvents maxima at *ca*. 510 nm with FWHM of *ca*. 23 nm were observed (Figure 2.18.B).

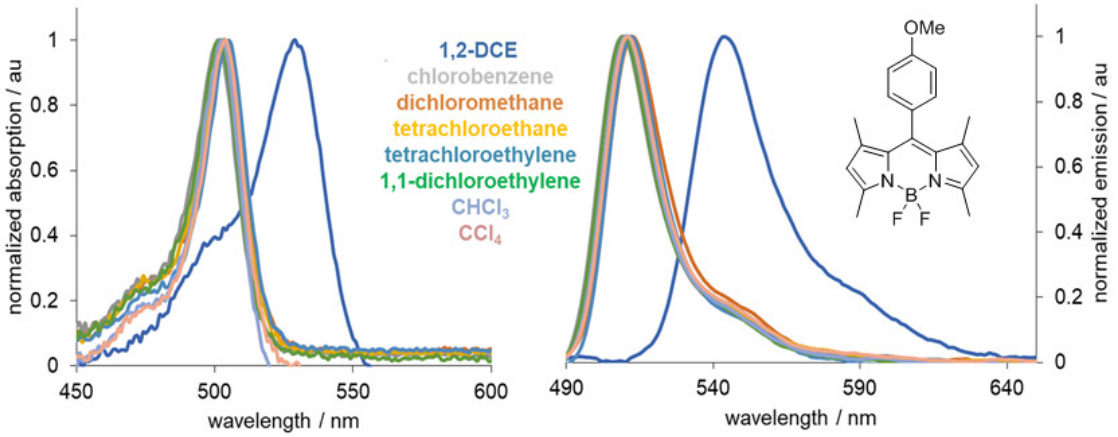

Figure 2.18 Normalized absorption (left) and emission (right) spectra of BODIPY **2** in chlorinated solvents. 1,2-DCE = 1,2-dichlroethane from ACROS/ for spectroscopy Conditions: [**2**] = 0.1 μM; λ_{ex} = 480 nm

Finally, in order to prove that the unique spectroscopic behavior of BODIPY dyes was due to the solvent rather than due to impurities that could have been introduced to the product during the manufacturing process, the photophysical properties of BODIPY **2** were investigated in a set of 1,2-DCE that were purchased from different vendors and were of different designations (Table 2.3). The results showed that in 1,2-DCE from ACROS/for spectroscopy, the absorbance and emission of BODIPY **2** were drastically different from all other 1,2-DCE samples (Figure 2.19, Table 2.3). Specifically, a 28 nm difference in the absorption maximum a 34 nm difference in the emission maximum, which were accompanied by a broadening of bands from 19 to 30 nm in absorbance and from 23 to 46 nm in emission, distinguished 1,2-DCE ACROS/for spectroscopy from all other samples of 1,2-DCE.

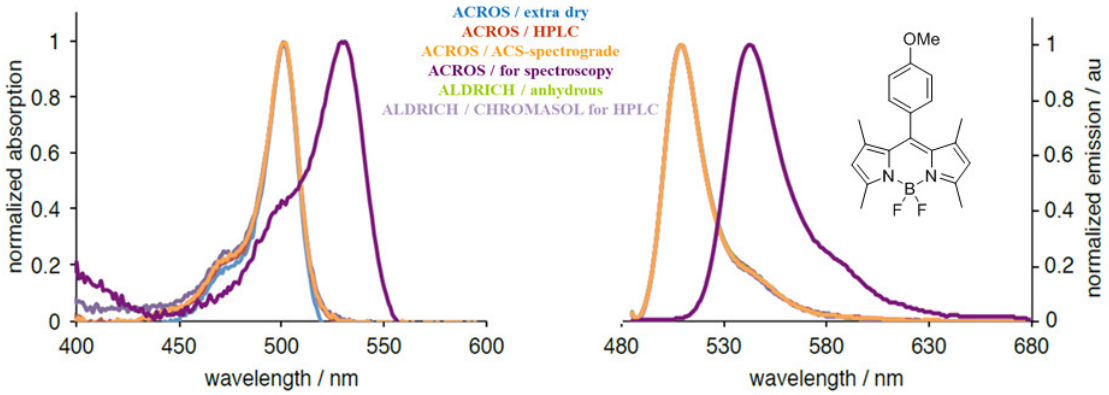

Figure 2.19 Normalized UV/visible absorbance and emission of BODIPY **2** 1,2-DCE of different grades and different vendors.
Conditions: [**2**] = 1.0 μM, λ_{ex} = 480 nm.

1,2-DCE Vendor/description	λ_{ab}^{max} / nm	λ_{em}^{max} / nm
ACROS / extra dry	501	509
ACROS / HPLC	501	509
ACROS / ACS-spectrograde	501	509
ACROS / for spectroscopy	**529**	**543**
ALDRICH / anhydrous	501	509
ALDRICH / CHROMASOL for HPLC	501	509

Table 2.3 Spectroscopic values of dye **2** in 1,2-DCE samples from various vendors grades

This study unambiguously showed that the observed unique behavior of BODIPY dyes in 1,2-DCE was not attributed to the few special properties of 1,2-DCE, but rather to an impurity. It was recognized that establishing the nature of the impurity that could cause the formation of various dye aggregates (or assemblies) might be important not only from the standpoint of spectroscopy, but also from the standpoint of supramolecular chemistry of BODIPY dyes.

Neither absorption nor emission spectroscopy showed any differences among 1,2-DCE samples. Furthermore, no significant differences among the samples were noted based on ^{1}H NMR, GC and HPLC analyses, which indicated that the potential impurity was present at a relatively small concentration and/or the chemical structure was fairly similar to 1,2-DCE that might have led to overlap with the main signals of 1,2-DCE.

Two samples, specifically 1,2-DCE ACROS/for spectroscopy and ACROS/ACS-spectrograde were subjected to gas chromatography with vacuum ultraviolet detector (GC-VUV). [136] GC-VUV is a versatile technique for highly sensitive quantitative and qualitative analysis, which overcomes the sensitivity issues of other UV-based GC techniques, which cannot distinguish among non-chromophoric species, i.e., compounds that do not absorb above 215-230 nm.[140]

It appeared that GC-VUV chromatogram of the two 1,2-DCE samples contained four common impurities in micrograms per milliliters amounts, disregarding oxygen from air and the vehicle solvent (methanol), such as water and chlorinated derivatives in comparable amounts in the two samples (Figure 2.20, Table 2.4). However, ACROS / for spectroscopy had an additional peak that was absent in ACROS / ACS-spectrograde, namely 1,1- dichloroethane, 1,1-DCE (Figure 2.20). Even though, the effect of other chlorinated solvents on spectral properties of BODIPY dyes were analyzed previously (Table 2.19), 1,1-DCE was never considered; mostly because, 1,1-DCE is not a commonly used solvent. It should be noted that it volatility (b.p. 57 ^{o}C), compared to some other chlorinated solvents. In addition, 1,1-DCE can be classified as polar aprotic, as it has a relative polarity of 0.269.[141]

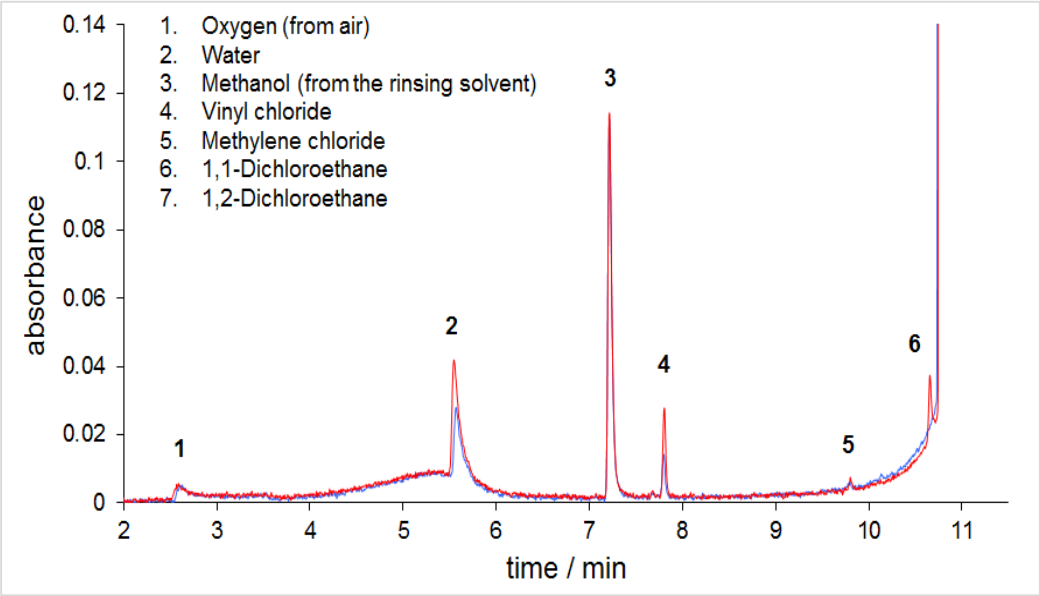

Figure 2.20 GC-VUV of 1,2-DCE ACROS/ACS-spectrograde (blue) and 1,2-DCE ACROS/for spectroscopy (red)

Impurity in 1,2-DCE	1,2-DCE / spectrograde µg/ml	1,2-DCE / ACROS µg/ml
Water (2)	192.0 ± 3.8	80.4 ± 2.9
vinyl chloride (4)	54.9 ± 1.8	19.10 ± 0.92
CH_2Cl_2 (5)	7.35 ± 0.22	6.04 ± 0.42
1,1-DCE (6)	**56.57 ± 0.78**	**-**

Table 2.4 Identity and amount of various impurities in different 1,2-DCE samples. Numbers refer to peaks in Figure 2.20

Notably, the concentration of 1,1-DCE at *ca*. 56 µg/ml corresponded to around 0.005 % (v/v). Even though this is a relatively small amount, the amount of dye 0.1 - 10.0 µM concentrations is about a thousand times smaller. Therefore, the solvation capabilities of 1,1-DCE are plausible.

Next, in order to corroborate the observed effect of 1,1-DCE on the aggregation of BODIPY dyes, photophysical properties of dye **2** were analyzed in 1,1-DCE. The stock solution of **2** was prepared in 1,1-DCE as well to avoid any interferences from other materials. It was found that the absorption maximum shifted from 527 nm to 501 nm as a function of dye's concentration (Figure 2.21). However, unlike the previous case (Figure 2.8, dye **2**), the shift took place at 12 μM concentration of the dye, which was a ten-fold higher as compared to the case when **2** was studied in 1,2-DCE ACROS/for spectroscopy, where 1,1-DCE was a minor impurity. The blue shift of the absorption spectra was also accompanied by a broadening of the band from 27 nm FWHM at 0.1 μM to 49 nm at 6 μM, while at 50 μM, FWHM was 25 nm. These changes of the absorption maxima as well as FWHM were suggestive of different assemblies being present in the ground state as a function of dye's concentration. Since no time-dependent changes were observed, and the results were reproducible, it could be assumed that the assemblies (*i.e.*, aggregates) were thermodynamically stable.

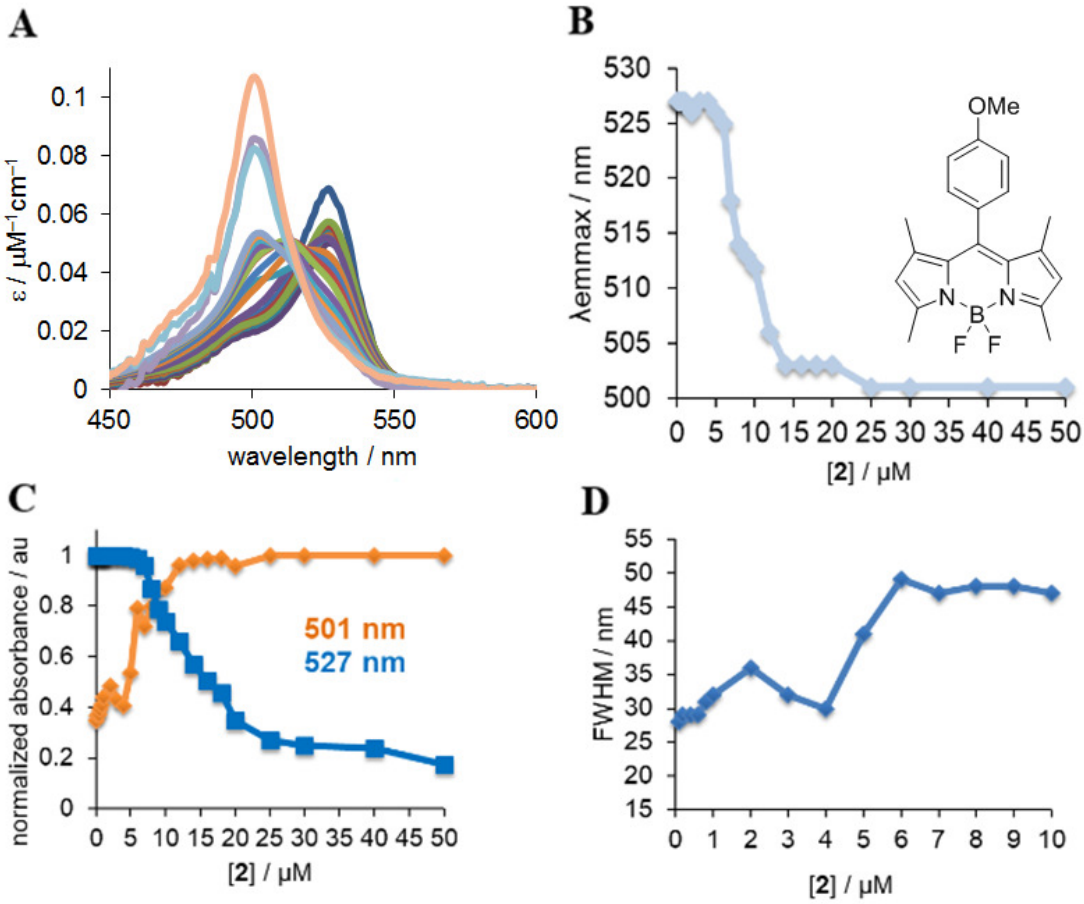

Figure 2.21 Concentration-dependent absorption characteristics of **2** in 1,1-DCE.
A: UV/visible spectra of BODIPY **2** in 1,1-DCE while increasing the concentration 0.1 - 10 μM
B: changes of the absorption maximum as a function of dye's concentration;
C: changes of the emission intensity as a function of dye's concentration at two maxima;
D: changes of the FWHM as a function of dye's concentration.

The emission profile of **2** in 1,1-DCE (Figure 2.22) appeared to be drastically different from that exhibited by **2** in 1,2-DCE with 1,1-DCE as an impurity (Figure 2.24). In this case, a single emission maximum over the range of concentrations (0.1 to 50 μM) was observed (Figure 2.22). The concentration depend changes were better illustrated by the difference emission spectra (Figure 2.22.B) which were obtained by subtracting the 50

μM spectrum from the other concentrations to show the variations on the shapes and deconvolute the signals. The shoulder at around 539 nm was increasing as a function of dye's concentration. Similarly to previous cases, bandwidth increased in the lower concentration range, reaching the maximum of 51 nm at 16 μM of **2**, and subsequently decreasing to 45 at higher concentrations.

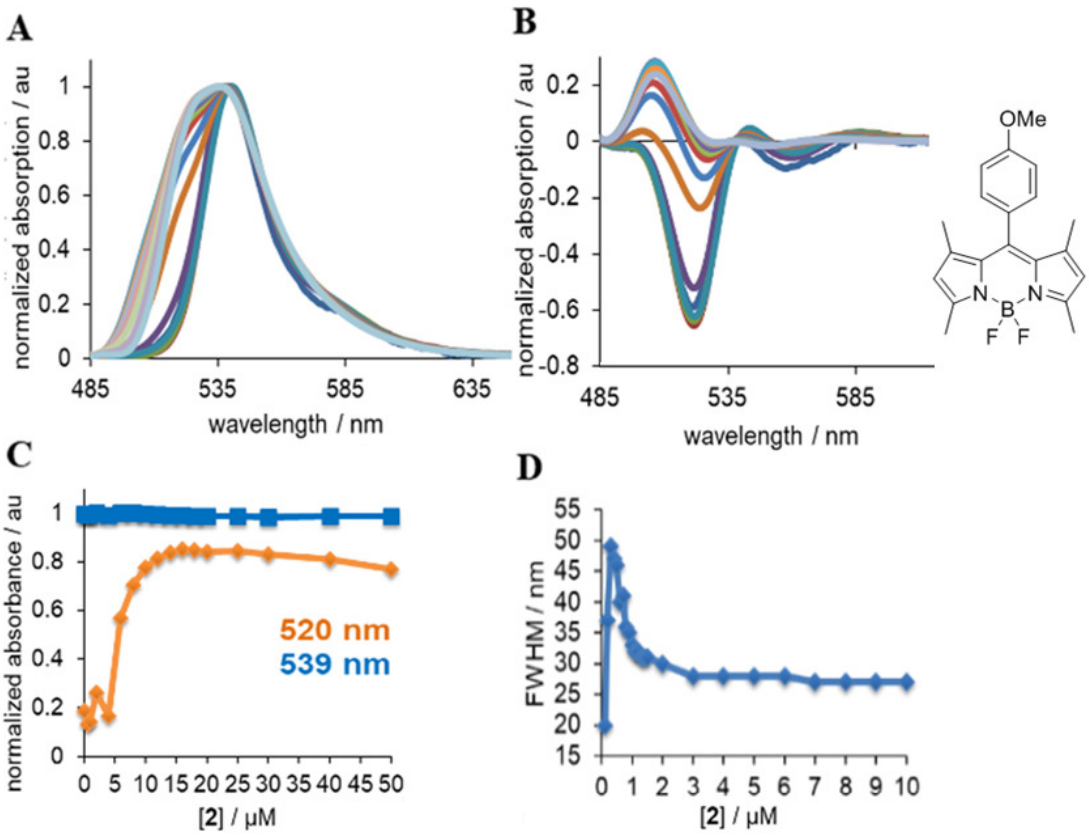

Figure 2.22 Concentration-dependent emission characteristics of **2** in 1,1-DCE
A: normalized, concentration-depend emission intensity of **2**;
B: difference concentration-dependent emission spectra;
C: changes of the emission intensity as a function of dye's concentration at two maxima, which were determined from the difference spectra, see B;
D: changes of the FWHM as a function of dye's concentration.
Conditions: λ_{ex} = 480 nm

Fluorescence lifetimes of dye **2** in 1,1-DCE indicated that no significant variations within the studied concentration range were observed (Figure 2.23). Importantly, comparison of fluorescence lifetimes of dye **2** in 1,1-DCE and two different 1,2-DCE samples (Table 2.5) revealed that at 0.1 and 1.0 μM concentrations of **2**, similar types of species were present in 1,1-DCE and 1,2-DCE ACROS/for spectroscopy (the sample that contained 1,1-DCE impurity). Notably, in 1,1-DCE a decrease of lifetime (by *ca*. 1.2 ns) was noted when the concentration of the dye increased to 10.0 μM, which was indicative of the formation of different assemblies. Based on the lifetime values, these assemblies might be somewhat comparable to those observed in 1,2-DCE ACROS/for spectroscopy. Further confirmation that 1,1-DCE was inducing distinct BODIPY assemblies came from that fact that the lifetime values of **2** in 1,2-DCE ACROS/ACS-spectrograde, which did not contain 1,1-DCE (Table 2.5), did not show any significant variations as a function of dye's the concentration, thus indicating that single types of species were present in this particular solvent.

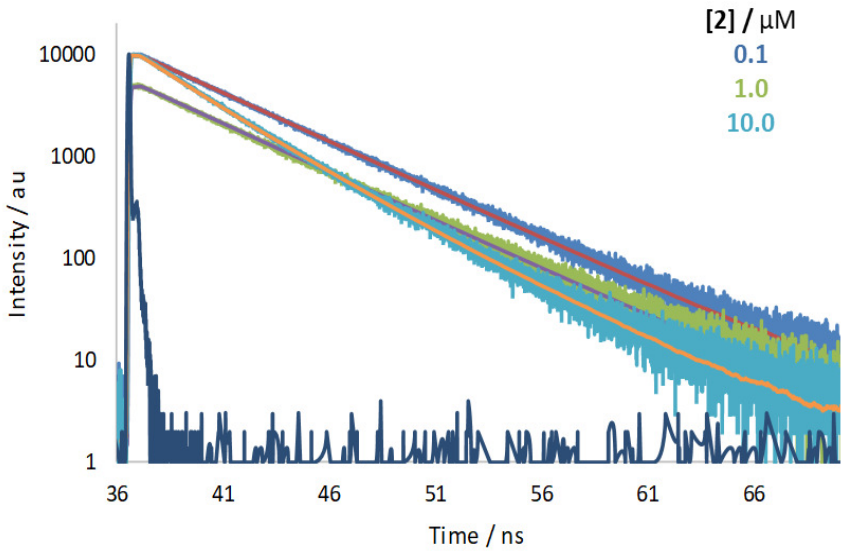

Figure 2.23 Fluorescence lifetime BODIPY **2** in 1,1-DCE

Solvent	Concentration / μM	Lifetime / ns
1,1-DCE	0.1	4.56 ± 0.02
	1.0	4.57 ± 0.02
	10.0	3.34 ± 0.03
1,2-DCE ACROS / for spectroscopy	0.1	4.15 ± 0.01
	1.0	4.12 ± 0.06
	10.0	3.45 ±0.02
1,2-DCE ACROS / ACS-spectrograde	0.1	3.12 ± 0.01
	1.0	3.10 ± 0.01
	10.0	3.19 ± 0.01

Table 2.5 Fluorescence amplitude lifetime BODIPY **2** in 1,1-DCE and 1,2-DCE

Considering that 1,1-DCE is not a common solvent (it is sold in small quantities, *i.e.*, 25 g or less), it was decided to investigate the effect of 1,1-DCE as an additive for common molecular organic solvents. After the addition of 5 % (v/v) of 1,1-DCE to a solution of ethanol and acetonitrile that contained dye **2**, a red shift of the absorption maxima was observed by 25 nm and 37 nm, respectively (Figure 2.24). On the other hand, in chloroform and dimethyl sulfoxide even after the addition of over 10 % (v/v) of 1,1-DCE, the absorption maxima wavenumber remained the same around 500 nm (Figure 2.25). Similar behavior, *i.e.*, no changes in the absorption maximum upon addition of 1,1-DCE, was observed in dichloromethane and carbon tetrachloride.

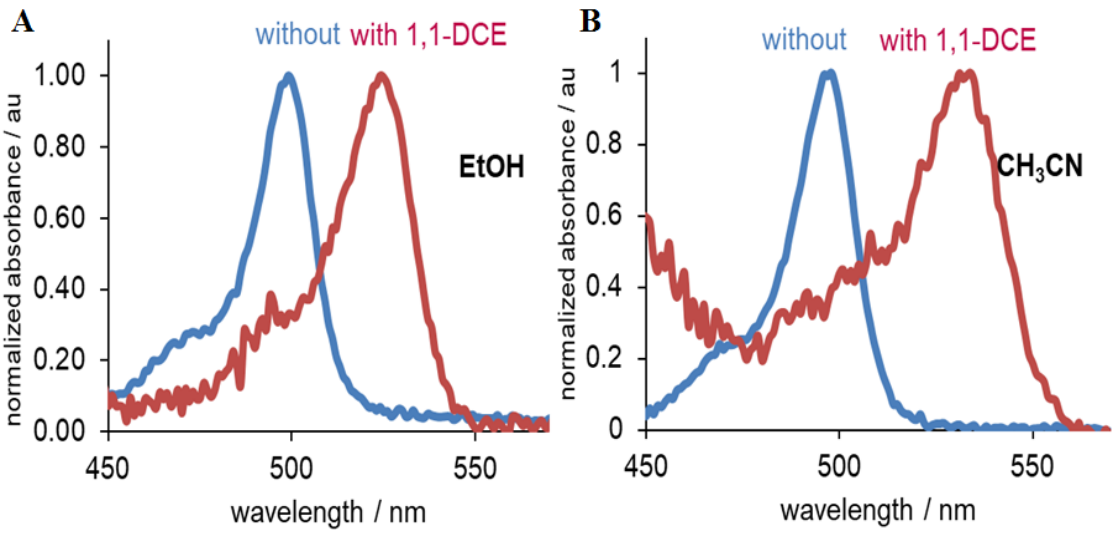

Figure 2.24 Normalized absorbance of BODIPY **2** in ethanol (A) and acetonitrile (B) in the absence (blue) and in the presence (red) of 1,1-DCE (5 % v/v).

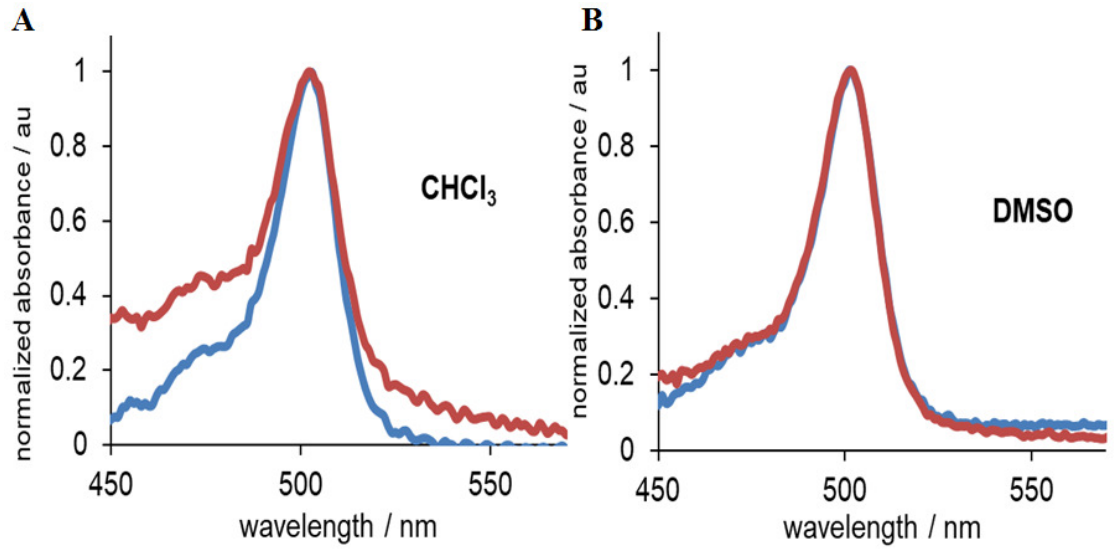

Figure 2.25 Normalized absorbance of BODIPY **2** in chloroform (A) and dimethyl sulfoxide (B) in the absence (blue trace) and in the presence (red trace) of 1,1-DCE (5 % v/v).

2.4 Conclusions

An unusual, previously unknown effect of 1,1-DCE that allows to modulate the aggregation state of BODIPY dyes has been discovered. With the aid of 1,1-DCE, for the first time, it was shown that in many organic solvents at μM concentration, BODIPY dyes exist as aggregates, rather than monomers. Furthermore, even small amounts of 1,1-DCE were able to induce a disaggregation of these aggregates and produce monomeric BODIPY species in such solvents as 1,2-DCE, ethanol and acetonitrile.

Although the exact nature of the BODIPY aggregates remains to be clarified perhaps through computational calculations, these results indicate that 1,1-DCE aid in evaluation and characterization of fluorophores and their assemblies, in general, and BODIPY-based dyes, in particular. Arguably, additive-induced disaggregation of fluorophore assemblies might constitute a viable approach towards tuning the supramolecular structures of fluorophore assemblies.

2.5. Experimental section

Materials and methods

All reagents and solvents were purchased from commercial sources (Sigma-Aldrich, Acros, Alfa, Aesar) and were used as received.

Absorbance and fluorescence measurements were performed on Agilent 8453 UV-visible and Shimadzu RF-5301PC instruments, respectively, using 1 cm quartz cells with a resolution of 1 nm. Fluorescence measurements were carried out as follows: excitation and emission width slits were 3 nm and 3 nm; intensity – high or low; samples were excited at

480 nm, and the obtained spectra were smoothed using manufacture provided software.

BODIPY dyes: all BODIPY dyes were prepared according to published procedures.[54,139]

1: ^{1}H NMR (400 MHz, $CDCl_3$): δ = 7.68 (d, *J* = 8.4 Hz, 2H), 7.53 (d, *J* = 8.4 Hz, 2H), 6.75 (d, *J* = 4.2 Hz, 2H), 6.40 (d, *J* = 4.3 Hz, 2H), 3.11 (q, *J* = 7.6 Hz, 4H), 1.38 (t, *J* = 7.6 Hz, 6H); ^{13}C NMR (100 MHz, $CDCl_3$): δ = 164.3, 141.6, 135.4, 134.1, 132.5, 130.7, 130.4, 123.6, 117.8, 81.8, 75.9, 22.3, 13.0; ^{19}F NMR (376 MHz, $CDCl_3$): δ = 145.24 (q, *J* = 32.7 Hz); HRMS (ESI; positive): $[M]^+$ *m/z* calcd for $C_{42}H_{36}B_2F_4N_4Na$ 717.2962, found 717.2954.[139]

2: ^{1}H NMR (300 MHz, $CDCl_3$) δ = 7.21 (d, *J* = 8.72, 2 H), 7.04 S6 (d, *J* = 8.72, 2 H), 5.98 (s, 2 H), 3.88 (s, 3 H), 2.56 (s, 6 H), 1.44 (s, 6 H); ^{13}C NMR (75 MHz, $CDCl_3$) δ: 160.12, 155.25, 143.20, 141.87, 131.86, 129.20, 127.02, 121.12, 114.54, 55.33, 14.59.[142]

3: ^{1}H NMR (300 MHz, $CDCl_3$): δ = 1.30 (s, 6H); 2.57 (s, 6H); 6.02 (s, 2H); 7.54 (d, *J* = 8.6 Hz, 2H); 8.41 (d, *J* = 8.6 Hz, 2H). ^{13}C NMR (75 MHz, $CDCl_3$): δ = 14.6, 121.8, 124.3, 129.6, 130.6, 138.3, 141.9, 142.5, 148.3, 156.6.[143]

4: ^{1}H NMR (400 MHz, $CDCl_3$) δ =7.77 (d, *J* =7.5, 2H), 7.46 (d, *J* = 7.5, 2H), 2.54 (s, 6H), 2.30 (q, *J* = 7.5, 4H), 1.25 (s, 6H), 0.98 (t, *J* = 7.5, 6H). ^{13}C NMR (100 MHz, $CDCl_3$) 154.6, 139.9, 138.1, 133.4, 131.5, 131.2, 130.5, 129.2, 126.14.[144]

5: ^{1}H NMR (400 MHz, $CDCl_3$) δ = 7.60 (d, *J* = 8.4 Hz, 2H), 7.46 (d, *J* = 8.4 Hz, 2H), 6.71 (d, *J* = 4.2 Hz, 2H), 6.36 (d, *J* = 4.2 Hz, 2H), 3.21 (s, 1H), 3.08 (q, *J* = 7.6 Hz, 4H), 1.34 (t, *J* = 7.6 Hz, 6H).[145]

6: ^{1}H NMR (300MHz, $CDCl_3$): δ = 7.47 (m, 5H), 6.73 (d, *J* = 4.1 Hz, 2H), 6.34 (d, *J* = 4.1 Hz, 2H), 3.08 (q, *J* = 7.6 Hz, 4H), 1.34 (t, *J* = 7.6 Hz, 6H).[146]

Stock and solution preparations for spectroscopic measurements.

1.0 mM stock solutions of BODIPY dye was prepared by dissolving a weighted amount of the dye in the appropriate solvent, followed by sonication for 30-40 sec. All stock solutions were prepared fresh and used within 24 hours. For all measurements the aliquots of the stock solutions were diluted to the appropriate solvent, thoroughly mixed and allowed to equilibrate for several minutes prior to the spectra acquisition.

CHAPTER 3: BODIPY DYES AS MOLECULAR VISCOMETERS

3.1 A triazine-based BODIPY trimer as a molecular viscometer

3.1.1 Overview

Viscosity is one of the major physical properties of various biological systems, having a major impact from microscopic up to systemic levels.[31] For biological applications, it is important to detect viscosity changes of various types of environments (*i.e.*, intracellular, intercellular, membrane, etc) using probes that provide fast response times and are not hindered neither by other components nor by other properties of the environments. Fluorescent molecular rotors fulfill these demands and provide high spatial and temporal responses.[147-149]

In general, fluorescent molecular rotors consist of two (or more) moieties that have the ability to rotate around each other. When such internal rotation is coupled to changes of the photophysical properties of the fluorophore and is dependent on the physical properties of the environment, molecular rotors could be used environmental-sensitive fluorescent probes. It is postulated that the photophysical principle of twisted intramolecular charge transfer (TICT), operates in the excited state, where the viscosity causes hindrance of the intramolecular rotation (Figure 1.5).[150,151]

Molecular rotors have been employed to measure micro-viscosity changes in a number of organic solvents as well as in biological systems. In general, a linear correlation of fluorescence lifetimes (or other photophyscial properties of the probes, such emission intensity and quantum yields) and the viscosity of the media.[152,153,57]

The fluorescence quantum yield Φ at the maximum wavelength can be related to the viscosity η in molecular rotors possessing TICT using the Forster-Hoffmann equation (1),

$$\Phi = Z\eta^{\alpha} \quad (1)$$

where α is positive constant that depends on the chromophore and Z is a constant on the interaction between the dye and the solvent. Considering that the quantum yield represents the radiative decay (κ_r) multiplied by the fluorescence lifetime (τ), equation (2) can be derived:

$$\tau = \frac{Z\eta^{\alpha}}{\kappa_r} \quad (2)$$

In this context, BODIPY dyes have shown great promise for determining the viscosity of various systems using the correlation with the corresponding fluorescence lifetimes, where the lifetime is expected to increase as the viscosity increases.[54,56,154,155]

Moreover, BODIPYs that are functionalized with groups in the *meso*-position have an activation energy for the internal rotation of the group that also have dependency on the changes of viscosity. In the case of a similar BODIPY monomer with a phenyl substituent in this position that has free rotation (dye **6** Figure 2.3) the energy was calculated as 2.6 kJ/mol, whereas the monomer with restricted rotation of the *meso*-position (or methyl groups on the side, dye **2** Figure 2.3) was determined as 7.7 kJ/mol.[156]

3.1.2 Synthesis of trimeric BODIPY dyes

In general, the preparation of BODIPY-based and other types of dyads reported in the literature features multistep synthetic routes.[154] Arguably, from the application and utility perspectives, multistep, non-modular approaches could be viewed as a limitation. To address this limitation, a homodimeric BODIPY dye **1** was prepared in two steps, with the first step being based on the mechanochemical, largely solvent-free synthesis of alkyne-containing BODIPY (Scheme 2.2). In this dye, the rotation of the two BODIPY groups around the middle moiety was shown to be sensitive to microviscosity.[139] Specifically, the potential of this dimeric rotor to act as a viscometer for molecular, ionic and cellular environments was explored. In addition, along with other literature accounts, the development and applications of the BODIPY dimer **1** also demonstrated a possibility that the extinction coefficient of the fluorogenic rotor could be enhanced by the addition of another BODIPY group.[157,158] Therefore, it was expected that a system that contains three BODIPY units would provide even a brighter dye, which would allow for utilization of smaller amounts of the probe, which in turn would assure lesser perturbations to the studies systems imposed by the addition of the probe.

In order to construct a trimer BODIPY rotor, cyanuric chloride was chosen as a scaffold, due to its well stablished and robust chemistry.[159] An approach similar to preparation of dimer **1** was chosen to make trimeric BODIPY rotor. Specifically, ethynyl-BODIPY was prepared using mechanochemical synthesis,[54] followed by metals catalyzed cross-coupling reaction that provided BODIPY rotor **7** in two synthetic steps (Scheme 3.1).[160-162]

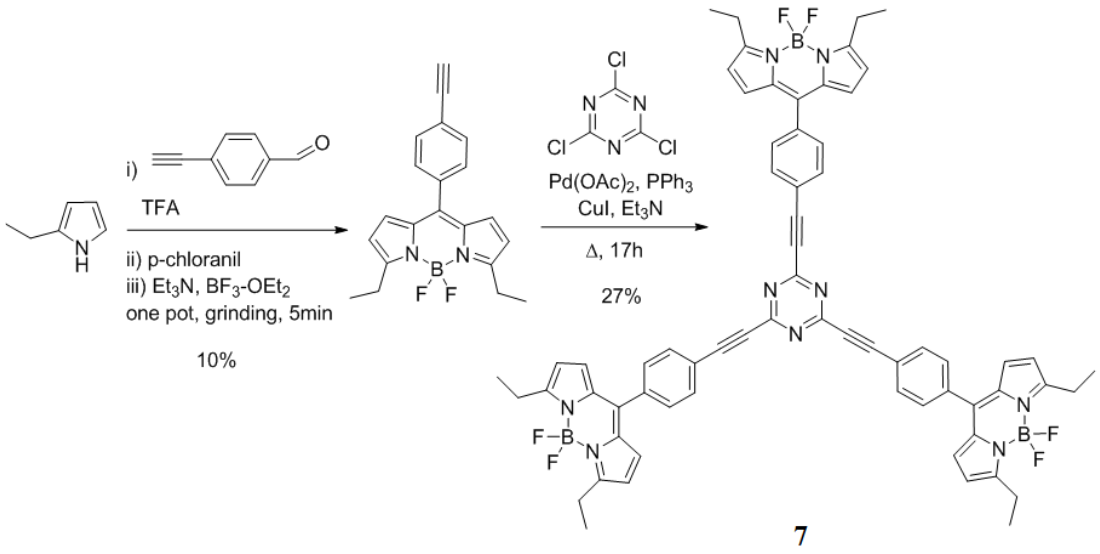

Scheme 3.1 Synthesis of BODIPY trimer **7**

Using a similar procedure, trimeric BODIPY non-rotor **8** was made (Scheme 3.2). The need for the non-rotor dye was driven by the fact that, typically in literature, no structural controls for molecular rotors are provided. In other words, the effects of viscosity on photophysical properties of molecular rotors are not backed up by the data that are obtained using probes, which do not have the rotating moieties. In this particular instance, the presence of methyl groups on the 1- and 7-positions of the BODIPY core sterically restricts the rotation of the substituent in the *meso*-position.

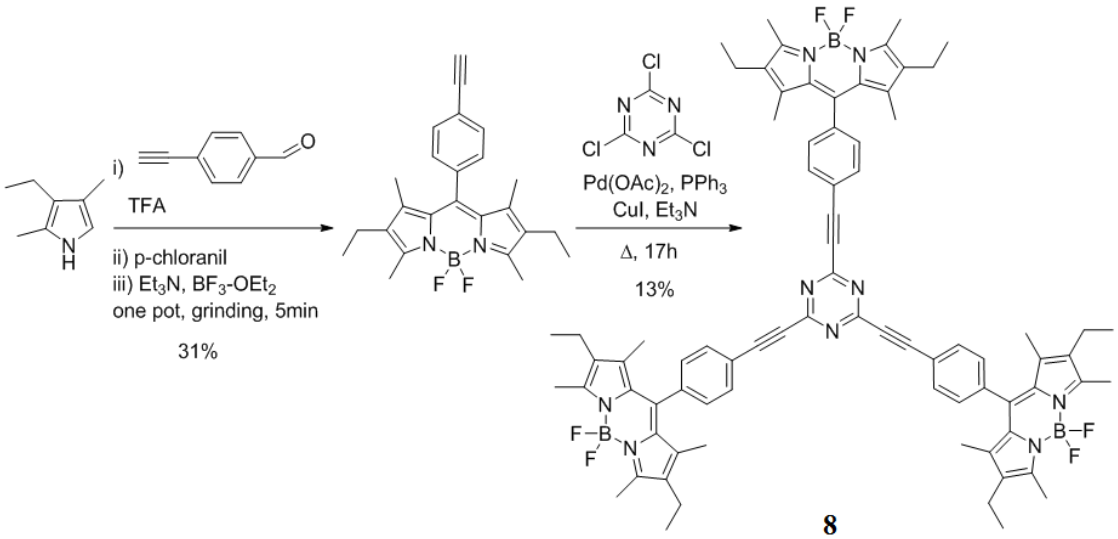

Scheme 3.2 Synthesis of BODIPY trimer **8**

3.1.3 Results

Since the goal for developing trimeric BODIPY rotors was driven by enhancement of the extinction coefficient, *i.e*., to make a brighter dye, the extinction coefficients of both rotor **7** and non-rotor **8** were determined in a range aqueous and organic solvents (Table 3.1). It should be pointed out that, monomeric BODIPY dyes have extinction coefficients in the range of 60,000-70,000 M^{-1} cm^{-1} (depending on the solvent). Thus, based on the obtained results (Table 3.1), it appeared that both trimeric BODIPY dyes **7** and **8** had the extinction coefficients that were some 3-fold larger than those observed for the monomer, and they supported that notion that incorporation of multiple BODIPY groups on a common scaffold would have an additive effect. Notably, the extinction coefficient for non-rotor **8** was larger over the range of solvent, due to the steric hindrance imposed by the methyl groups, *i.e*., restricted rotation of the substituent in the meso-position, which prevented charge transfer between the two units. Furthermore, both BODIPY trimers **7** and

8 had the lowest extinction coefficients in aqueous solution (*e.g.*, PBS buffer).

Solvent	BODIPY 7 ε / M^{-1} cm^{-1}	BODIPY 8 ε / M^{-1} cm^{-1}
ethanol	206,000	235,000
glycerol	99,000	99,000
ethanol/glycerol 90/10 (v/v)	189,000	232,000
ethanol/glycerol 50/50 (v/v)	193,000	325,000
ethanol/glycerol 10/90 (v/v)	92,000	75,000
1,2-DCE	174,000	242,000
DMSO	150,000	216,000
PBS buffer, pH 7	62,000	99,000

Table 3.1 Extinction coefficient of BODIPY **7** and **8** in organic solvents and aqueous buffer.

In order to establish that rotor **7** could be used solely as a viscometer, *i.e.,* to prove that the photophysical properties would be changing only due to changes of media's viscosity, the effect of media's polarity was tested (Figures 3.1 and 3.2). Absorption and emission spectra of trimer **7** in organic and aqueous solvents with different polarities indicated that there were no significant variations for a range of organic solvents studied, with absorption maxima centered around 515 nm (Figure 3.1). Interestingly, a broadening of the visible band of the dye in water might be attributed to aggregation of the dye, considering relatively high hydrophobicity and relatively low solubility of **7** in water. The

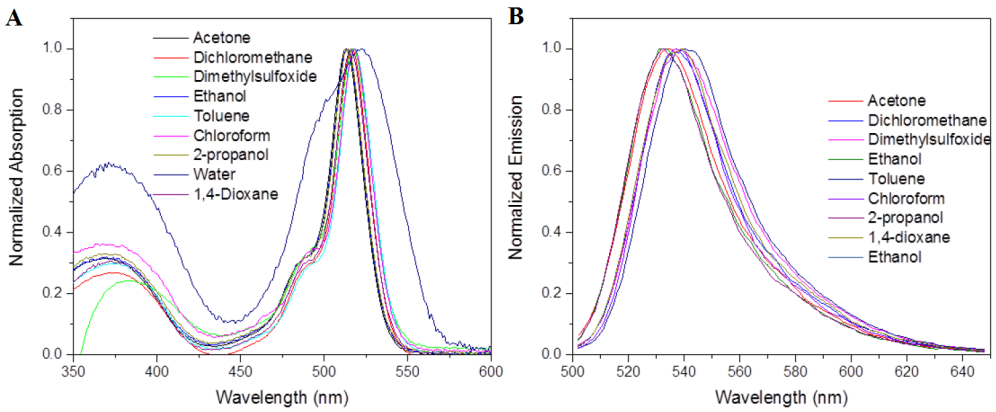

Figure 3.1 Normalized absorbance (A) and normalized emission (B) spectra of BODIPY trimer **7**; taken from ref: 145
Conditions: [**7**] = 0.5 μM, λ_{ex} = 480 nm; DMSO = 1 % v/v

emission of **7** in organic solvents exhibited a single peak, with the emission maxima in the range between 528 and 539 nm. It should be pointed out that the stock solution of trimer **7** in DMSO was made (at 1 mM concentration), and it was diluted to various solvents to the specified final concentration. Thus, all studied solutions contained small amounts of DMSO (*i.e.*, ca. 1 % v/v), but this amount is considered small enough to cause any changes to the spectral properties of the dyes. Importantly, this is a common practice reported in a number of literature accounts.

Similar characteristics and trends were observed for the non-rotor **8**: absorption maxima were centered around 525 nm, and a broader transition noted for the absorbance in water, whereas the emission maximum was found to be centered around 540 nm (Figure 3.2).

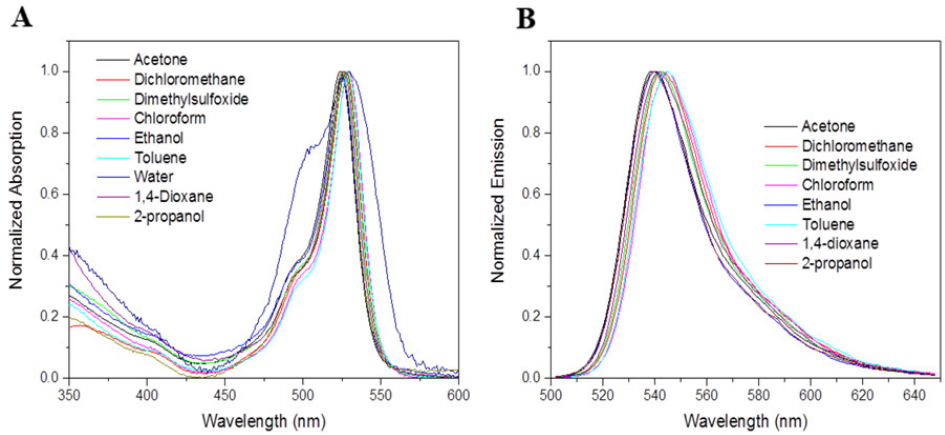

Figure 3.2 Normalized absorbance (left) and normalized emission (right) spectra of BODIPY trimer **8**; taken from ref: 145
Conditions: [**8**] = 0.5 μM, λ_{ex} = 480 nm; [DMSO] = 1 % v/v

Next, the effect of media's viscosity on the steady-state fluorescence intensity of rotor **7** was tested using standard ethanol / glycerol mixtures. It was determined that as the viscosity was continuously varied from ethanol (η = 1.2 cP) to glycerol (η = 1457 cP) both the emission intensity and the quantum yield of the fluorophore **7** increased (Figure 3.3)

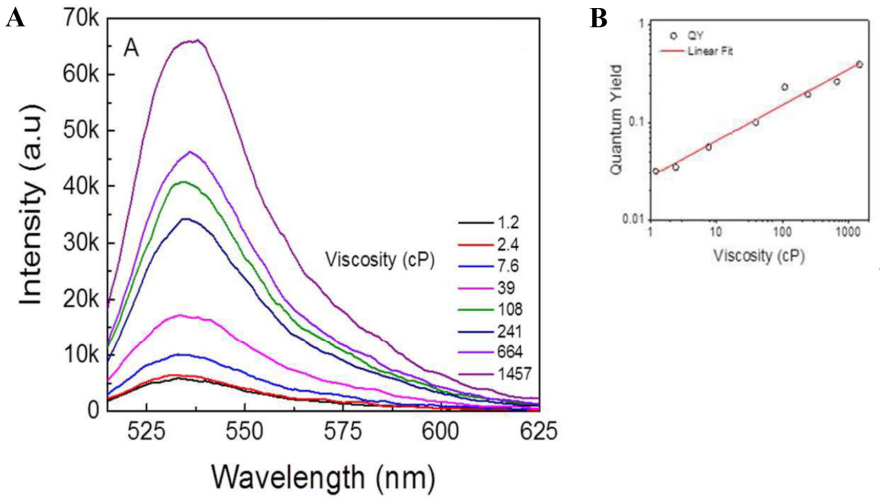

Figure 3.3 Emission spectra of BODIPY rotor **7** in media of different viscosities (A); Effect of viscosity on the quantum yield of **7** (B); taken from ref: 145

It is known that both emission intensity and quantum yields could be influenced by a number of factors, such as dyes' concentration, for example.[145] Thus, other photophysical characteristics of the fluorophores should be considered as well, when establishing their ability to act as environment-sensitive probes. Fluorescence lifetime decays are known to be independent on the fluorophore's concentration of the dye but are sensitive to the microenvironment around the dye. Thus, fluorescent lifetimes for rotor **7** were measured in solutions of various viscosities that comprised a range of some 1,500 cP units (Figure 3.4) The decays became slower as the viscosity of the environment increased: from *ca*. 180 ps observed in ethanol to 3245 ps observed in more viscous glycerol. Arguably, the rotation in the excited state, became restricted as the viscosity of the media increased.

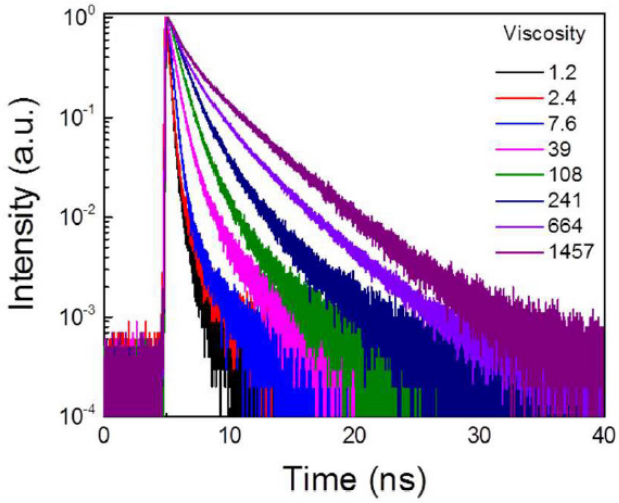

Figure 3.4 Fluorescence lifetimes of BODIPY trimer **7** in media of various viscosities; taken from ref: 145

Importantly, the non-rotor **8** showed no significant increase of the fluorescence lifetimes as the viscosity was variations over the same 1.2 to 1457 cP range (Figure 3.5). Specifically, lifetime of 3.44 ns was noted in ethanol, while 4.97 ns lifetime was recorded in glycerol. Thus, it appeared that BODIPY trimer **7** could act as a molecular viscometer.

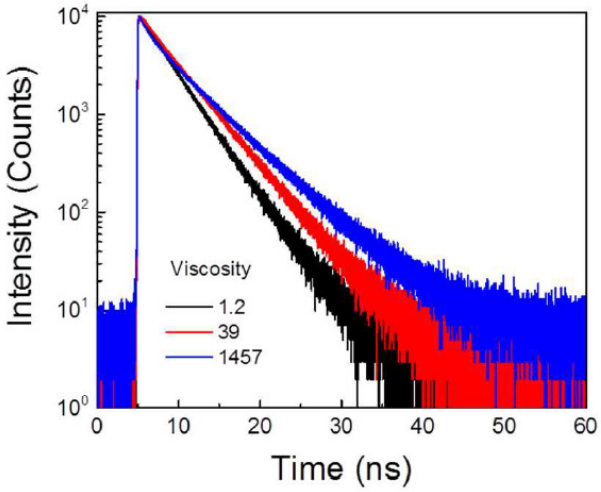

Figure 3.5 Fluorescent lifetimes of BODIPY non-rotor **8** in media of different viscosities; taken from ref: 145

To gain further proof that the internal rotation within trimer **7** was indeed controlled by the viscosity, the obtained set of data (Figure 3.4) was evaluated using the Foster-Hoffmann equation (3).[163] Within this approach, the rotor-like behavior is determined when the linear correlation between photophysical property of a fluorophore and the physical property of the media (such as viscosity) is obtained, and the slope is larger than 0.1; and ideal molecular rotor has the slope of 0.66.[163]

$$ln\,(\tau) = ln\left(\frac{Z}{\kappa_r}\right) + \alpha ln\,(\eta) \qquad (3)$$

In the case of rotor **7**, the slope was measured to be 0.44 (Figure 3.6), which was in a good agreement with both theoretical estimation and literature results, which typically show the slope of the correlation in the range of 0.2 to 1.4. In addition, a decrease on the non-radiative decay as a function of the viscosity, which was also expected for molecular rotors, due to decreasing the TICT of non-emissive relaxation was observed, while no variation of the radiative decay was detected, which is the expected behavior for molecular rotors where the no-radiative decay is affected by the viscosity of the environment (Figure 3.6).[31]

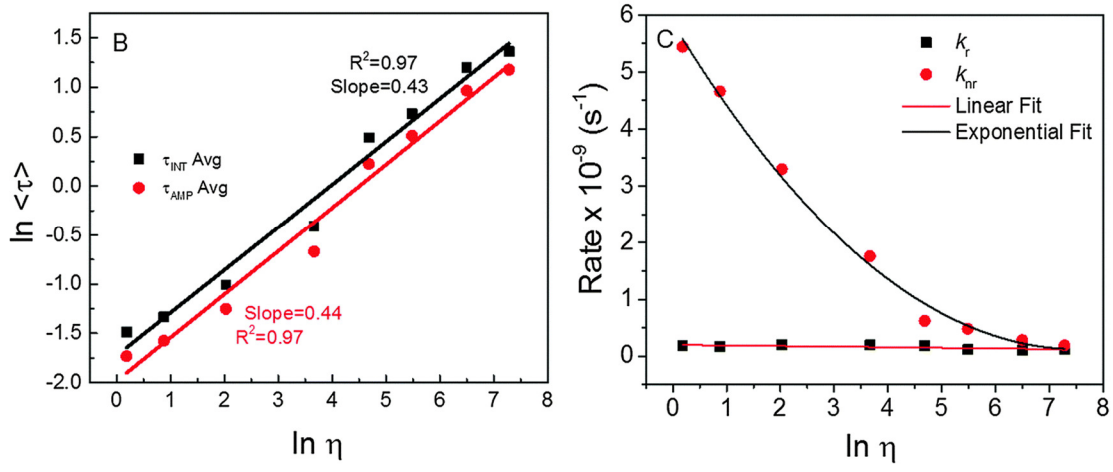

Figure 3.6 Fluorescence lifetime (A) and radiative/non-radiative decays (B) of BODIPY-rotor trimer **7** as a function of media viscosities; taken from ref: 145

In addition, the effect of solvent polarity on the fluorescence lifetimes of both rotor **7** and non-rotor **8** in several organic solvents was evaluated, and the results indicated that no significant changes in the lifetimes were noted over a range of polarities (Table 3.2). It should be pointed out, however, that a ten-fold difference in fluorescence lifetime values was observed between non-rotor and rotor trimers.

Solvent	**BODIPY 7 Lifetime / ns**	**BODIPY 8 Lifetime / ns**
1,4-dioxane	0.27	3.70
2-propanol	0.24	3.40
chloroform	0.27	3.50
ethanol	0.19	3.50
toluene	0.30	3.30
DCM	0.21	3.40
acetone	0.14	2.95
DMSO	0.23	3.20

Table 3.2 Fluorescence lifetime amplitude of BODIPY dyes **7** and **8** in organic solvents of various polarities.

In addition, the chromophores were studied in several types of confined environments, including lipid vesicles made of 1,2-dimyristoyl-sn-glycero-3-phosphocholine (DMPC) (Figure 3.7). Notably, DMPC vesicles exhibit a bilayer structure that is relevant and similar to biological membrane environments.

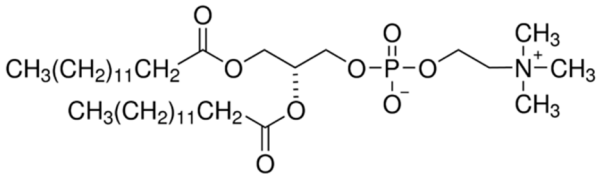

Figure 3.7 Chemical structure of DMPC.

The fluorescence lifetime of rotor **7** in DMPC decreased as a function of temperature from 15 ˚C to 30 ˚C (Figure 3.8). Arguably, with increasing temperature, the amount of rotor encapsulated in DMPC decreases. In other words, in more restricted environments the rotor showed a longer (about two-fold increase) lifetime. These results were in accord with viscosity measurements, where an increase in the lifetimes was correlated to viscosity. Using **7**'s lifetimes, the viscosity of the vesicles was estimated to change from 60 cP to 270 cP as the temperature decreased. Notably, similar measurements, which were conducted with the non-rotor **8**, demonstrated that the lifetimes remained largely unchanged over the same range of temperature. Overall, similarly to rotor **1**,

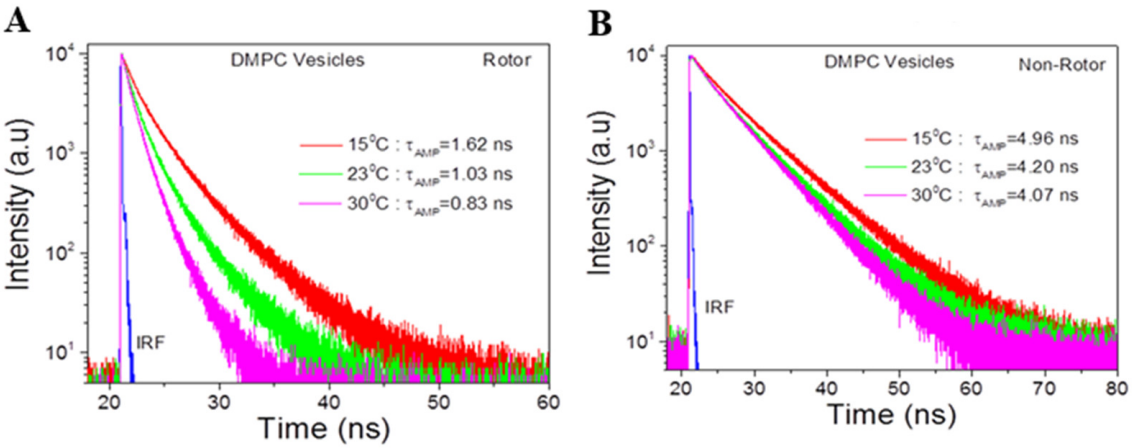

Figure 3.8 Fluorescence lifetime intensity of BODIPY **7** (A) and **8** (B) in DMPC vesicles; taken from ref: 145

trimeric rotor **7** appeared to be a promising molecular probe for various biologically relevant environments.

To further demonstrate that **7** could be used in biological types of settings, the photophysical behavior of BODIPY rotor **7** was investigated using cellular lines of adenocarcinoma of the lung (Calu-3) and prostate cancer (DU145) using fluorescence lifetime image microscopy (FLIM) (Figure 3.9). The distribution of the dye appeared to concentrate in the cytoplasm of the cells in a punctuate manner. The fluorophore also appeared to accumulate more in the hydrophobic pockets of the cells, which is consistent with the somewhat lipophilic nature of this BODIPY rotor **7**. Overall, imaging of cancer cells with good to moderate signal-to-noise ratio was achieved by using rotor **7**.

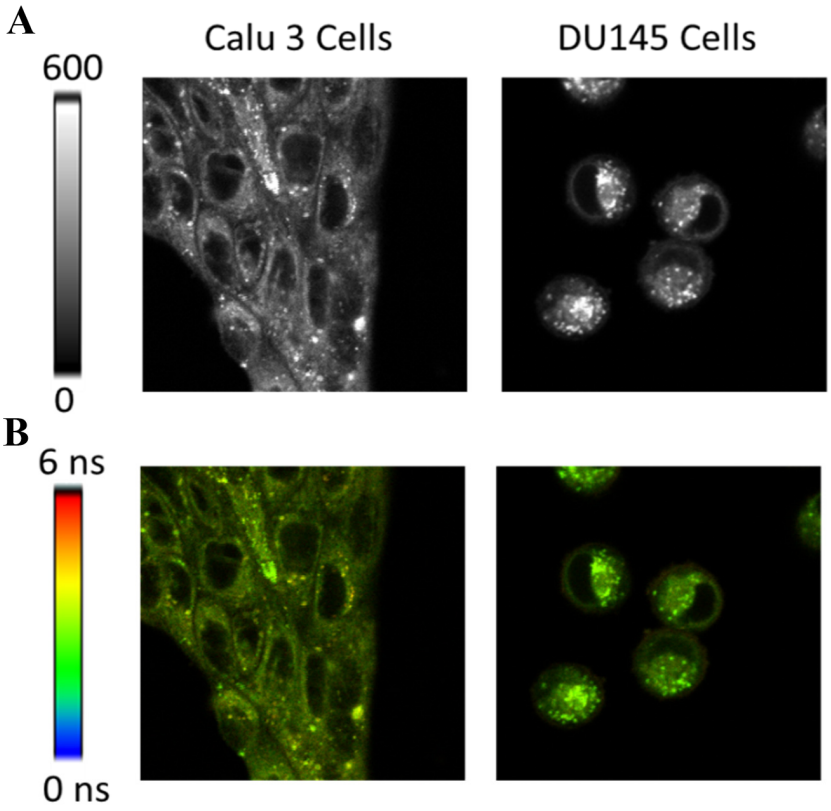

Figure 3.9 Bright field microscopy of BODIPY **7** in cells (A); fluorescence lifetime imaging microscopy (FLIM) of BODIPY **7** (B). Taken from ref: 145

In addition, the ability of rotor **7** to interact with common, ubiquitous proteins was investigated (Figure 3.10). The results illustrated the notion that rotor **7** appeared to interact with albumins, specifically human serum albumin (HSA) and bovine serum albumin (BSA). On the other hand, the fluorescent lifetime of **7** in the presence of lysozyme were drastically different from those observed in the case of albumin and was virtually the same as that exhibited by **7** in solution that was free from any proteins (Figure 3.10).

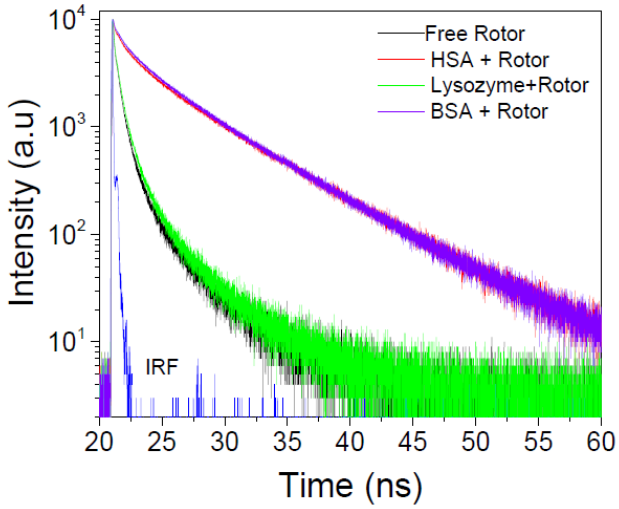

Figure 3.10 Fluorescence lifetime of BODIPY **7** in presence of proteins. Taken from ref: 145

3.1.4 Conclusions

BODIPY trimers were prepared by assembling three BODIPY moieties onto triazine core. Modular synthetic procedure allowed to obtain both rotor and non-rotor dyes. Rotor **7** was shown to be a viable probe for assessing micro-viscosity of the various types of media, whereas non-rotor **8** unambiguously demonstrated that the observed

photophysical changes were strictly due to viscosity variations. Moreover, some biological studies revealed the capability of **7** to distinctly interact with several abundant biomacromolecules, such as albumins and lysozyme, which might be useful protein sensing applications.

3.1.5. Experimental section

All chemicals and solvents were from commercial sources (Aldrich, Acros, TCI America), they were of highest grade possible and were used as received. ^{1}H, ^{13}C, ^{11}B and ^{19}F NMR spectra were recorded on a Bruker (400 MHz) spectrometer; the chemical shifts are reported in ppm (δ) downfield from tetramethylsilane in $CDCl_3$.

Synthesis of dye **7**:

In a hood behind the protecting shield, 2-ethylpyrrole (2.0 ml, 19.53 mmol) and 4-ethynylbenzaldehyde (1.14 g, 8.76 mmol) were mixed in a mortar with a pestle to form a suspension. Trifluoroacetic acid (TFA; 4-5 drops) was slowly added while grinding, which resulted in an almost instantaneous formation of a brown sticky paste. CH_2Cl_2 (*ca*. 2 ml) was added, followed by grinding to obtain homogeneous mixture. Next, p-chloranil (2.37g, 9.64 mmol) was added and grinded followed until deep red paste was obtained. Subsequently, Et_3N (10 ml, 71.65 mmol) was added, until the color of the mixture turned into a green/brown paste. Next, BF_3-OEt_2 (10 ml, 81 mmol) was added and grinded until a red metallic paste was formed. The resulting mixture was transferred into the separatory funnel with 400 ml of CH_2Cl_2 and carefully (without vigorous shaking, to avoid producing

stable emulsion) washed with saturated K_2CO_3 solution (200 ml x 2) followed by brine (200 ml x 2). Volatiles were removed *in vacuo*, and the residue was purified by column chromatography (SiO_2/$CHCl_3$) to yield dye **5** (0.328 g, 11 %) as a red solid. A screwcap vial containing a stirring bar was subsequently charged with alkyne BODIPY (4.5 eq, 20 mg, 57 µmol), cyanuric chloride (2.3 mg, 12.7 µmol), CuI (4.8 mg, 1.28 µmol), $Pd(OAc)_2$ (1.2 mg, 1.28 µmol), PPh_3 (2.0 mg, 6.38 µmol), and Et_3N (0.2 ml), capped and stirred under reflux for 17 hours. After cooling to room temperature, the mixture was quenched with HCl (1M, 20 ml) and extracted with CH_2Cl_2 (20 ml x 2). Organic fractions were combined, rotovaped, and the crude material was purified by column chromatography ($CHCl_3$/hexanes – 3/1 (v/v)) to obtain the triad **7** (0.0076 g, 26 % yield) as a red solid.

^{1}H NMR (400 MHz, $CDCl_3$) δ = 7.66 (d, *J* = 8.5 Hz, 6H), 7.50 (d, *J* = 8.4 Hz, 6H), 6.73 (d, *J* = 4.2 Hz, 6H), 6.37 (d, *J* = 4.2 Hz, 6H), 3.09 (q, *J* = 7.6 Hz, 12H), 1.35 (t, *J* = 7.6 Hz, 18H). ^{13}C NMR (100 MHz, $CDCl_3$) δ = 164.2, 141.5, 135.4, 134.1, 132.4, 130.7, 130.33, 123.5, 117.7, 81.7, 77.4, 75.8, 22.2, 12.9. ^{19}F NMR (376 MHz, $CDCl_3$) δ = –145.23 (q, *J* = 33 Hz). ^{11}B NMR (128 MHz, $CDCl_3$) δ = 0.97 (t, *J* = 33 Hz).

Synthesis of dye **8**:

In a hood behind a protective shield, 3-ethyl-2,4-dimethyl-1H-pyrrole (2.2 ml, 16.23 mmol) and 4-ethynylbenzaldehyde (0.93 g, 7.13 mmol) were grinded with a pestle to obtain a suspension. TFA (3-5 drops) was slowly added which results in an almost instantaneous formation of a brown sticky mixture. CH_2Cl_2 (*ca*. 2 ml) was added, followed by grinding to obtain homogeneous mixture. Next, p-chloranil (1.91 g, 7.76 mmol) was added while grinding to obtain a dark red paste. Subsequent addition of Et_3N (10 ml, 71.65 mmol) while

grinding produced a green/brown mixture, to which BF_3-OEt_2 (10 ml, 81 mmol) was added dropwise under grinding to produce a metallic red paste. The mixture was transferred into a separatory funnel using CH_2Cl_2 (500 ml) and carefully (without vigorous shaking, which produces stable emulsion) washed with saturated K_2CO_3 solution (200 ml x 2), followed by brined (200 ml x 2). Volatiles were removed *in vacuo* and the residue was purified by column chromatography (silica gel / $CHCl_3$) to obtain dye non-rotor monomer (0.885 g, 31 %) as a dark red solid.

A screwcap vial was sequentially charged with a stirring bar, alkyne BODIPY non-rotor monomer (50 mg, 124 mol), Et_3N (0.25 ml) cyanuric chloride (5.0 mg, 27 µmol), CuI (1.6 mg, 8.2 µmol), $Pd(OAc)_2$ (1.8 mg, 8.2 µmol) and PPh_3 (4.3 mg, 16.5 µmol). The vial was capped and stirred under reflux for 17 h. After cooling to room temperature, the mixture was diluted with CH_2Cl_2 (20 ml), washed with HCl (1M, 20 ml x 2), and the volatiles removed *in vacuo*. The residue was subjected to column chromatography (silica gel, $CHCl_3$) to obtain triad **8** (4.6 mg, 13 % yield) as a red solid.

^{1}H NMR (400 MHz, $CDCl_3$) δ =7.67 (d, *J* = 8.5 Hz, 6H), 7.31 (d, *J* = 8.5 Hz, 6H), 2.54 (s, 6H), 2.31 (q, *J* = 7.5 Hz, 12H), 1.32 (s, 18H), 0.99 (t, *J* = 7.5 Hz, 18H).

^{13}C NMR (100 MHz, $CDCl_3$) δ =154.4, 138.9, 138.2, 137.2, 133.3, 133.2, 130.6, 128.9, 122.4, 81.7, 77.4, 75.0, 17.2, 14.8, 12.7, 12.1. ^{19}F NMR (376 MHz, $CDCl_3$) δ =–145.8 (q, *J* = 33 Hz). ^{11}B NMR (128 MHz, $CDCl_3$) δ =0.78 (t, *J* = 33 Hz).

Spectroscopic Measurements

UV-Vis absorption and fluorescence spectra were obtained using a Cary 50 bio UV–visible spectrophotometer (Varian) and Cary Eclipse spectrofluorometer (Varian), respectively.

All measurements were conducted using quartz 0.4 x 1cm cuvettes at room temperature with optical density below 0.05, unless mentioned otherwise. In order to measure the quantum yield, absorption spectra of the BODIPY trimers were collected followed by measuring the integrated fluorescence intensity of the sample. A solution of rhodamine B in ethanol was used as a reference (quantum yield: 0.7).

Preparation of Lipid Vesicles

Lipid unilamellar vesicles were prepared using 1,2-dimyristoyl-sn-glycero-3-phosphocholine (DMPC). Briefly, appropriate amount of lipid stock (725 μL of 1.4 mM $CHCl_3$ stock) and BODIPY trimers (10 μL of 100 μM DMSO stock) were mixed (lipid:dye ratio was *ca*. 1000:1) in glass bottles. The solvents were evaporated under moisture -free nitrogen stream and left overnight to remove any traces of organic solvents. Next, 1 mL of PBS buffer (pH 7.4) was added, followed by sonication at about 40 ^{o}C for 10 min to obtain multilamellar vesicles. In order to obtain unilamellar vesicles, these mutlilamellar vesicles were passed through 100 μm and 0.02 μm membrane filters attached to syringe filter in a cascade manner once to obtain unilamellar vesicles.

Fluorescence Microscopy and FLIM

Calu 3 (human epithelial lung cancer cells) and DU145 (human epithelial prostate cancer cells) cancer cell lines were obtained from the American Type Culture Collection (ATCC), Manassas, VA (USA) and were grown to 70 % confluence in RPMI supplemented with 10% FBS and 1% Pen-Strep. Cells were trypsinized using 0.25 % Trypsin EDTA and seeded on 20 mm round glass-bottom petri dishes. After 24 hours, the cells were stained

with 500 nM solution of BODIPY trimer in DMSO for 20 min at 37 ^{o}C (10 μL DMSO in 1 mL of cell media). Next, the media was washed 3 times using PBS and fresh PBS was added followed by FLIM imaging on Olympus IX7 microscope. Laser excitation was provided by a pulsed laser diode (PDL-470) emitting 470 nm light and driven by a PDL 828 "Sepia II" driver (operated at 20 MHz).

Measurements were performed on a MicroTime 200 time-resolved, confocal microscope (PicoQuant). The excitation and emission light were focused by a 60X 1.2 NA Olympus objective in an Olympus IX71 microscope, and the emission light was filtered by a 488 long wave pass filter before passing through a 50 μm pinhole. The detection was achieved by a hybrid photomultiplier assembly. The resolution of the time correlated single photon counting (TCSPC) module was set to 4 ps/bin in order to facilitate the detection at highest possible resolution. All data analysis was performed using the SymPhoTime software, version 5.3.2. All experimental equipment and the SymPhoTime software were provided by PicoQuant, GmbH as part of the MicroTime 200 system.

3.2 BODIPY-rotor for imaging viscosity of intragranular mucin matrix in cystic fibrosis cells

3.2.1 Overview of cystic fibrosis

Cystic fibrosis (CF) is a disease characterized by overproduction of mucus, which leads to airways obstruction, infections, pancreatic malabsorption and ultimately death.[164] However, in addition to their pathological role, mucus secretions have important physiological functions, since they possess protective and lubricant properties, by covering epithelial surfaces throughout the body. Mucin is a viscous glycoprotein, and it is the most abundant macromolecule in mucus cells. This protein is known to undergo many conformational changes due to covalent or non-covalent interactions, and it have shown high propensity for aggregation, polymerization, sol-to-gel transition.[165] In addition, the exact viscosity of neither mucus nor mucin are known. Although viscosity of mucus was measured upon secretion, the values range from 50 cP to 10,000 cP. This is not surprising, given a great diversity of conditions for the viscosity determination.[166] In regard to intracellular, *i.e*., intragranular, viscosity of mucin (mucus), there are no methods that allow assessing it without destroying the mucin granules. Due to the lack of suitable non-invasive methods to determine viscosity of mucin, it is not possible to even speculate on how rheological properties of mucin might be related to the disease.

As shown previously, the determination of microviscosity in biological environment could be done with good spatial and temporal resolution using small-molecule rotors, including those based on BODIPY core.[60,167-170] Yet, until this account the study of micro-viscosity of mucin in mucus cells of CF was not reported.

3.2.2 BODIPY rotors and mucin granules

In order to investigate intragranular viscosity of mucin, cells from CF and non-CF patients were collected by the researchers at the University of Montreal (the group of Professor Ryszard Grygorczyk).[146] The ability of BODIPY rotors to act as viable probes for various types of media, including the cellular environments (Figure 3.11, dimer **1** and trimer **7**).[145,54] In addition, monomeric BODIPY **6** (Figure 3.11.C) was also considered.

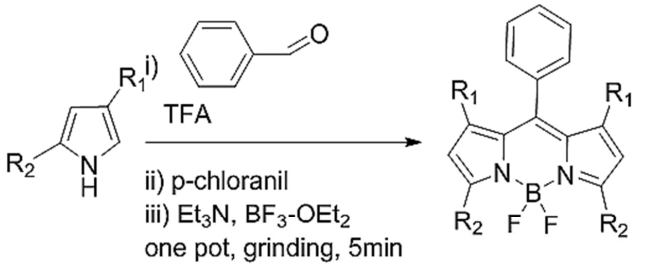

R_1= H, R_2=Et
6 (rotor)

R_1= R_2=Me
9 (non-rotor)

Scheme 3.3 Synthesis of BODIPY rotor **6** and non-rotor **9**

3.2.3 Results

Based on previous successful utilization of BODIPY rotors **1** and **7** for viscosity determination of cell cultures, the initial investigation of viscosity distributions of airways epithelial cells was performed using these dyes (Figure 3.9). Regretfully, inability of rotor **1** to report on the viscosity of CF cell was noted (Figure 3.9.A). Although somewhat more promising (a relatively moderate image of the system), FLIM imaging of rotor **7** (Figure

3.9.B) indicated that the changes of the fluorescent lifetimes were too small for this rotor to serve as a meaningful probe. Unexpectedly, the simple BODIPY rotor **6** gave the highest variation of lifetimes that span over a range of several ns (Figure 3.11.C).

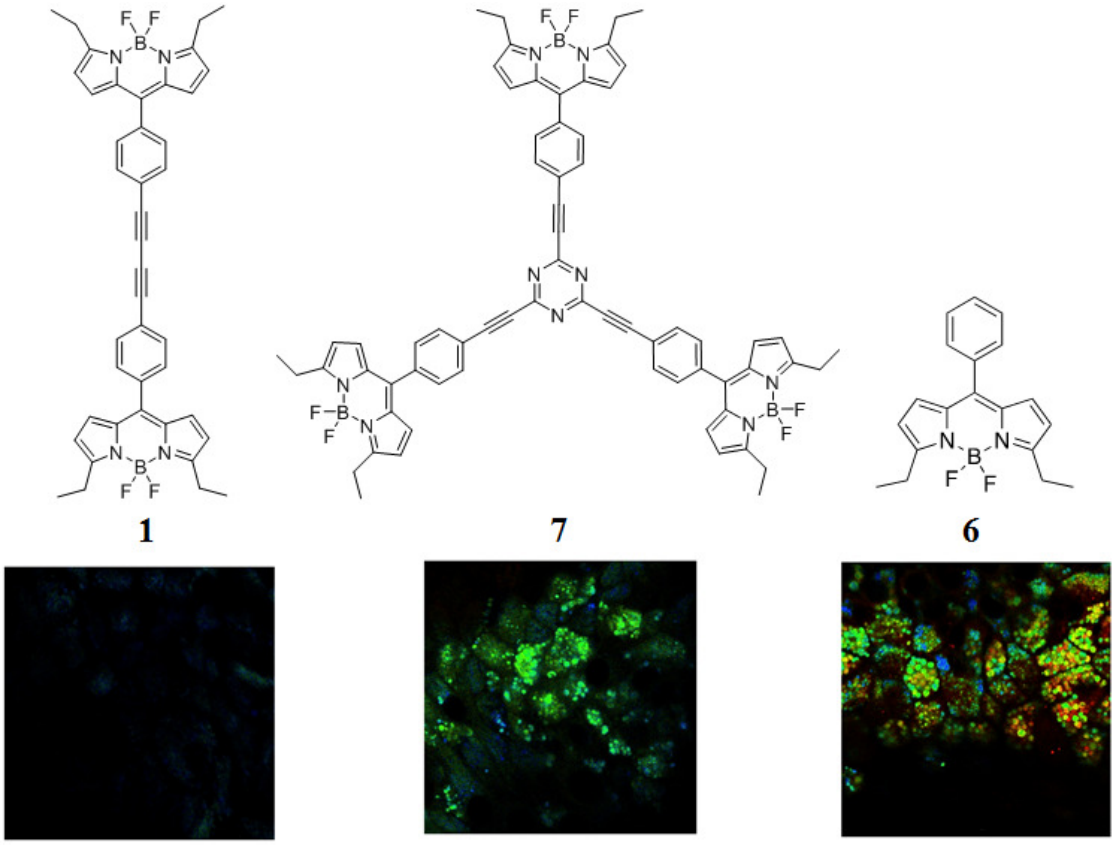

Figure 3.11 Fluorescence lifetime imaging microscopy of BODIPY rotors **7** (A), **1** (B) and **6** (C) of mucin granules from CF cells.
Taken from ref: 146

In order to prove that the observed changes with rotor **6** were only attributed to viscosity variations with mucin granules, several approaches were undertaken. First, the non-rotor **9** was examined (Scheme 3.2). In this compound rotation of the phenyl-group in the *meso*-position around the BODIPY core is restricted by the methyl-groups in 1- and 7-

positions. Thus, as expected, no or significantly smaller variations of lifetimes were observed for this compound as compared to the rotor **6**, when these dyes were added to CF cells (Figures 3.11C and 3.15).

Subsequent evaluation of lifetimes of both **6** and **9** in standard water-glycerol mixtures confirmed that dye **6** followed the predicted behavior of the rotor, while dye **9** demonstrated the behavior that was expected for a non-rotor (Figure 3.12). Specifically, for a linear correlation between lifetime of the dye and media's viscosity, the slope of less than 0.1 suggests a non-rotor-like behavior, whereas a slope of higher than 0.1 indicates a rotor-like behavior.[163]

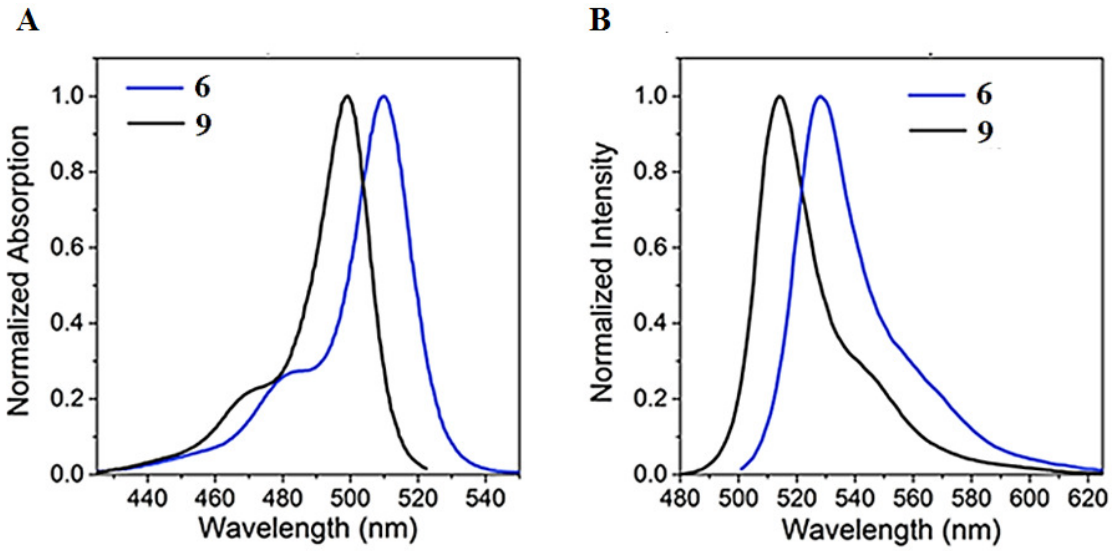

Figure 3.12 Normalized absorbance (A) and emission (B) spectra of BODIPY **6** and **9** in methanol; taken from ref: 146
Conditions: [dye] = 2.3 μM, λ_{ex} = 470 nm; taken from ref: 146

Spectroscopic characterization of both **6** and **9** various types of media was conducted. As expected, the absorption and emission spectra of both dyes in methanol

appeared to be similar (Figure 3.12). Slight red-shifts (*ca*. 10-15 nm; **6**: λ_{ab}^{max} = 511 nm, λ_{em}^{max} = 526 nm; **9**: λ_{ab}^{max} = 501 nm, λ_{em}^{max} = 511 nm) in the case of **6** as compared to **9** were likely due to the presence of a planar conformation that is attainable by the rotor **6**, *i.e*., an extended conjugation between phenyl substituent and the BODIPY core, which is not attainable for the non-rotor **9**, for which twisted conformation dominates.

Next, since pH and polarity of the environment could affect photophysical properties of the dyes, the lifetimes of both **6** and **9** were measured in media of various pH (a physiological range of pH value was chosen) and organic solvents of different polarities (Figure 3.13). The obtained results proved that no significant variations on the lifetimes for both rotor **6** and non-rotor **9** were noted.

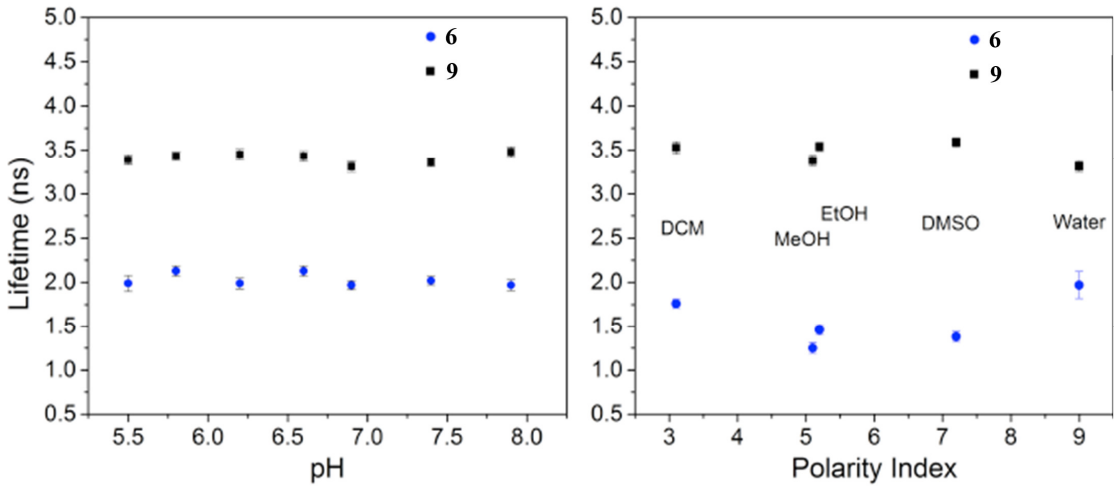

Figure 3.13 Fluorescence lifetimes of BODIPY **6** and **9** as a function of pH and polarity index; taken from ref: 146

Overall, the above results indicated that BODIPY rotor **6** could be used as a molecular viscometer, whereas non-rotor **9** could be used as a control It should be noted

that both dyes could be easily obtained through a one-pot procedure from commercially available materials. On the other hand, for a great number of molecular viscometers reported in literature, either the control (non-rotor) compound cannot be obtained and/or multistep synthetic procedures are utilized.

Once the viability of both dyes to act as a viscometer (rotor **6**) and as a control (non-rotor **9**) were established, it became of interest to use **6** to not only measure viscosity of intragranular mucin, but also to differentiate between the CF and non-CF intragranular viscosities. Towards this goal airway epithelial cells were isolated from bronchial tissues collected from CF patients who underwent lung transplantation, and non-CF cells were from healthy patients.[146] Both types of cells were cultured, and treated with rotor **6** (Figure 3.14). FLIM unambiguously demonstrated that **6** was capable to distinguish between these two different types of cells: significant changes of lifetimes (about two-fold, from 2.5 to 5 ns) were observed in the case of CF-cells, while no significant changes of lifetimes (around 3.5-4.0 ns) were noted in the case of the non-CF-cells (Figure 3.14). Importantly, when

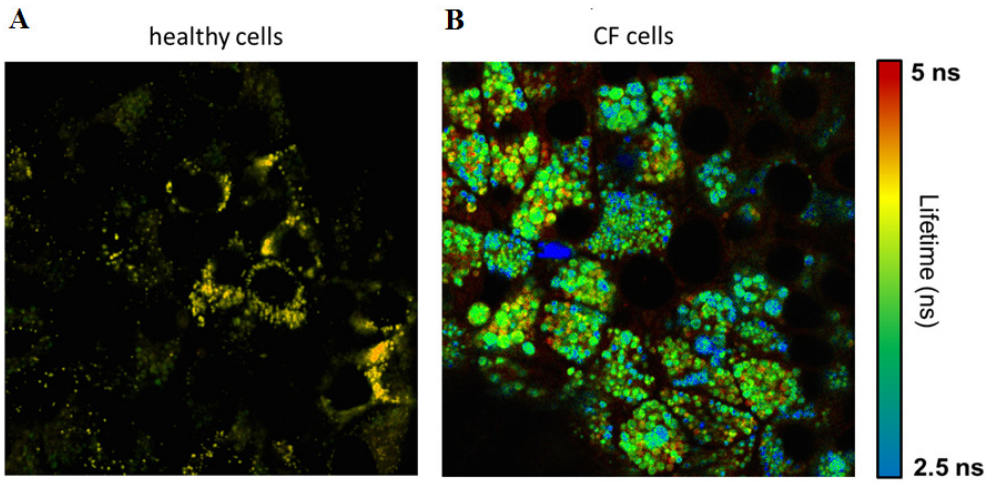

Figure 3.14 Fluorescence lifetime imaging microscopy of BODIPY rotor **6** in healthy (A) and CF (B) cells; taken from ref: 146

similar studies were done with non-rotor **9** no variations between CF and non-CF cells were observed (Figure 3.15).

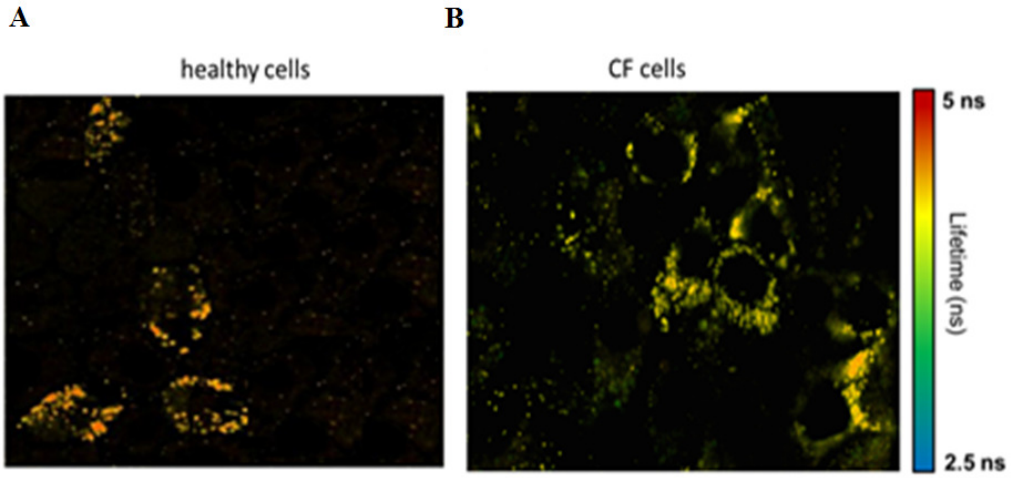

Figure 3.15 Fluorescence lifetime imaging microscopy of BODIPY non-rotor **9** in healthy (A) and CF (B) cells; taken from ref: 146

In order to removed user bias during the analysis of the results and analyze numerous images in a relatively high-throughput screening manner, a machine learning algorithm was developed to calculate the viscosity variations using FLIM images.[146] This analysis demonstrated that viscosity distributions in non-CF cells was a relatively narrow distributed, with main fraction of viscosities centered around 520 cP (Figure 3.16.A). Unexpectedly, in the case of the CF-cells two major populations of viscosities were observed: smaller population had a viscosity of ca. 500 cP and larger population with lower viscosity around 160 cP (Figure 3.16.B). Thus, it appeared that more viscous mucin could be attributed to healthy condition, whereas pathological mucin exhibited low viscosities.

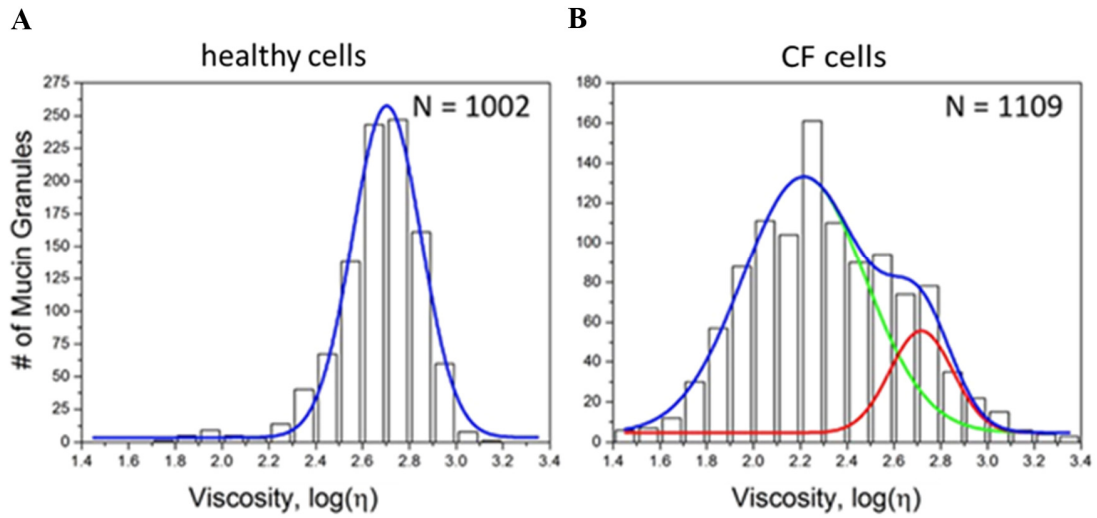

Figure 3.16 Viscosity distributions of intragranular mucin matrices as determined by analysis of several FLIM images using BODIPY **6** in CF-cells (A) and non-CF-cells (B); N is the number of analyzed granules; Blue line: overall fit, green line: lower viscosity populations, red line: higher viscosity populations; taken from ref: 146

3.2.4 Conclusions

For the first time, CF cells were imaged using a small-molecule fluorescence rotor **6** using FLIM, which is a noninvasive method. This BODIPY dye **6** was able to show a difference in viscosity distributions of intragranular mucin of CF and non-CF cells. Specifically, it was determined that in CF cell, mucin's viscosity exhibited a wide range of viscosities, whereas a narrow distribution of viscosities was noted in non-CF-cell. It is plausible that these results might pave the way for determining quantitative relationships between the disease and the viscosity of mucus, which might aid in a better understanding of the disease, and potentially provide viable ways for therapeutic intervention.

3.3.5 Experimental part.

Synthesis of rotor and non-rotor BODIPY dyes.

All chemicals and solvents used for the synthesis of BODIPY dyes were of the highest grade possible and used as received from commercial vendors. BODIPY rotor and non-rotor were prepared according to previously published procedure.[54]

Rotor **6**: ^{1}H NMR (300MHz, $CDCl_3$): δ = 7.47 (m, 5H), 6.73 (d, *J* = 4.1 Hz, 2H), 6.34 (d, *J* = 4.1 Hz, 2H), 3.08 (q, *J* = 7.6 Hz, 4H), 1.34 (t, *J* = 7.6 Hz, 6H).

Non-rotor **9**: ^{1}H NMR (300 MHz, $CDCl_3$): δ = 7.48 (m, 3H), 7.28 (m, 2H), 5.98 (s, 2H), 2.56 (s, 6H), 1.37 (s, 6H).

Viscosity of water-glycerol mixtures.

Mixtures of various viscosities were prepared using commonly used glycerol-water mixtures, by varying the volume fraction of a mixture of Milli-Q ultrapure water (EMD Millipore, MA, USA) and spectroscopic grade glycerol (Sigma-Aldrich, MA, USA) in 10% increments3.

Steady state fluorescence measurements.

All measurements were performed using 1.0 cm path length quartz cuvettes. Absorption measurements were acquired on a Varian Cary 50 Bio UV–Vis spectrophotometer (Agilent Technologies, CA, USA). Fluorescence measurements were performed on a Cary Eclipse spectrofluorometer (Agilent Technologies, CA, USA). Fluorescein (Sigma-Aldrich, MA, USA) in 0.1 M NaOH with a quantum yield of 0.95 was used as the standard for quantum yield calculations.

Fluorescence lifetime imaging microscopy.

CF and non-CF primary human AEC were incubated with BODIPY rotor and non-rotor (2.3 μM each) for 30 min at 37 °C, under 5% CO_2 atmosphere with mild agitation. Cells were washed twice for 2 minutes in HBSS w/o Ca^{2+} and Mg^{2+}, mounted between coverslips, and examined using the Time-Correlated Single Photon Counting system. An MT-200 (PicoQuant, Berlin, Germany) confocal microscopy system with a 60 × 1.2 NA Olympus water immersion objective and 50 μm pinhole was used with an Olympus IX71 inverted microscope with a piezoelectric scanning stage (Physik Instrumente, Karlsruhe, Germany) for all fluorescence imaging measurements and lifetime measurements. A PDL-470 (470 nm wavelength) laser operated at 20 MHz repetition rate by a PDL 828 "Sepia II" was used as the excitation source in all measurements. A 488 nm LP filter (Semrock, NY, USA) was used to remove the excitation from the collection. Symphotime V 4.2 (PicoQuant, Berlin, Germany) software was used to analyze and fit fluorescence lifetime decays.

CHAPTER 4: CONFORMATIONAL BEHAVIOR OF RATIOMETRIC FLUORESCENCE PORPHYRIN ROTOR IN ORGANOGELS

4.1 Overview of porphyrin rotor as a molecular probe

Porphyrin dimer (**PD**) is a molecular rotor containing two chromophores linked by a diyne moiety that allows for a free rotation of the porphyrin cores around each other, and produces an array of conformers, with twisted and planar conformation being the two extremes (Figure 4.1). **PD** is an *in vitro* photodynamic therapy agent for treatment of cancer, which has efficient two-photon excitation.[171] Additionally, **PD** was shown to be a viable fluorescent molecular rotor, with the relative emission intensities exhibiting good correlation with solvents' viscosity.[158]

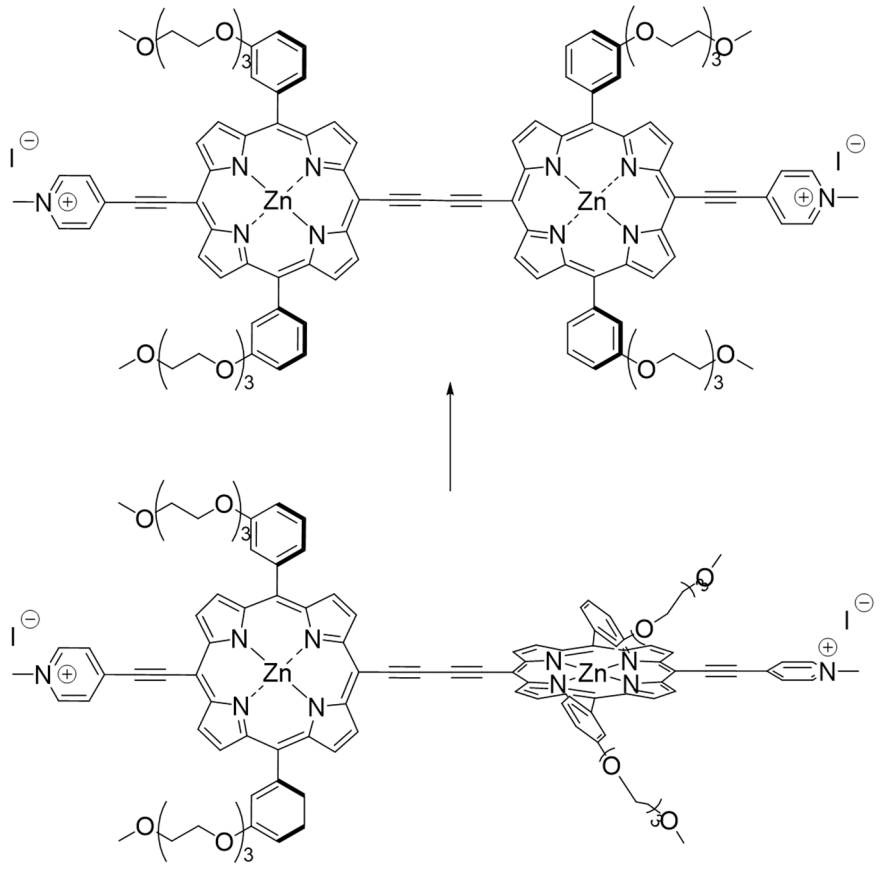

Figure 4.1 Planar (top) and twisted (bottom) conformations of **PD**.[174]

In molecular solvents state with low viscosities, such as ethanol, (viscosity 0.6 cP), the planar conformation of **PD** in the excited exhibits an emission maximum at around 780 nm, while in the excited state the twisted conformation, which is predominant in high viscosity solvents, such as glycerol (viscosity 950 cP), emission at around 720 nm is noted (Figure 4.2).[158] Although fluorescence lifetime of **PD** was shown to be sensitive to media's viscosity,[172] the operational ease of steady-state emission spectrophotometry contributes to the rotational sensitivity of **PD** made it an interesting probe to study various types of environments. Specifically, the effect of confinement was probed on the conformation of **PD**, by using reverse micelles that contained either molecular solvents or imidazolium-based ionic liquid.[173] Furthermore, **PD** was incorporated in polyvinyl alcohol films, and conformational integrity was explored as a function of the stretching/shrinking of the film at room temperature as well as at elevated temperatures.[174] Recently, the effect of macromolecular crowding on the conformational preference of **PD** was reported. It appeared that in the crowding environment, the amount of twisted conformation was decreasing with the increasing amounts of the crowding agent, *i.e.*, polyethylene glycol; this increase in the amount of crowding agent correlated with the increase of media's viscosity. It was proposed that the twisted conformation which occupies more space would be disfavored under such conditions, whereas the planar conformation of **PD**, the one that can fit better within the network of crowding agent, should be the more dominant one.[175] On the other hand, theorical calculations on a similar porphyrin dimer with *meso-meso* butadiyne linker and different substituents have shown that the torsional energy barrier is around 3 - 4 kJ/mol from planar to twisted. Also, specify the planar position as the most stable conformer and the twisted as the one that requires the largest activation energy.[176]

From a practical stand-point, the study indicated that since macromolecular crowding is highly prevalent in biological types of media, the applicability of **PD** as a molecular viscometer should be taken with caution. From the more fundamental stand-point, modulating the conformational integrity of **PD** by additives, solutes in various types of media might provide an additional, interesting and potentially useful aspect on controlling the internal rotation of molecular rotors.

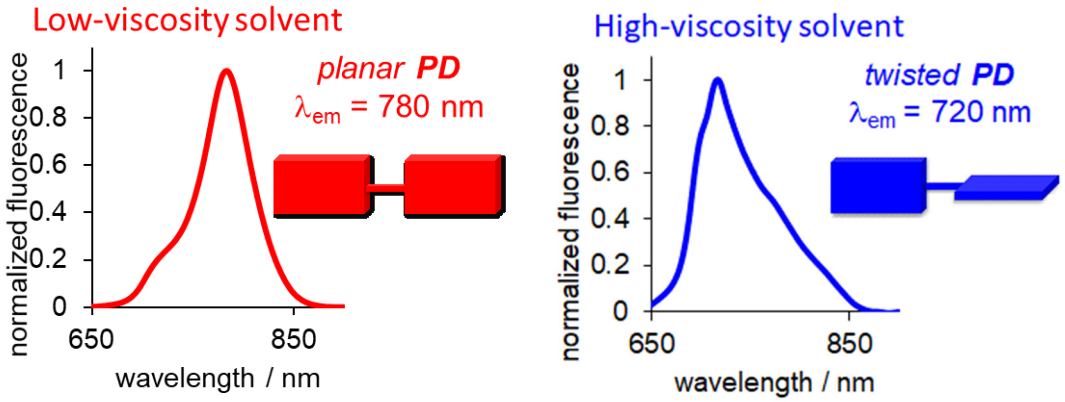

Figure 4.2 Emission spectra of **PD** in solvents of different viscosities.

To further expand on using **PD** as a molecular probe of different types of media, studies were initiated to address the spectroscopic behavior of **PD** in organogels. Organogels are a soft matter, which has received a lot of attention due to their unique properties that could be viewed as transient between liquids and solids. Gel-like formation is induced by so-called low molecular weight gelators, *i.e.,* small molecules, and results in the formation of a three-dimensional supramolecular network. Typically, this network is supported by non-covalent interactions which trap solvent molecules, and restrict their mobility, thus producing a solid-like system.[177] The mechanisms of gel formation, and

especially structural features that would be responsible for the gel formation in any particular case are not completely understood.[177] In the majority of cases, gelators are serendipitously discovered, and a rational design of organogelators is somewhat illusive. Notably, in some instances, fluorescence probes have been employed to study organogels in order to understand the processes of fiber formation and growth, as a fundamental study to prove the possibility of using fluorescence probes for characterizing self-organization of materials.[178]

For this work, a low molecular weight gelator **G** (Figure 4.3) was chosen due to ease of synthesis, and its ability to gel a wide range of organic solvents with different chemical properties.[179] The organogelator **G** was also utilized in the room-temperature ionic liquid assisted gelation of DMSO.[180]

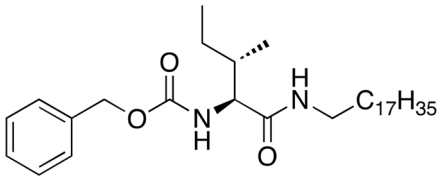

G

Figure 4.3 Structure of organogelator **G**.

It should be pointed out that, in general, gel formation of a solvent is typically done by heating a small amount of gelator in the solvent in a capped vial until a homogenous solution is obtained. Subsequently, the vial is allowed to cool to room temperature, and the successful gel formation is confirmed by inverting the vial upside down, and observing no fluid running down the walls.

4.2 Synthetic approach toward PD

With the purpose of constructing two-photon PDT photosensitizers, **PD** was synthetized *via* a multi-step approach (Scheme 4.1). It should be noted that zinc-containing porphyrins, which were decorated with ethylene glycol side-chains to enhance water

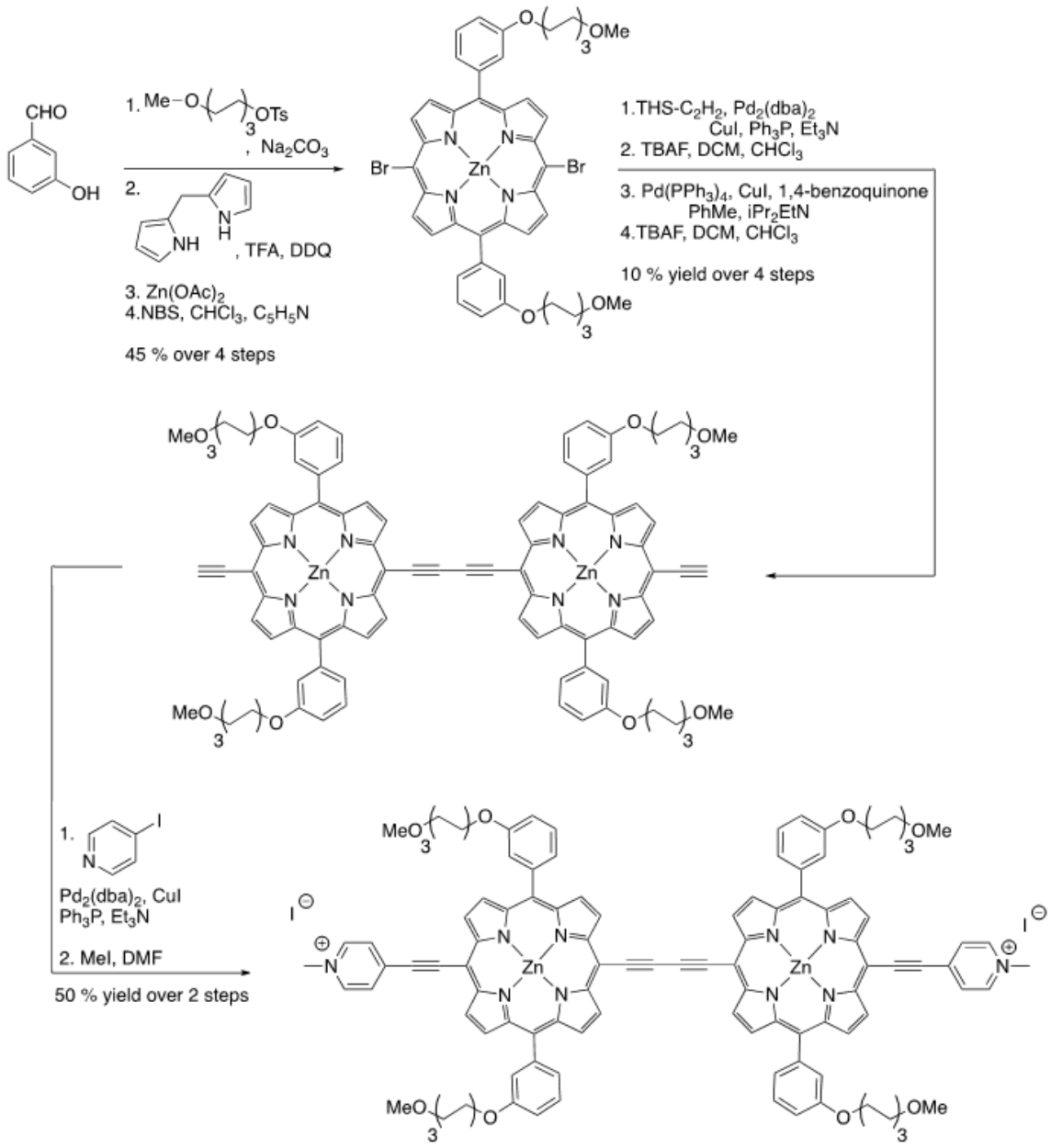

Scheme 4.1 Synthesis of **PD**.

solubility and prevent aggregation of the porphyrin,[45] The sample of **PD** that was used in this work was a gift from Professor Milan Balaz laboratory (University of Wyoming, WY, US and Yonsei University, Republic of Korea).

4.3 Results

In order to introduce **PD** into the gel-like environment a protocol was developed to assure homogenous distribution of **PD** in the gel. Specifically, gel of DMSO was prepared using 10 mg/ml of **G** (i.e., minimum gelation concentrations),[179] heated to induce gel-to-sol transition and transferred hot into a spectroscopic cell, which was placed into the Peltier heating unit of a spectrophotometer. The cell was heated to 70 ^{o}C in the instrument, and **PD** were added to this solution, mixed and the cell was removed from the instrument and allowed to cool to room temperature. This procedure provided reproducible results and assured that thermosensitive **PD** was not exposed to temperatures higher than 70 ^{o}C.

Initially, the absorption spectra of **PD** were measured at 20 $^{\circ}$C, *i.*e., in the gel state, and at 70 $^{\circ}$C, *i.e.,* in the solution state (Figure 4.4). The absorption maxima in both states was around 470 nm, *i.e.,* the Soret band. Two-distinct peaks were noted in the region with the maxima at 782 nm (at 20 $^{\circ}$C) and 766 nm at (70 $^{\circ}$C) with a shoulder at *ca*. 700 nm under both conditions. Some studies indicated that the longer-wavelength band was attributed to planar conformation, while the shorter-wavelength band was reflecting the twisted conformation.[181] Thus, in the ground state, **PD** appeared to be mostly in the planar conformation in both solution and gel states (Figure 4.4). However, in general, due to broad, ill-defined nature of the bands, UV-vis spectroscopy is not commonly used for

assessing conformational preference of **PD**. Therefore, the majority of the work described here was accomplished using fluorescence spectroscopy.

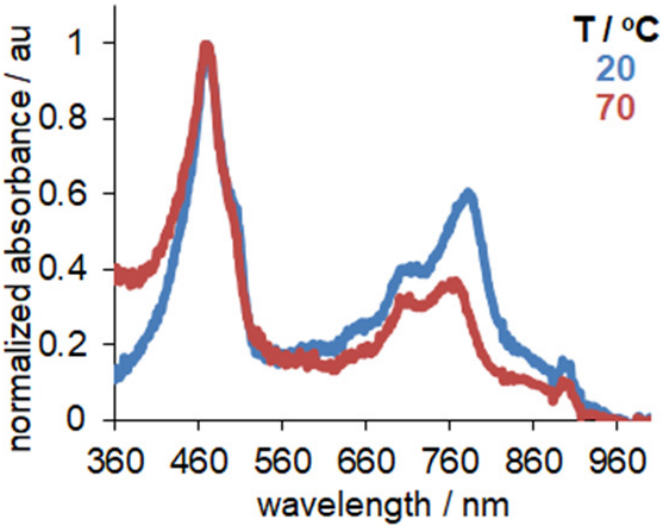

Figure 4.4 Temperature-dependent, normalized absorbance spectra of **PD** in DMSO gel and solution.
[**PD**] = 2μM, [**G**] = 10 mg/mL

The emission spectra of **PD** were obtained upon excitation at 475 nm of DMSO gel (Figure 4.5). Upon gel-to-sol transition, *i.e.,* by heating the gel from 20 °C to 70 °C, an increase of the amount of the twisted conformation in the excited state, as judged by the increase of the rotation between the 720 nm peak, associated with twisted **PD**, 787 nm peak, associated with planar conformation of **PD**, was observed. Considering that the viscosity of the media decreases upon melting of the gel, *i.e.,* during gel-to-sol transition, the observed conformational changes were in complete contrast with previous reports.[179] In general, it was shown that as the viscosity of the media decreases, the amount of twisted conformation decreases as well in the excited state. This is consistent with the idea that the

conformational twisting in the excited state depends on viscosity (Figure 4.5.A). Therefore, in the presence of the gelator, a unique behavior of **PD** was uncovered.

The gel system was subjected to two more heating cycles, *i.e.,* the spectroscopic cell was heated from 20 °C to 70 °C, then cooled to room temperature (2nd cycle), and once the gel formed, the cell was heated from 20 °C to 70 °C, then cooled to room temperature (3nd cycle) (Figure 4.5, B and C). As a result of these three heating/cooling cycles, a continuous, irreversible, incremental increase of the twisted conformation of **PD** was observed (Figure 4.5). This experiment was repeated over four times to confirm the

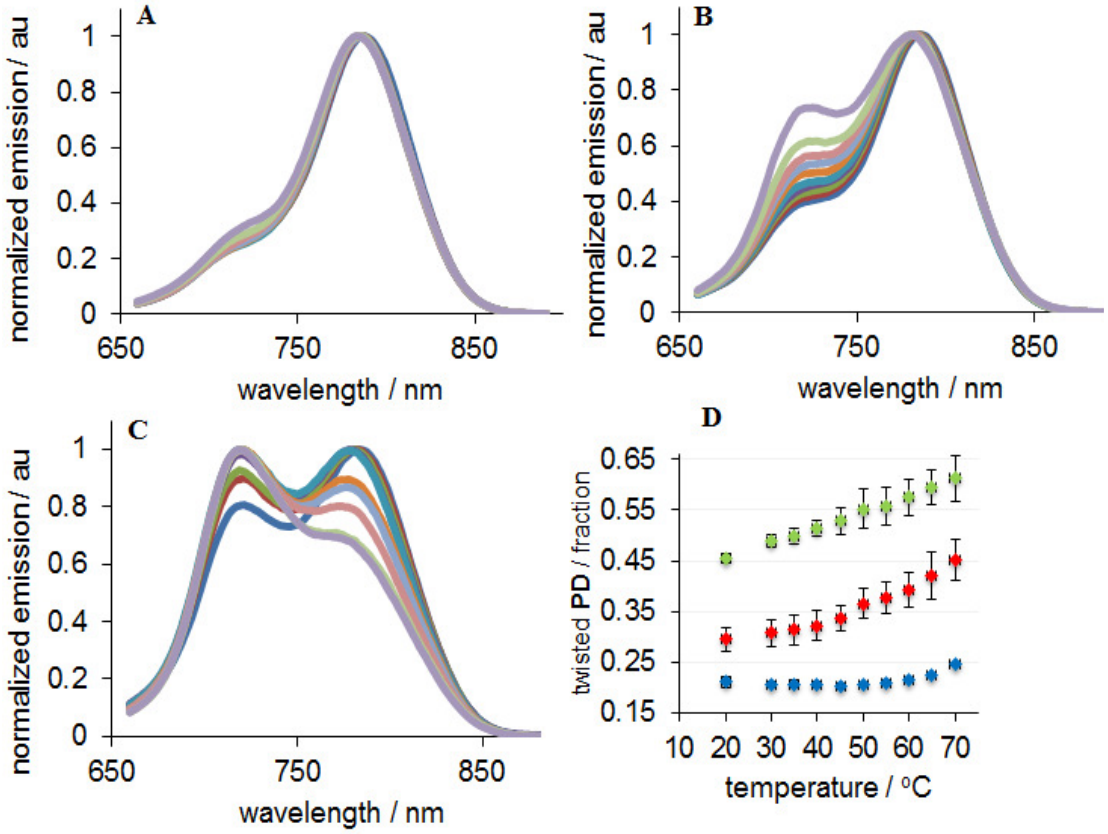

Figure 4.5 Normalized fluorescence emission of **PD** in DMSO gel as a function of temperature in three heating / cooling cycles.
Conditions: [**PD**] = 2 μM, [**G**] = 10 mg/mL, λ_{ex} = 475 nm
A: 1st heating cycle, **B**: 2nd heating cycle, **C**: 3rd heating cycle, **D**: 1st cycle (blue), 2nd cycle (red), 3rd cycle (green) error bars indicate the standard deviation on three experiments.

reproducibility of this conformational change of **PD**. The fraction of twisted **PD** (Figure 4.5 D) was calculated diving the emission at 720 nm (twisted) over the sum of the emission at 780 nm (planar) and 720 nm.

Moreover, fluorescence of **PD** was examined at several temperatures along a range of excitation wavelengths on the Soret band or the intense band in the blue region (Figure 4.6), observing specially the temperature where the sol-to-gel transition occurs at 30 °C. It was established that the ratio of twisted structure varied along the excitation wavelengths, which according to literature reports suggested the presence of the two conformers in the system.

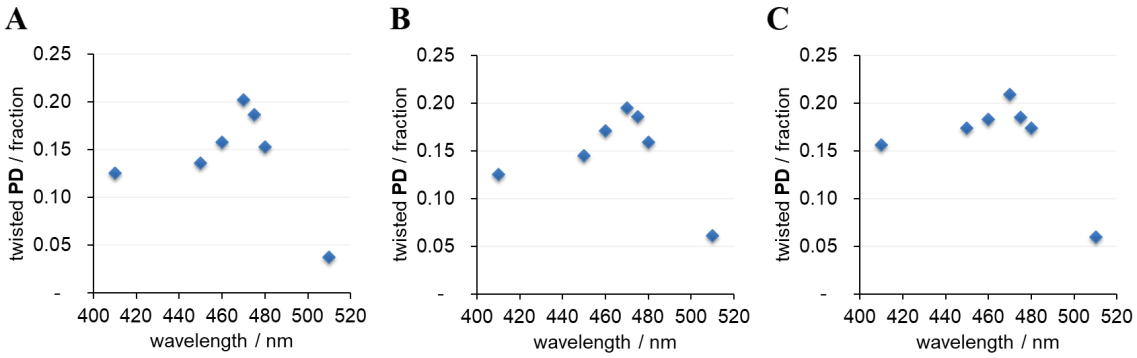

Figure 4.6 Ratio of twisted of **PD** in DMSO gels as a function of excitation wavelength at 20 °C (A), 30 °C (B) and 30 °C (C)
Conditions: [**PD**] = 2μM, [**G**] = 10 mg/mL

As a control, the spectroscopic response of **PD** in DMSO without gelator was examined (Figure 4.7). It appeared that in the absence of **G**, by subjecting **PD** to three heating / cooling cycles no noticeable conformational variations were observed.

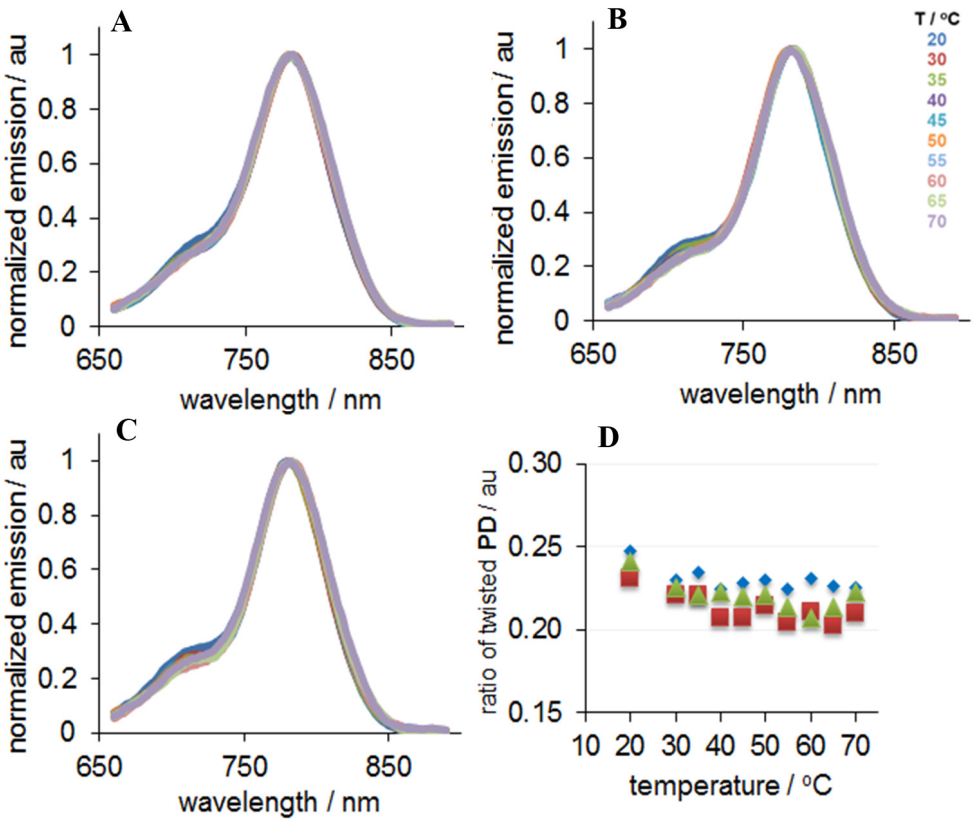

Figure 4.7 Normalized emission intensity of **PD** in DMSO as a function of temperature during three heating / cooling cycles.
Conditions: [**PD**] = 2 μM, [**G**] = 10 mg/mL, λ_{ex} = 475 nm;
A: 1st heating cycle, B: 2nd heating cycle, C: 3rd heating cycle, D: 1st cycle (blue), 2nd cycle (red), 3rd cycle (green)

Additionally, due to the fact that DMSO gel was white and opaque, which might have caused some artifacts during spectroscopic measurements, a microscopy evaluation was performed at several temperatures, to test **PD** behavior in both gel state and solution state, *i.e.*, at 23 °C to 60 °C, respectively (Figure 4.8). The fluorescence microscopy was measured upon excitation at 475 nm and imaging at wavelengths of the twisted and planar geometries, 720 nm and 780 nm, respectively.

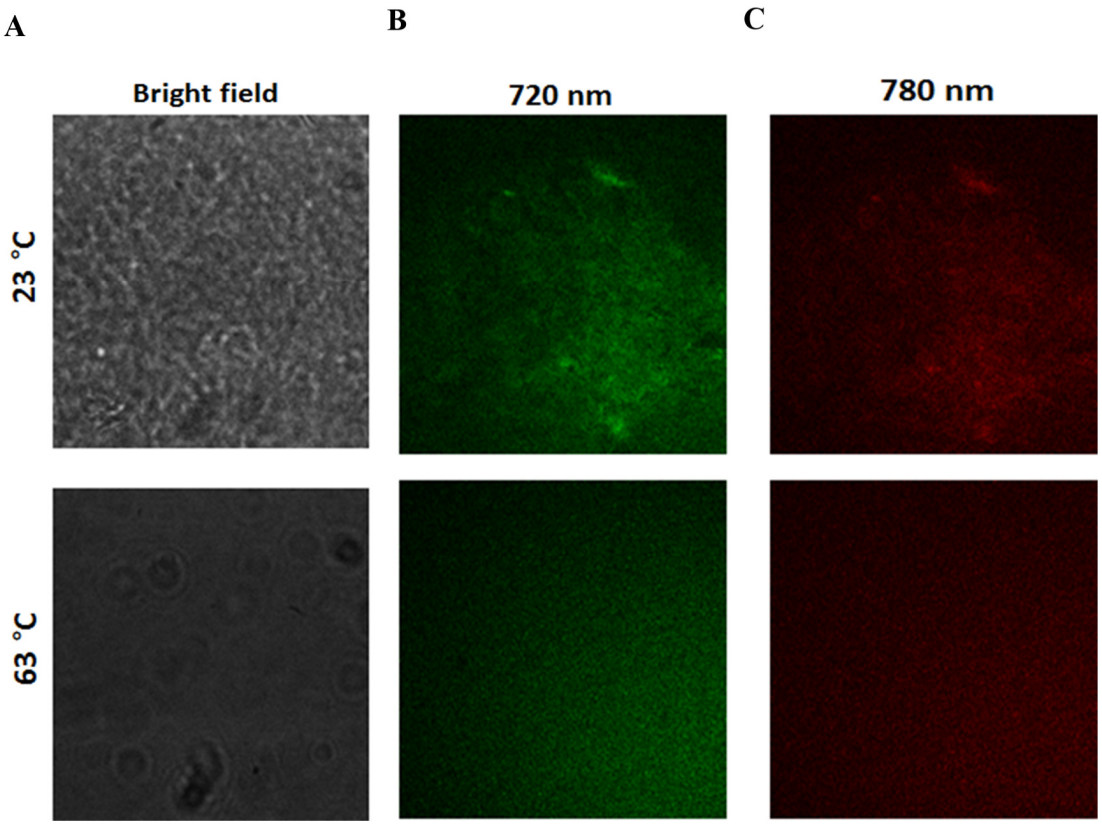

Figure 4.8 Temperature dependent bright field image (A) and fluorescence microscopy at two λem (B and C) of **PD** in gel of DMSO.
Conditions: [**PD**] = 2 μM, [**G**] = 10 mg/mL, λ_{ec} = 475 nm

Average emission intensity signal of the image was utilized to calculate the amount of conformer along the range of temperatures (Figure 4.9). A rapid increase of the twisted conformation even after one heating cycle up to *ca*. 0.7 was observed, while the twisted conformation of PD plateaued at *ca.* 0.8 ration upon the subsequent two heating cycles (Figure 4.9 B and C), Although an irreversible conformational behavior that was similar to that observed in steady state fluorescence was noted (Figure 4.9), the "kinetics" of the

conformational change was different. However, this discrepancy is likely to be expected due to different conditions, especially considering that different amounts of the gels that were used in steady-state fluorescence set-up (about 0.5 ml) and imaging (0.05 ml).

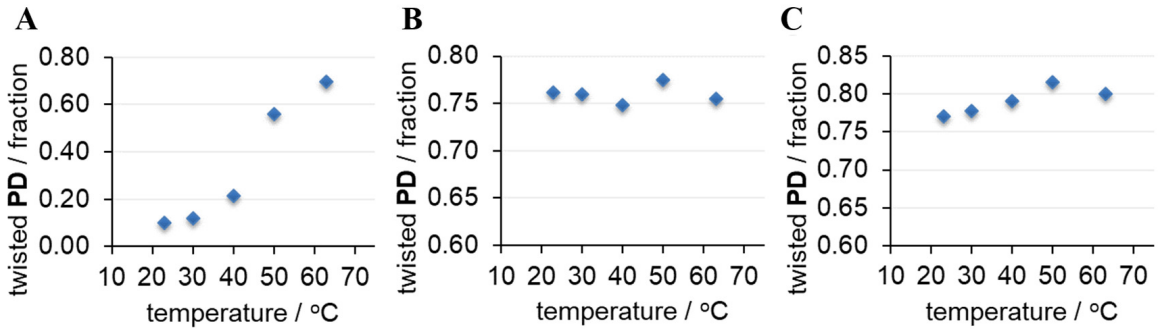

Figure 4.9 Conformational changes of **PD** in DMSO gel as a function of heating cycles assessed by microscopy.
Conditions: [**PD**] = 2 μM, [**G**] = 10 mg/mL, λ_{ex} = 475 nm
A: 1st heating cycle, B: 2nd heating cycle, C: 3rd heating cycle
Data obtained using average emission intensities of fluorescence microscopy images (see text for details).

Collectively, the aforementioned results suggested that the interaction between **G** and **PD** could be responsible for the conformational change. It is plausible that while in the monomeric form, **G** would not be affecting the conformation of **PD**, the aggregated form of **G** might promote such a change. Arguably, due to its structure (*i.e.*, a long alkyl chain and a polar amino acid tail), organogeltor **G** might form micelle-like structures, which could interact with **PD**. Since confined environment was shown to affect planar-twisted equilibrium of **PD**,[173] the micelle-like structures of **G** might be affecting **PD**'s conformation as well. These assemblies of **G** might not completely disaggregate to the monomeric form upon heating of the gels, *i.e.*, during gel-to-sol transitions, and they might be responsible for locking a particular amount of twisted **PD** after each heating/cooling

cycle. These assemblies were not large enough to be observed by the microscope. Therefore, dynamic light scattering (DLS) measurements were performed on the solution state of DMSO gel, *i.e.*, 10 mg/mL of **G** was dissolved in DMSO followed by heating. However, no aggregates where observed. Furthermore, even when these measurements were done in the presence of **PD** (in case **PD** was acting as a template for the assembly of **G**), no micelle-like structures could have been detected. Albeit unsuccessful, these experiments did indicate that a) **G** was important for the conformational change, due to amount and/or the type of environment that is created by **G**, and b) heating of the system in the presence of **G** was essential for inducing the conformational change.

To address the first notion, the emission of **PD** was measured in a range of gelator concentrations (Figure 4.10). It should be noted that at the concentration of **G** below 10 mg/ml (minimum gelation concentration), *i.e.*, at 2, 5, and 8 mg/ml (Figure 4.10 B-D), no gel formation was noted when **G** was dissolved in DMSO upon heating followed by cooling to room temperature. Thus, in this concentration range the conformational behavior of **PD** was studied in the solution state at all temperatures. However, at 10 and 20 mg/ml (Figure 4.10, E and F), conformational change of **PD** was taking place during gel-to-sol transition.

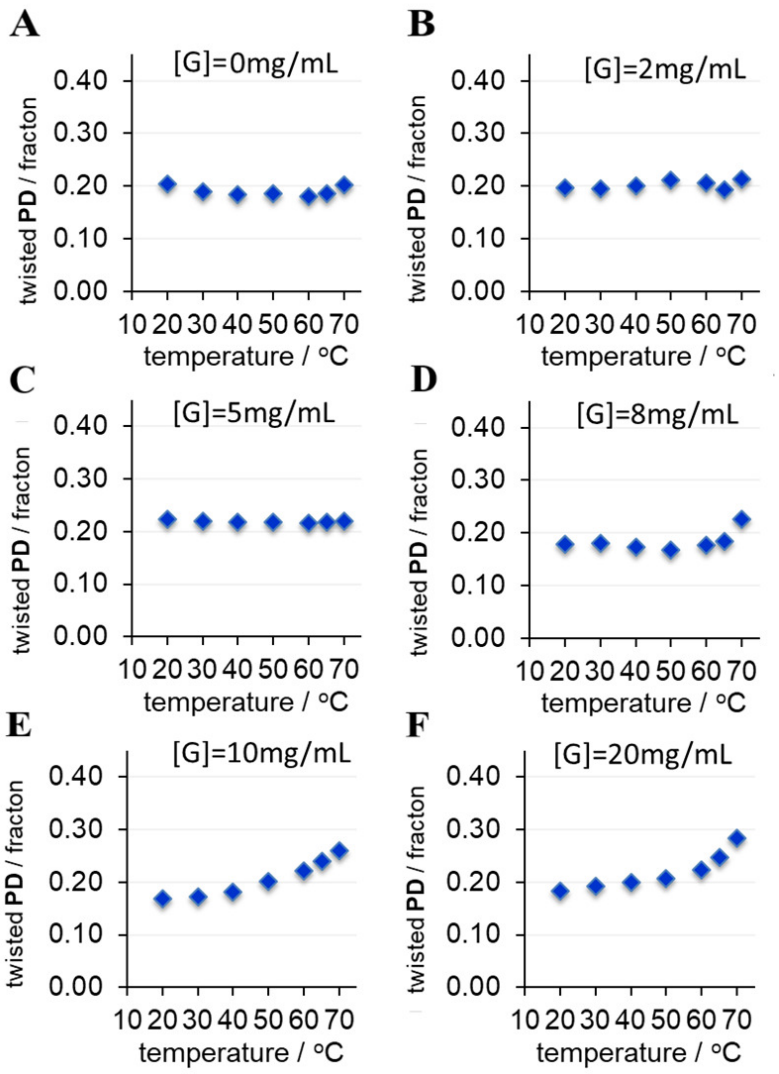

Figure 4.10 Ratio of twisted **PD** conformation in gels of DMSO with different concentration of gelator **G** after one heating cycle.
Conditions: [**PD**] = 2 μM, λ_{ex} = 475 nm

It appeared that in the presence of low concentrations of **G**, the amount of twisted conformation of **PD** did not change appreciably with the change of temperature, and remained at around 20 %, as it resembled the amount of twisted **PD** found in neat DMSO, *i.e.*, in the absence of **G**.

Next, in order to address whether the gel formation could induce the conformational change, it was decided to use a system that would allow to distinguish between the effect of gelation and the effect of temperature. Such gelation would need to be conducted at room temperature, *i.e.,* without exposure of the gelation system to elevated temperatures. The ability of imidazolium-based, BF_4-containing ionic liquids to gel DMSO in the presence of small amounts of **G** at room temperature was recently established.[180] Adaptation of this procedure allowed to evaluate the effect of gelation on conformation of **PD** without heat (Figure 4.11). The system was prepared by dissolving 2 mg/mL of **G** in DMSO (the minimum gelator concentration is 10 mg/mL), followed by dissolution of **PD** at room temperature; subsequently gelation was induced by addition of [C_4-mim]BF_4 (20 % v/v) at room temperature. The results clearly demonstrated that gelation did not induce conformational change of **PD** (Figure 4.11). The amount of twisted conformation was 22 % in DMSO+**G** solution (*i.e.*, prior gelation), and this amount did not change appreciably upon gelation, which was caused by addition of the ionic liquid (Figure 4.11). Small

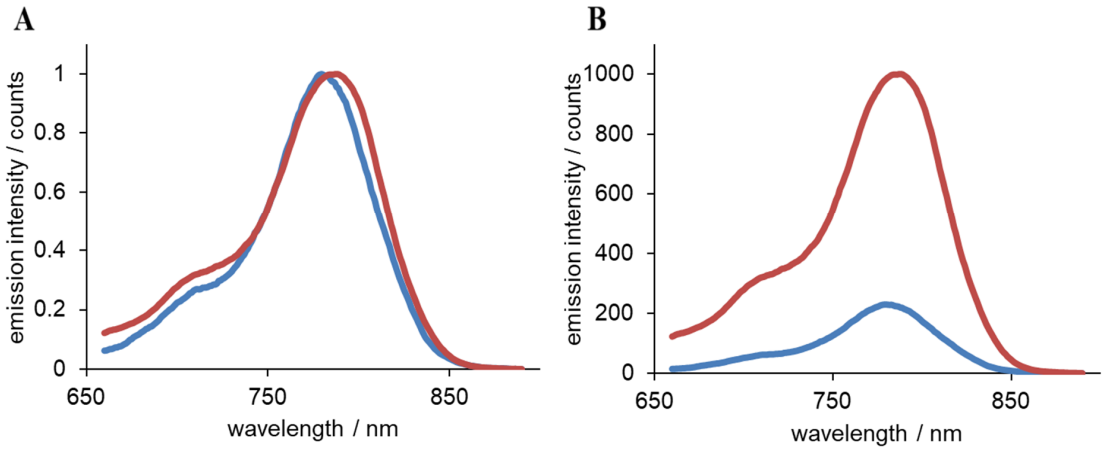

Figure 4.11 Normalized emission intensity of PD before (blue; solution state) and after (red, gel state) addition of [C_4-mim]BF_4 (A) emission intensity of PD before (blue; solution state) and after (red, gel state) addition of [C_4-mim]BF_4 (B)
Conditions: [**PD**] = 2μM, [**G**] = 2 mg/mL, [C_4-mim]BF_4 = 20 % v/v, λ_{exc} = 475 nm

changes in the position of the emission maxima were expected since the polarity ad the nature of the system changed upon addition of the ionic liquid to DMSO.

To assure that the presence of [C_4-mim]BF_4 did not induce conformational change, emission of **PD** was investigated in DMSO-[C_4-mim]BF_4 mixtures in the presence and absence of **G** (Figure 4.12). In the absence of the gelator, *i.e.*, in solutions of DMSO-[C_4-mim]BF_4, conformation of **PD** did not undergo any appreciable changes upon heating these solutions (Figure 4.12). However, in the presence of **G** (2 mg/mL), a small increase on the twisted conformation as a function of temperature was noted (Figure 4.12).

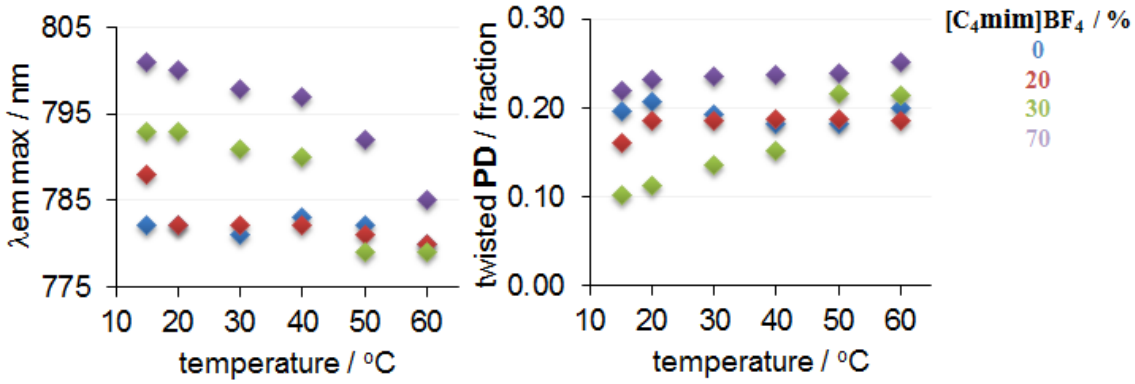

Figure 4.12 Changes of emission maxima of **PD** as a function of temperature (A) and amount of twisted **PD** (B) in DMSO/ionic liquid gels as a function of temperature during the 1st heating cycle.
Conditions: [**PD**] = 2 μM, [**G**] = 2 mg/mL λ_{ex} = 475 nm

In addition, to investigate the temperature dependence, a gel in DMSO was heated at 70 °C for three hours, measuring the steady-state emission every 10 minutes (Figure 4.13.A). The results show a shift to the shorter wavelength or twisted conformation emission of **PD**. Moreover, the in DMSO without gelator, no variations were observed as a function of time as the system was kept at 70 °C (Figure 4.13.B). The drastic differences

between the gel in DMSO and without **G** (Figure 4.13.C) prompt to continue investigate the gelator as the potential reason for the increase in the twisted fraction.

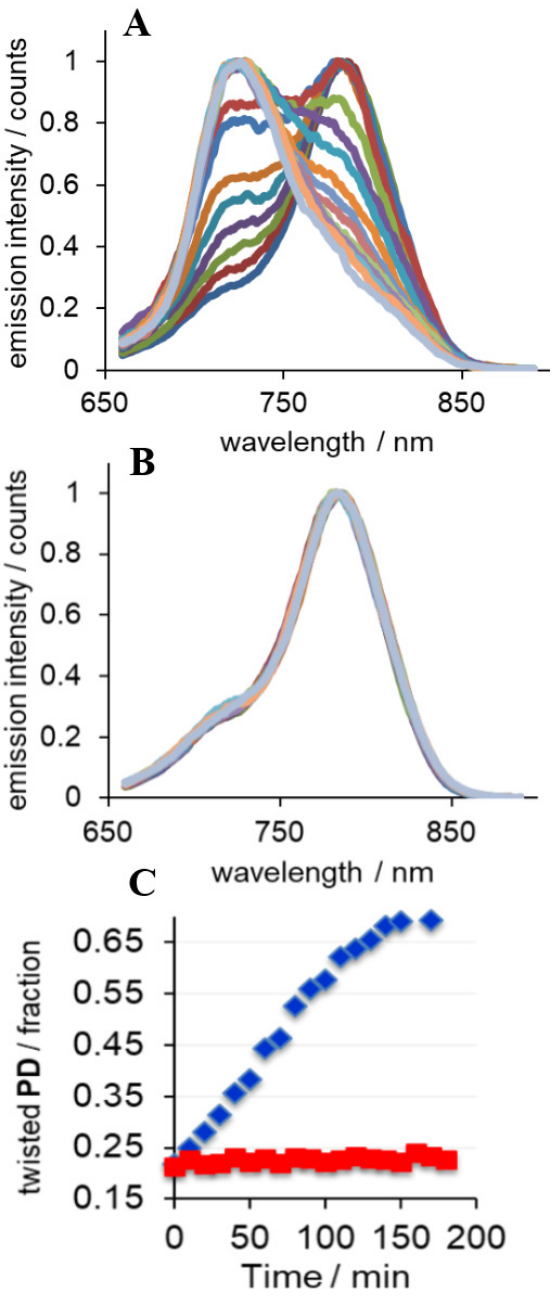

Figure 4.13 Normalized emission intensity of **PD** in DMSO gel (A) and neat DMSO (B) at 70 °C over 180 minutes; amount of twisted **PD** as a function of heating time (C). Conditions: [**PD**] = 2μM, [G] = 10 mg/mL λ_{exc} = 475 nm

The following step was to evaluate the effect of temperature on the conformational preference of **PD** in the presence of various amounts of **G**. Time-dependent, steady-state emission measurements unambiguously demonstrated that increase of the twisted conformation of **PD** was solely dependent on the presence of **G** (Figure 4.14). However, the relationships appeared to be not very straightforward. For example, it was expected that increasing the amount of the gelator would lead to the increase of the twisted conformation, and consistent with that notion, as the amount of **G** increased from 2 to 10 mg/ml the rate of formation of twisted conformation increased as well (Figure 4.14). On the other hand, when concentration of **G** was increased to 20 mg/ml (twice the amount of the minimum gelation concentration), the rate of twisted conformation of **PD** decreased (Figure 4.14). This fact is quite interesting, and it might indicate that the structural identity of the gel network might be dependent on the amount of the gelator.

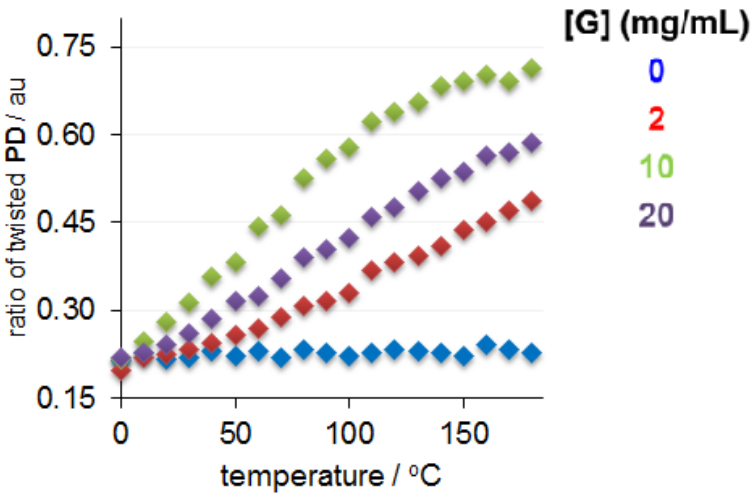

Figure 4.14 Amount of twisted **PD** in DMSO gels/solutions as a function of organogelator concentration upon heating at 70 °C for 180 minutes.
Conditions: [**PD**] = 2 μM, λ_{ex} = 475 nm

Finally, as **G** was reported to gel several organic solvents besides DMSO, more organogels were prepared and studied, utilizing in all cases the minimum gelator concentration reported.[179] Solvents with different physical characteristics, such as polarity, density and refractive index were chosen. Similarly, as previous studies (Figure 4.13), the emission of **PD** was measured at 70 °C over a period of 3 hours (Figure 4.15). The results indicated that in DMF and DMSO, the rate of formation of twisted conformation of **PD** was the largest, while the changes in other solvents were less pronounced (Figure 4.15).

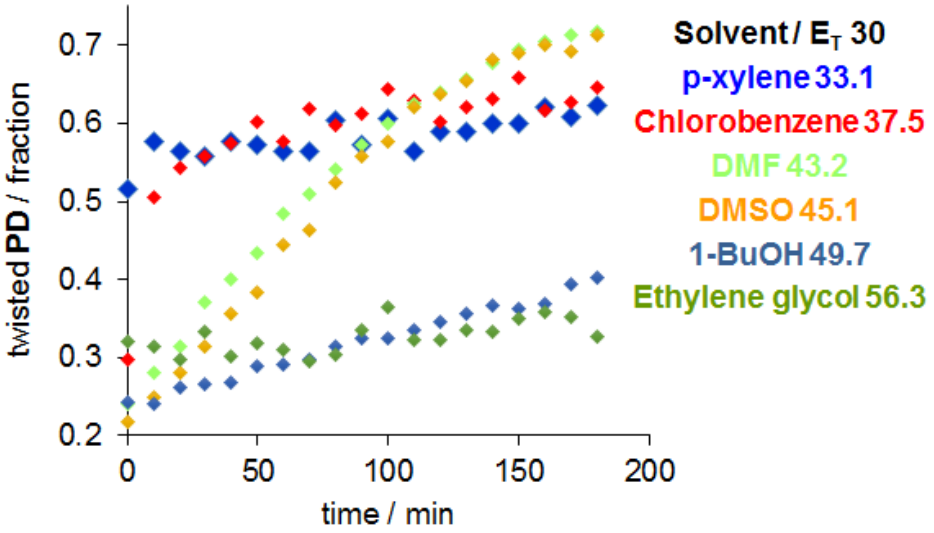

Figure 4.15 Amount of twisted PD in organogels as a function of time at 70 °C.
Conditions: [**PD**] = 2 μM, λ_{exc} = 475 nm
p-xylene: [**G**] = 17 mg/mL
chlorobenzene: [**G**] = 30 mg/mL
DMF: [**G**] = 20 mg/mL
DMSO: [**G**] = 10 mg/mL
1-BuOH: [**G**] = 19 mg/mL
ethylene glycol: [**G**] = 23 mg/mL

Surprisingly, when the emission of **PD** was measured in neat solvents, *i.e.*, in the absence of **G**, conformational change was noted in a number of solvents (Figure 4.16).

Specifically, in neat DMF and 1-BuOH, a conformational change from planar to twisted was induced within 3 hours of heating (Figure 4.16). Thus, in these solvents conformational change of **PD** could be achieved without the gelator. This phenomenon has not been reported previously, and it might provide additional tools for controlling conformational integrity of molecular rotors.

In addition, in aromatic solvent, such as chlorobenzene, even without exposure to elevated temperature, twisted conformation appeared to be the most dominant. It should be noted that in p-xylene, only one emission maximum (as opposed to typically observed two maxima) was observed. Thus, estimation of the amount of twisted conformation was not possible. Based on literature report,[182] which suggested that aggregation of **PD** in toluene was taking place, it is plausible that in aromatic molecular solvents, the evaluation of conformational behavior of **PD** is much more complex than in other molecular solvents.

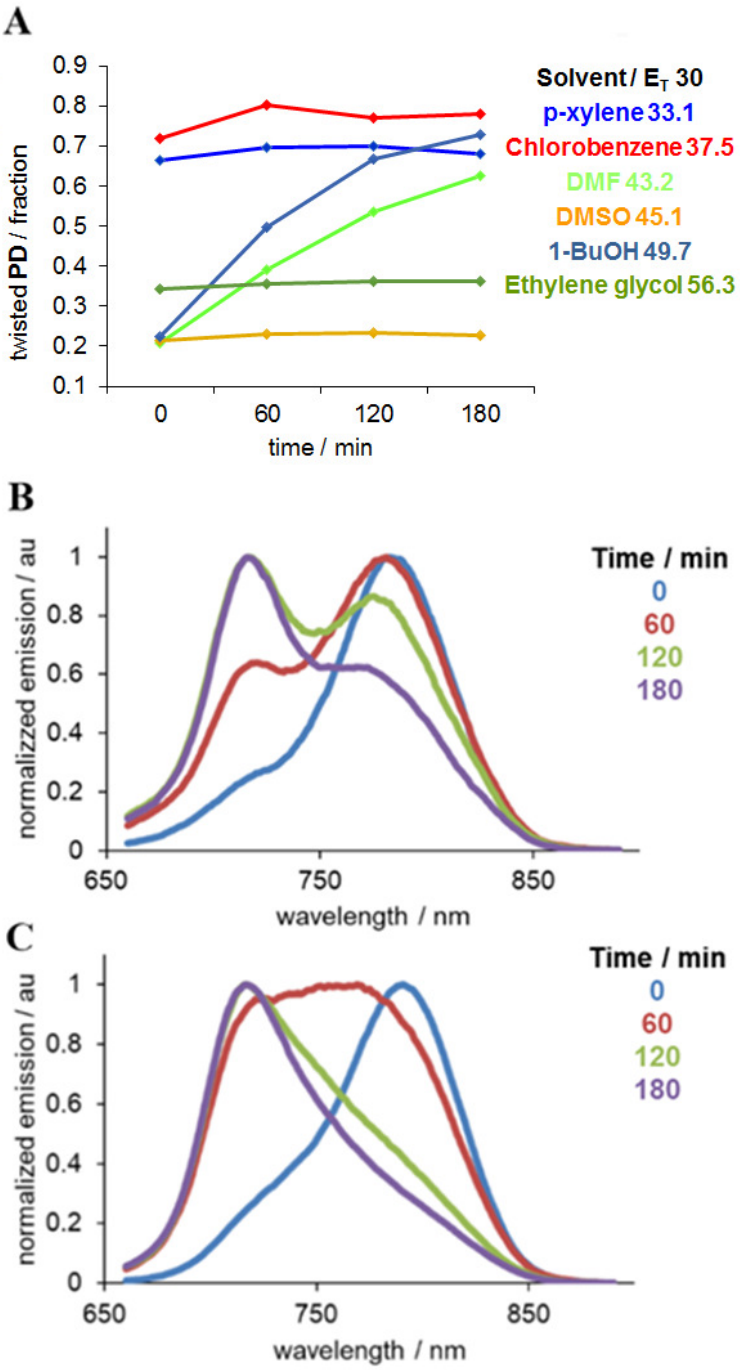

Figure 4.16 Effect of molecular organic solvents on the amount of twisted **PD** (A), normalized emission intensity of **PD** in DMF (B), 1-buthanol (C) Conditions: [**PD**] = 2 μM, λ_{ex} = 475 nm, temperature = 70 °C

4.4 Conclusions

Porphyrin dimer **PD**, a known PDT agent and fluorescent molecular viscometer for several types of environments, was utilized to probe the gelation of a diverse set of organogels. In sharp contrast to previously reported accounts, where the amount of twisted conformation was shown to increase with increasing of media's viscosity, it was discovered that the amount of the twisted conformation of **PD** in the gels of organic solvents and ionic liquids, increased as the viscosity of the organogel decreases (*i.e.,* upon gel-to-sol transition or melting of the gel). This effect appeared to be due to a combination of factors, including the amount of the gelator, heating time, and the nature of the organic solvent, while formation of the gel network did not have a pronounced effect.

Surprisingly, the amount of twisted conformation of **PD** was found to increase in common organic solvents, such as DMF and 1-butanol simply upon heating the solution of **PD** at 70 °C for three hours. This behavior was not observed in DMSO, ethanol, dioxane, and a range of other molecular solvents and ionic liquids. This is the first report on the temperature-dependent conformational change of **PD** in molecular organic solvents. The results strongly suggest that conformational flexibility of **PD** might be affected not only by physical properties of the environment or by the presence of additives, such as organogelators or crowding agents, etc, but also by interactions with the solvent molecules. In light of this, the use of **PD** as a molecular viscometer should be taken with caution, and proper controls should be performed to unambiguously utilize it as an environment-sensitive probe.

4.5. Experimental part

All solvents and other materials were purchased from Sigma-Aldrich and were used as received. **PD** was prepared according to literature procedure the structure and purity were confirmed by MALDI-TOF spectrometry and HPLC. A 1 mM concentration stock solution of **PD** in DMSO was prepared fresh prior to experiments and it was used for all spectroscopic measurements and protected from a direct light exposure during storage.

Absorbance and emission measurements.

All measurements were performed using 0.5 cm path length quartz cuvettes. Absorption measurements were acquired on a Varian Cary 50 Bio UV–Vis spectrophotometer (Agilent Technologies, CA, USA). Fluorescence measurements were performed on a Cary Eclipse spectrofluorometer (Agilent Technologies, CA, USA)

Imaging.

All confocal microscopic analysis was performed using an Olimpus IX82 microscope (Physik Instrumente, Karlsruhe, Germany), with Hamamatsu ImagEM digital fluorescent camera using a laser operated Pico Quant Diode Laser PDL 828 “Sepia II” was used as the excitations source, and a Temperature controller Warner Instrument Corporation TC-344B.

REFERENCES

[1] L. Ruan, M. Ge, X. Huang and J. Ren, "Assay of single-cell apoptosis by ensemble and single-molecule fluorescence methods: annexin-V/polyethylene glycol functionalized quantum dots as probes," *Langmuir,* vol. 34, pp. 10040-10047, 2018.

[2] S. Brown, I. Heinisch, E. Ross, K. Shaw, C. D. Buckley and J. Savill, "Apoptosis disables CD31-mediated cell detachment from phagocytes promoting binding and engulfment.," *Nature,* vol. 418, pp. 200-203, 2002.

[3] P. Bosch, F. Catalina, T. Corrales and C. Peinado, "Fluorescent probes for sensing processes in polymers," *Chem Eur. J.,* vol. 11, pp. 4214-4325, 2005.

[4] Z. Wang, Z. Huang, N. Zhou, X. H. Dong, X. Zhu and Z. Zhang, "Quantitatively monitoring polymer chain growth and topology formation based on monodisperse polymers," *Polym. Chem.,* vol. 8, pp. 2346–2352, 2017.

[5] L. H. Jones, "Reactive chemical probes: beyond the kinase cysteinome," *Angew.Chem. Int. Ed.,* vol. 57, pp. 9220-9223, 2018.

[6] L. L. Lock, C. D. Reyes, P. Zhang and H. Cui, "Tuning cellular uptake of molecular probes by rational design of their assembly into supramolecular nanoprobes," *J. Am. Chem. Soc.,* vol. 138, pp. 3533-3540, 2016.

[7] E. A. Legenzov, S. Muralidharan, L. B. Woodcock, G. R. Eaton, S. S. Eaton, G. M. Rosen and J. P. Y. Kao, "Designing molecular probes to prolong intracellular retention: application to nitroxide spin probes," *Bioconjugate Chem.,* vol. 27, pp. 2923-2930, 2016.

[8] B. A. Smith and B. D. Smith, "Biomarkers and molecular probes for cell death imaging and targeted therapeutics," *Bioconjugate Chem,* vol. 22, pp. 1989-2006, 2012.

[9] M. Y. Berezin and S. Achilefu, "Fluorescence lifetime measurements and biological imaging," *Chem. Rev., 2010, 110, 2641–2684,* vol. 110, pp. 2641-2684, 2010.

[10] J. R. Lakowicz, Principles of fluorescence spectroscopy, Singapore: Springer Science+Bussines Media, LLC, 2006.

[11] I. Roy, S. Bobbala, J. Zhou, M. T. Nguyen, S. K. M. Nalluri, Y. Wu, D. P. Ferris, E. A. Scott and M. K. Wasielewski, "ExTzBox: a glowing cyclophane for live-cell imaging." *J. Am. Chem. Soc.,* vol. 140, pp. 7206-7212, 2018.

[12] M. Fernández-Suárez and A. Y. Ting, "Fluorescent probes for super-resolution imaging in living cells," *Nat. Rev. Mol. Cell Biol.,* vol. 9, pp. 929-943, 2008.

[13] M. Grossi, M. Morgunova, S. Cheung, D. Scholz, E. Conroy, M. Terrile, A. Panarella, J. C. Simpson, W. M. Gallagher and D. F. O'Shea, "Lysosome triggered near-infrared fluorescence imaging of cellular trafficking processes in real time," *Nat. Commun.,* vol. 7, pp. 10855-10868, 2016.

[14] L. Long, M. Huang, N. Wang, Y. Wu, K. Wang, A. Gong, Z. Zhang and J. L. Sessler, "A mitochondria-specific fluorescent probe for visualizing endogenous hydrogen cyanide fluctuations in neurons," *J. Am. Chem. Soc.,* vol. 140, pp. 1870-1875, 2018.

[15] X. Huang, H. Zhou, Y. Huang, H. Jiang, N. Yang, S. A. Shahzad, L. Meng and C. Yu, "Silver nanoparticles decorated and tetraphenylethene probe doped silica nanoparticles: a colorimetric and fluorometric sensor for sensitive and selective detection and intracellular imaging of hydrogen peroxide," *Biosens. Bioelectron.,* vol. 121, pp. 236-242, 2018.

[16] J. Xu, X. Wang, Z. Teng, G. Lu, N. He and Z. Wang, "Multifunctional yolk-shell mesoporous silica obtained via selective etching the shell: a therapeutic nanoplatform for cancer therapy," *ACS. Appl. Mater. Interfaces,* vol. 10, pp. 24440-24449, 2018.

[17] F. Chen, K. Ma, L. Zhang, B. Madajewski, P. Zanzonico, S. Sequeira, M. Gonen, U. Wiesner and M. S. Bradbury, "Target-or-clear zirconium-89 labeled silica nanoparticles for enhaced cancer-directed uptake in melanoma: a comparison of radiolabeling strategies," *Chem. Mater.,* vol. 29, pp. 8269-8281, 2017.

[18] S. Wang, C. J. Zeman, J. Jiang, Z. Pan and K. S. Schanze, "Intercalation of alkynylplatinum(II) terpyridine complexes into a helical poly(phenylene ethynylene) sulfonate: application to protein," *ACS Appl. Mater. Interfaces ,* vol. 9, pp. 33461-33469, 2017.

[19] X. Ma, C. Xu, J. Wang and H. Tian, "Amorphous pure organic polymersfor heavy-atom-free efficient room-temperature phosphorescence emission," *Angew. Chem. Int. Ed.,* vol. 57, pp. 10854-10858, 2018.

[20] Y. Yang, K. Z. Wang and D. Yan, "Ultralong persistent room temperature phosphorescence of metal coordination polymers exhibiting reversible ph-responsive emission," *ACS Appl. Mater. Interfaces,* vol. 8, pp. 15489–15496, 2016.

[21] G. Wei, Y. Jiang and F. Wang, "A new click reaction generated AIE-active polymer sensor for Hg2+ detection in aqueous solution," *Tetrahedron Lett.,* vol. 59, pp. 1476-1479, 2018.

[22] S. Bi, Y. Li, S. Zhang, J. Hu, L. Wang and H. Liub, "A diketopyrrolopyrrole-based fluorescent porous organic polymer as fluoride sensing monolithic device," *J. Mater. Chem. C,* vol. 6, pp. 3961-3967, 2018.

[23] W. J. Peveler, R. F. Landis, M. Yazdani, J. W. Day, R. Modi, C. J. Carmalt, W. M. Rosenberg and R. V. M., "A rapid and robust diagnostic for liver fibrosis using a multichannel polymer sensor array," *Adv. Mater.,* vol. 30, pp. 1800634-1800640, 2018.

[24] X. Zhen, C. Xie and K. Pu, "Temperature-correlated afterglow of a semiconducting polymer nanococktail for imaging-guided photothermal therapy," *Angew. Chem. Int. Ed.,* vol. 57, pp. 3938-3942, 2018.

[25] S. R. G. Fernandes, R. Fernandes, B. Sarmento, P. M. R. Pereira and J. P. C. Tome, "Photoimmunoconjugates: novel synthetic strategies to target and treat cancer by photodynamic therapy," *Org. Biomol. Chem.,* vol. 17, pp. 2579-2593, 2019.

[26] T. Senthilkumar, L. Zhou, Q. Gu, L. Liu, F. Lv and S. Wang, "Conjugated polymer nanoparticles with appended photo-responsive units for controlled drug delivery, release and imaging," *Angew. Chem. Int. Ed.,* vol. 57, pp. 13114-13119, 2018.

[27] X. Zhang, Y. Jiang and N. Xiao, "Monitoring ADP and ATP in vivo using a fluorescent Ga(III) probe complex," *Chem. Commun.,* vol. 54, pp. 12812-12815, 2018. 2018.

[28] Y. Yang, L. Guo, Z. Tian, Y. Gong, H. Zheng, S. Zhang, Z. Xu, X. Ge and Z. Liu, "Novel and versatile imine-N-heterocyclic carbene half-sandwich iridium(III) complexes as lysosome-targeted anticancer agents," *Inorg. Chem.,* vol. 57, pp. 11087-11098, 2018.

[29] W. Streciwilk, A. Terenzi, X. Cheng, L. Hagerm, Y. Dabiri, P. Prochnow, J. E. Bandow, S. Wolfl, B. K. Keppler and I. Ott, "Fluorescent organometallic rhodium(I) and ruthenium(II) metallodrugs with 4-ethylthio-1,8-naphthalimide ligands: antiproliferative effects, cellular uptake and DNA-interaction," *Eur. J. Med. Chem.,* vol. 156, pp. 148-161, 2018.

[30] D. S. Viswanath, T. K. Ghosh, D. H. L. Prasad, N. V. K. Dutt and K. Y. Rani, Viscosity of liquids: theory, estimation, experiment, and data, The Netherlands: Springer, 2007.

[31] M. K. Kuimova, "Mapping viscosity in cells using molecular rotors," *Phys. Chem. Chem. Phys.,* vol. 14, pp. 12671-12686, 2012.

[32] R. Paris, I. Quijada-Garrido, O. Garcia and M. Liras, "BODIPY-conjugated thermo-sensitive fluorescent polymers based on 2-(2-methoxyethoxy)ethyl methacrylate," *Macromolecules,* vol. 44, pp. 80-86, 2011.

[33] Roopa, N. Kumar, V. Bhalla and M. Kumar, "Development and sensing applications of fluorescent motifs within the mitochondrial environment," *Chem. Commun.,* vol. 51, pp. 15614-15628, 2015.

[34] D. Su, C. L. Teoh, N. Gao, Q. H. Xu and Y. T. Chang, "A simple BODIPY-based viscosity probe for imaging of cellular viscosity in live cells," *Sensors,* vol. 16, pp. 1397-1406, 2016.

[35] P. S. Nabavi Zadeh, M. Z. V. Gomes, M. Abrahamsson, A. E. C. Palmqvist and B. Akerman, "Measuring viscosity inside mesoporous silica using protein-bound molecular rotor probe," *Phys. Chem. Chem. Phys.,* vol. 20, pp. 23202-23213, 2018.

[36] R. Kotani, H. Sotome, H. Okajima, S. Yokoyama, Y. Nakaike, A. Kashiwagi, C. Mori, Y. Nakada, S. Yamaguchi, A. Osuka, A. Sakamoto, H. Miyasaka and S. Saito, "Flapping viscosity probe that shows polarity-independent ratiometric fluorescence," *J. Mater. Chem. C,* vol. 5, pp. 5248-5256, 2017.

[37] S. C. Lee, J. Heo, J. W. Ryu, C. L. Lee, S. Kim, J. S. Tae, B. O. Rhee, S. W. Kima and O. Kwon, "Pyrrolic molecular rotors acting as viscosity sensors with high fluorescence contrast," *Chem. Commun.,* vol. 52, pp. 13695-13698, 2016.

[38] Z. Lou, Y. Hou, K. Chen, J. Zhao, S. Ji, F. Zhong, Y. Dede and B. Dick, "Different quenching effect of intramolecular rotation on the singlet and triplet excited states of bodipy," *J. Phys. Chem. C ,* vol. 122, p. 185-193, 2018.

[39] L. Wang, J. Zhang, B. Kim, J. Peng, S. N. Berry, Y. Ni, D. Su, J. Lee, L. Yuan and Y. T. Chang, "Boronic acid: a bio-inspired strategy to increase the sensitivity and selectivity of fluorescent NADH probe," *J. Am. Chem. Soc.,* vol. 138, pp. 10394-10397, 2016.

[40] J. V. Jun, E. J. Petersson and D. M. Chenoweth, "Rational design and facile synthesis of a highly tunable quinoline-based fluorescent small-molecule scaffold for live cell imaging," *J. Am. Chem. Soc.,* vol. 140, pp. 9486-9493, 2018.

[41] G. Ulrich, R. Ziessel and A. Harriman, "The chemistry of fluorescent bodipy dyes: versatility unsurpassed," *Angew. Chem. Int. Ed.,* vol. 47, pp. 1184-1201, 2008.

[42] K. Xu, D. Luan, X. Wang, B. Hu, X. Liu, F. Kong and B. Tang, "An ultrasensitive cyclization-based fluorescent probe for imaging native HOBr in live cells and zebrafish," *Angew. Chem. Int. Ed.,* vol. 55, pp. 12751-12754, 2016.

[43] K. Cao, K. Elbel, J. L. Cifelli, J. Cirera, C. J. Sigurdson, F. Paesani, E. A. Theodorakis and J. Yang, "Solvation-guided design of fluorescent probes for discrimination of amyloids," *Sci. Rep.,* vol. 8, pp. 6950-6963, 2018.

[44] B. Li, L. Lu, M. Zhao, Z. Lei and F. Zhang, "An efficient 1064 nm NIR-II excitation fluorescent molecular dye for deep-tissue high-resolution dynamic bioimaging," *Angew. Chem. Int. Ed.,* vol. 57, pp. 7483-7487, 2018.

[45] M. Balaz, H. A. Collins, E. Dahlstedt and H. L. Anderson, "Synthesis of hydrophilic conjugated porphyrin dimers for one-photon and two-photon photodynamic therapy at NIR wavelengths," *Org. Biomol. Chem.,* vol. 7, pp. 874-888, 2009.

[46] Y. Zhou, M. Maiti, A. Sharma, M. Won, L. Yu, L. X. Miao, J. Shin, A. Podder, K. N. Bobba, J. Hand, S. Bhuniyab and K. J. S., "Azo-based small molecular hypoxia responsive theranostic for tumorspecific imaging and therapy," *J. Control. Release,* vol. 288, pp. 14-22, 2018.

[47] S. Das, K. Aich, L. Patra, K. Ghoshal, S. Gharami, M. Bhattacharyya and T. K. Mondal, "Development of a new fluorescence ratiometric switch for endogenous hypochlorite detection in monocytes of diabetic subjects by dye release method," *Tetrahedron Lett.,* vol. 59, pp. 1130-1135, 2018.

[48] H. W. Liu, L. Chen, C. Xu, Z. Li, H. Zhang, X. B. Zhang and W. Tan, "Recent progresses in small-molecule enzymatic fluorescent probes for cancer imaging," *Chem. Soc. Rev.,* vol. 47, pp. 7140-7180, 2018.

[49] M. Pawlicki, H. A. Collins, R. G. Denning and H. L. Anderson, "Two-photon absorption and the design of two-photon dyes," *Angew. Chem., Int. Ed.,* vol. 48, pp. 3244-3266, 2009.

[50] R. Feng, L. Li, B. Li, J. Li, D. Peng, Y. Yu, Q. Mu, N. Zhao, X. Yu and Z. Wang, "A small-molecule with a large two-photon absorption cross-section serves as a membrane permeable ribonucleic acid (RNA) probe for live," *New J. Chem.,* vol. 42, pp. 14325-14331, 2018.

[51] Y. W. Jun, T. Wang, S. Hwang, D. Kin, D. Ma, K. H. Kim, S. Kim, J. Jung and K. H. Ahn, "A ratiometric two-photon fluorescent probe for tracking lysosomal ATP: direct in cellulo observation of lysosomal membrane fusion," *Angew. Chem. Int. Ed.,* vol. 57, pp. 10142-10147, 2018.

[52] N. Boens, B. Verbelen and W. Dehaen, "Postfunctionalization of the BODIPY core: synthesis and spectroscopy," *Eur. J. Org. Chem.,* pp. 6577-6595, 2015.

[53] T. Kowada, H. Maeda and K. Kikuchi, "BODIPY-based probes for the fluorescence imaging of biomolecules in living cells," *Chem. Soc. Rev.,* vol. 44, pp. 4953-4972, 2015.

[54] L. P. Jameson and S. V. Dzyuba, "Expeditious, mechanochemical synthesis of BODIPY dyes," *Beilstein J. Org. Chem.,* vol. 9, pp. 786-790, 2013.

[55] A. Bessetteab and G. S. Hanan, "Design, synthesis and photophysical studies of dipyrromethene-based materials: insights into their applications in organic photovoltaic devices," *Chem. Soc. Rev.,* vol. 43, pp. 3342-3405, 2014.

[56] I. Lopez-Duarte, T. T. Vu, M. A. Izquierdo, J. A. Bull and M. K. Kuimova, "A molecular rotor for measuring viscosity in plasma membranes of live cells," *Chem. Commun.,* vol. 50, pp. 5282-5284, 2014.

[57] M. R. Dent, I. López-Duarte, C. J. Dickson, N. D. Geoghegan, J. M. Cooper, I. R. Gould, R. Krams, J. A. Bull, N. J. Brooks and M. K. Kuimova, "Imaging phase separation in model lipid membranes through the use of BODIPY based molecular rotors," *Phys. Chem. Chem. Phys.,* vol. 17, p. 18393, 2015.

[58] J. Zou, Z. Yin, K. Ding, Q. Tang, J. Li, W. Si, J. Shao, Q. Zhang, W. Huang and X. Dong, "BODIPY derivatives for photodynamic therapy: influence of configuration versus heavy atom effect," *ACS Appl. Mater. Interfaces,* vol. 9, pp. 32475-32481, 2017.

[59] G. Zhang, N. Zhao, P. Bobadova-Parvanova, M. Wang, F. R. Fronczek, K. M. Smith and M. G. H. Vicente, "Syntheses, spectroscopic properties, and computational study of (E,Z)-ethenyl and ethynyl-linked BODIPYs," *J. Phys. Chem. A ,* vol. 122, pp. 6256-6265, 2018.

[60] Z. Yang, Y. He, J. H. Lee, N. Park, M. Suh, W. S. Chae, J. Cao, X. Peng, H. Jung, C. Kang and J. S. Kim, "A self-calibrating bipartite viscosity sensor for mitochondria," *J. Am. Chem. Soc.,* vol. 135, pp. 9181-9185, 2013.

[61] T. Uppal, X. Hu, F. R. Fronczek, S. Maschek, P. Bobadova-Parvanova and M. G. H. Vicente, "Synthesis, computational modeling, and properties of benzo-appended BODIPYs," *Chem. Eur. J. ,* vol. 18, p. 3893-3905, 2012.

[62] A. Savoldelli, Q. Meng, R. Paolesse, F. R. Fronczek, K. M. Smith and M. G. H. Vicente, "Tetrafluorobenzo-fused BODIPY: a platform for regioselective synthesis of BODIPY dye derivatives," *J. Org. Chem.,* vol. 83, pp. 6498-6507, 2018.

[63] Z. Zhou, J. Zhou, L. Gai, A. Yuan and Z. Shen, "Naphtho[b]-fused BODIPYs: one pot Suzuki–Miyaura–Knoevenagel synthesis and photophysical properties," *Chem. Commun.,* vol. 53, pp. 6621-6624, 2017.

[64] M. Zhu, Y. Zhou, L. Yang, L. Li, D. Qi, M. Bai, Y. Chen, H. Du and Y. Bian, "Synergistic coupling of fluorescent “turn-off” with spectral overlap modulated fret for ratiometric Ag+ sensor," *Inorg. Chem.,* vol. 53, pp. 12186-12190, 2014.

[65] M. K. Panda, T. Lazarides, G. Charalambidis, V. Nikolaou and A. G. Coutsolelos, "Five-coordinate indium(III) porphyrins with hydroxy and carboxy BODIPY as axial ligands: synthesis, characterization and photophysical studies," *Eur. J. Inorg. Chem.,* pp. 468-477, 2015.

[66] M. D. Weber, V. Nikolaou, J. E. Wittmann, A. Nikolaou, P. A. Angaridis, G. Charalambidis, C. Stangel, A. Kahnt, A. G. Coutsolelos and R. D. Costa, "Benefits of using BODIPY–porphyrin dyads for developing deep-red lighting sources," *Chem. Commun.,* vol. 52, pp. 1602-1605, 2016.

[67] L. J. Patalag, L. P. Ho, P. G. Jones and D. B. Werz, "Ethylene-bridged oligo-BODIPYs: access to intramolecular J-aggregates and auperfluorophores," *J. Am. Chem. Soc.,* vol. 139, pp. 15104-15113, 2017.

[68] W. Zhang, W. Sheng, C. Yu, Y. Wei, H. Wang, E. Hao and L. Jiao, "One-pot synthesis and properties of well-defined butadiynylene-BODIPY oligomers," *Chem. Commun.,* vol. 53, pp. 5318-5321, 2017.

[69] B. Verbelen, S. Boodts, J. Hofkens, N. Boens and W. Dehaen, "Radical C-H arylation of the BODIPY core with aryldiazonium salts: synthesis of highly fluorescent red-shifted dyes," *Angew. Chem. Int. Ed.,* vol. 54, pp. 4612-4616, 2015.

[70] F. Lv, Y. Yu, E. Hao, C. Yu, H. Wang, L. Jiao and N. Boens, "Copper-catalyzed α-benzylation of BODIPYs via radical-triggered oxidative cross-coupling of two C-H bonds," *Chem. Commun.,* vol. 54, pp. 9059-9062, 2018.

[71] E. Palao, T. Slanina and P. Klan, "Construction of the carbon–chalcogen (S, Se, Te) bond at the 2,6-positions of BODIPY via Stille cross-coupling reaction," *Chem. Commun.,* vol. 52, pp. 11951-11954, 2016.

[72] M. Chapran, E. Angioni, N. J. Findlay, B. Breig, V. Cherpak, P. Stakhira, T. Tuttle, D. Volyniuk, J. V. Grazulevicius, Y. A. Nastishin, O. D. Lavrentovich and P. J. Skabara, "An ambipolar BODIPY derivative for a white exciplex OLED and cholesteric liquid crystal laser toward multifunctional devices," *ACS Appl. Mater. Interfaces,* vol. 9, pp. 4750-4757, 2017.

[73] C. Tahtaoui, C. Thomas, F. Rohmer, P. Klotz, G. Duportail, Y. Mely, D. Bonnet and M. Hibert, "Convenient method to access new 4,4-dialkoxy- and 4,4-diaryloxy-diaza-s-indacene dyes: synthesis and spectroscopic evaluation," *J. Org. Chem.,* vol. 72, pp. 269-272, 2007.

[74] D. Sirbu, A. C. Benniston and A. Harriman, "One-pot synthesis of a mono-O,B,N-strapped BODIPY derivative displaying bright fluorescence in the solid state," *Org. Lett.,* vol. 19, pp. 1626-1629, 2017.

[75] H. Manzano, I. Esnal, T. Marqués-Matesanz, J. Bañuelos, I. López-Arbeloa, M. J. Ortiz, L. Cerdán, A. Costela, I. García-Moreno and J. L. Chiara, "Unprecedented J-aggregated dyes in pure organic solvents," *Adv. Funct. Mater.,* vol. 26, pp. 2756-2769, 2016.

[76] X. D. Jiang, J. Zhang, T. Furuyama and W. Zhao, "Development of mono- and di-aco substituted bodipys on the boron center," *Org. Lett.,* vol. 14, pp. 248-251, 2012.

[77] H. Chen, X. He, M. Su, W. Zhai, H. Zhang and C. Li, "A general strategy toward highly fluorogenic bioprobes emitting across the visible" *J. Am. Chem. Soc.,* vol. 139, pp. 10157-10163, 2017.

[78] K. N. Bobba, M. Won, I. Shim, N. Velusamy, Z. Yang, J. Qu, J. S. Kim and S. Bhuniya, "A BODIPY-based two-photon fluorescent probe validates tyrosinase activity in live cells," *Chem. Commun.,* vol. 53, pp. 11213-11216, 2017.

[79] Y. S. Marfin, A. V. Solomonov, A. S. Timin and E. V. Rumyantsev, "Recent advances or individual bodipy and bodipy-based functional materials in medical diagnostics and treatment," *Curr. Med. Chem.,* vol. 24, pp. 2745-2772, 2017.

[80] A. Sampedro, A. Ramos-Torres, C. Schwoppe, C. Muck-Lichtenfeld, I. Helmers, A. Bort, I. Diaz-Laviada and G. Fernandez, "Hierarchical self-assembly of BODIPY dyes as a tool to improve the antitumor activity of capsaicin in prostate cancer," *Angew. Chem. Int. Ed.,* vol. 57, pp. 17235-17239, 2018.

[81] J. Zhou, Y. Zhang, G. Yu, M. R. Crawley, C. R. P. Fulong, A. E. Friedman, S. Sengupta, J. Sun, Q. Li, F. Huang and T. R. Cook, "Highly emissive self-assembled BODIPY-platinum supramolecular triangles," *J. Am. Chem. Soc.,* vol. 140, pp. 7730-7736, 2018.

[82] W. Ren, J. Zhang, C. Peng, H. Xiang, J. Chen, C. Peng, W. Zhu, R. Huang, H. Zhang and Y. Hu, "Fluorescent imaging of β-amyloid using BODIPY based near-infrared off-on fluorescent probe," *Bioconjugate Chem.,* vol. 29, p. 3459-3466, 2018.

[83] C. L. Teoh, D. Su, S. Sahu, S. W. Yun, E. Drummond, F. Prelli, S. Lim, S. Cho, S. Ham, T. Wisniewski and Y. T. Chang, "Chemical fluorescent probe for detection of Aβ oligomers," *J. Am. Chem. Soc.,* vol. 137, p. 13503-13509, 2015.

[84] N. Makukhin, V. Tretyachenko, J. Moskovitz and J. Misek, "A ratiometric fluorescent probe for imaging of the activity of methionine sulfoxide reductase A in cells," *Angew. Chem. Int. Ed.,* vol. 55, pp. 12727-12730, 2016.

[85] M. Ono, H. Watanabe, H. Kimura and H. Saji, "BODIPY-based molecular probe for imaging of cerebral β-amyloid plaques," *ACS Chem. Neurosci.,* vol. 3, pp. 319-324, 2012.

[86] F. Sozmen, S. Kolemen, H. O. Kumada, M. Ono, H. Sajib and E. U. Akkaya, "Designing BODIPY-based probes for fluorescence imaging of β-amyloid plaques," *RSC Adv.,* vol. 4, pp. 51032-51037, 2014.

[87] A. Vysniauskas, I. Lopez-Duarte, N. Duchemin, T. T. Vu, Y. Wu, E. M. Budynina, Y. A. Volkova, E. Pena-Cabrera, D. E. Ramırez-Ornelas and M. K. Kuimova, "Exploring viscosity, polarity and temperature sensitivity of BODIPY-based molecular rotors," *Phys. Chem. Chem. Phys.,* vol. 19, pp. 25252--25259, 2017.

[88] M. Kubankova, E. Lopez-Duarte, D. Kiryushko and M. K. Kuimova, "Molecular rotors report on changes in live cell plasma membrane microviscosity upon interaction with beta-amyloid aggregates," *Soft Matter,* vol. 14, pp. 9466-9474, 2018.

[89] C. Wang, X. Song, L. Chen and Y. Xiao, "Specifically and wash-free labeling of SNAP-tag fused proteins with a hybrid sensor to monitor local micro-viscosity," *Biosens. Bioelectron.,* vol. 91, pp. 313-320, 2017.

[90] A. H. Futerman and G. van Meer, "The cell biology of lysosomal storage disorders," *Nat. Rev. Mol. Cell. Biol.,* vol. 5, pp. 554-565, 2004.

[91] H. Wang, Y. Wu, Y. Shi, P. Tao, X. Fan, X. Su and G. C. Kuang, "BODIPY-based fluorescent thermometer as a lysosome-targetable probe: how the oligo(ethylene glycols) compete photoinduced electron transfer," *Chem. Eur. J.,* vol. 21, pp. 3219-3223, 2015.

[92] L. Wang, Y. Xiao, W. Tian and L. Deng, "Activatable rotor for quantifying lysosomal viscosity in living cells," *J. Am. Chem. Soc.,* vol. 135, pp. 2903-2906, 2013.

[93] L. L. Li, K. Li, M. Y. Li, L. Shi, Y. H. Liu, H. Zhang, S. L. Pan, N. Wang, Q. Zhou and X. Q. Yu, "BODIPY-based two-photon fluorescent probe for real-time monitoring of lysosomal viscosity with fluorescence lifetime imaging microscopy," *Anal. Chem. ,* vol. 90, pp. 5873-5878, 2018.

[94] S. P. Singh and T. Gayathri. Evolution of BODIPY dyes as potential sensitizers for dye-sensitized solar cells. Eur. J. Org. Chem., vol. 2014, pp. 4689-4707, 2014.

[95] D. Sirbu, J. K. G. Karlsson and A. Harriman, "Nonradiative decay channels for a structurally-distorted, monostrapped BODIPY derivative," *J. Phys. Chem. A,* vol. 122, p. 9160–9170, 2018.

[96] A. Bessette and G. S. Hanan, "Design, synthesis and photophysical studies of dipyrromethene-based materials: insights into their applications in organic photovoltaic devices," *Chem. Soc. Rev.,* vol. 43, pp. 3342-3405, 2014.

[97] T. Li, J. Benduhn, Y. Li, F. Jaiser, D. Spoltore, O. Zeika, Z. Ma, D. Neher, K. Vandewal and K. Leo, "Boron dipyrromethene (BODIPY) with mesoperfluorinated alkyl substituents as near infrared donors in organic solar cells," *J. Mater. Chem. A,* vol. 6, pp. 18583-18591, 2018.

[98] M. Kyeong, J. Lee, K. Lee and S. Hong, "BODIPY-based conjugated polymers for use as dopant-free hole transporting materials for durable perovskite solar cells: selective tuning of HOMO/LUMO levels," *ACS Appl. Mater. Interfaces,* vol. 10, pp. 23254-23262, 2018.

[99] R. S. Rao, A. Bagui, G. H. Rao, V. Gupta and S. P. Singh, "Achieving the highest efficiency using a BODIPY core decorated with dithiafulvalene wings for small molecule based solution-processed organic solar cells," *Chem. Commun.,* vol. 53, pp. 6953-6956, 2017.

[100] N. Yesilgul, O. Seven, R. Guliyev and E. U. Akkaya, "Energy harvesting in a BODIPY-functionalized rotaxane," *J. Org. Chem. ,* vol. 83, pp. 13228-13232, 2018.

[101] R. Mishra, B. Basumatary, R. Singhal, G. D. Sharma and J. Sankar, "Corrole-BODIPY dyad as small-molecule donor for bulk heterojunction solar cells," *ACS Appl. Mater. Interfaces,* vol. 10, pp. 31462-31471, 2018.

[102] B. M. J. M. Suijkerbuijk and R. J. M. Klein Gebbink, "Merging porphyrins with organometallics: synthesis and applications," *Angew. Chem. Int. Ed. ,* vol. 47, pp. 7396-7421, 2008.

[103] S. Hiroto, Y. Miyake and H. Shinokubo, "Synthesis and functionalization of porphyrins through organometallic methodologies," *Chem. Rev.,* vol. 117, pp. 2910-3043, 2017.

[104] M. O. Senge, "Stirring the porphyrin alphabet soup-functionalization reactions for porphyrins," *Chem. Commun.,* vol. 47, pp. 1943-1960, 2011.

[105] T. D. Lash, "Porphyrin Synthesis by the “3 + 1” Approach: new applications for an old methodology," *Chem. Eur. J.,* vol. 2, pp. 1197-1200, 1996.

[106] S. Shanmugathasan, C. Edwards and R. W. Boyle, "Advances in modern synthetic porphyrin chemistry," *Tetrahedron ,* vol. 56, pp. 1025-1046, 2000.

[107] S. Pisarek, K. Maximova and D. Gryko, "Strategies toward the synthesis of amphiphilic porphyrins," *Tetrahedron,* vol. 70, pp. 6685-6715, 2014.

[108] P. R. Kumar, N. J. Britto, A. Kathiravan, A. Neels, M. Jaccob and E. M. Mothi, "Synthesis and electronic properties of A3B-thienyl porphyrins: experimental and computational investigations," *New J. Chem.,* vol. 43, pp. 1569-1580, 2019.

[109] M. A. Rajora, J. W. H. Louac and G. Zheng, "Advancing porphyrin’s biomedical utility via supramolecular chemistry," *Chem. Soc. Rev.,* vol. 46, pp. 6433-6469, 2017.

[110] F. Bryden and R. W. Boyle, "Metalloporphyrins for medical imaging applications," *Adv. Inorg. Chem.,* vol. 68, pp. 141-221, 2016.

[111] M. Zhu, J. Zhang, Y. Zhou, P. Xing, L. Gong, C. Su, D. Qi, H. Du, Y. Bian and J. Jiang, "Two-photon excited FRET dyads for lysosome-targeted imaging and photodynamic therapy," *Inorg. Chem. ,* vol. 57, pp. 11537-11542, 2018.

[112] H. Zhang, X. T. Tian, Y. Shang, Y. H. Li and X. B. Yin, "Theranostic Mn-porphyrin metal−organic frameworks for magnetic resonance imaging-guided nitric oxide and photothermal synergistic therapy," *ACS Appl. Mater. Interfaces,* vol. 10, pp. 28390-28398, 2018.

[113] X. Zhao, Z. Zhang, X. Cai, B. Ding, C. Sun, G. Liu, C. Hu, S. Shao and M. Pang, "Postsynthetic ligand exchange of metal organic framework for photodynamic therapy," *ACS Appl. Mater. Interfaces,* vol. 11, p. 7884-7892, 2019.

[114] D. Moukheiber, U. Chitgupi, K. A. Carter, D. Luo, B. Sun, S. Goel, C. A. Ferreira, J. W. Engle, D. Wang, J. Geng, Z. Y. J. Xia, W. Cai and L. J. F. , "Surfactant-stripped pheophytin micelles for multimodal tumor imaging and photodynamic therapy," *ACS Appl. Bio Mater.,* vol. 2, pp. 544-554, 2019.

[115] K. Ding, Y. Zhang, W. Si, X. Zhong, Y. Cai, J. Zou, J. Shao, Z. Yang and X. Dong, "Zinc(II) metalated porphyrins as photothermogenic photosensitizers for cancer photodynamic/photothermal synergistic therapy," *ACS Appl. Mater. Interfaces,* vol. 10, pp. 238-247, 2018.

[116] D. Ni, C. A. Ferreira, T. E. Barnhart, V. Quach, B. Yu, D. Jiang, W. Wei, H. Liu, J. W. Engle, P. Hu and W. Cai, "Magnetic targeting of nanotheranostics enhances Cerenkov radiation-induced photodynamic therapy," *J. Am. Chem. Soc.,* vol. 140, pp. 14971-14979, 2018.

[117] S. Supriya, V. Shetti and G. Hegde, "Conjugated systems of porphyrin–carbon nanoallotropes: a review," *New J. Chem.,* vol. 42, pp. 12328-12348, 2018.

[118] U. Mazur and K. W. Hipps, "A systematic approach toward designing functional ionic porphyrin crystalline materials," *J. Phys. Chem. C,* vol. 122, pp. 22803-22820, 2018.

[119] H. Song, Q. Liu and Y. Xie, "Porphyrin-sensitized solar cells: systematic molecular optimization, coadsorption and cosensitization," *Chem. Commun.,* vol. 54, pp. 1811-1824, 2018.

[120] A. Mahmood, Y. J. Hu, B. Xiao, A. Tang, X. Wang and E. Zhou, "Recent progress in porphyrin-based materials for organic solar cells," *J. Mater. Chem. A,* vol. 6, pp. 16769-16797, 2018.

[121] V. Cuesta, R. Singhal, P. de la Cruz, G. D. Sharma and F. Langa, "Near-IR absorbing D-A-D Zn-porphyrin-based small molecule donors for organic solar cells with low voltage loss," *ACS Appl. Mater. Interfaces,* vol. 11, pp. 7216-7225, 2019.

[122] W. T. Hadmojo, D. Yim, H. Aqoma, D. Y. Ryu, T. J. Shin, H. W. Kim, E. Hwang, W. D. Jang, I. H. Jung and S. Y. Jang, "Artificial light-harvesting n-type porphyrin for panchromatic organic photovoltaic devices," *Chem. Sci.,* vol. 8, pp. 5095-5100, 2017.

[123] S. Basak, N. Nandi, A. Abhishek Baral and A. Banerjee, "Tailor-made design of J- or H-aggregated naphthalenediimide-based gels and remarkable fluorescence turn on/off behaviour depending on solvents," *Chem. Commun.,* vol. 51, pp. 780-783, 2015.

[124] Q. Zhao, J. Liu, H. Wang, M. Li and K. Zhou, "Balancing the H- and J-aggregation in DTS($PTTh_2$)$_2$/$PC_{70}BM$ to yield a high photovoltaic efficiency," *J. Mater. Chem. C,* vol. 3, pp. 8183-8192, 2015.

[125] M. Vybornyi, A. V. Rudnev, S. M. Langenegger, T. Wandlowski, G. Calzaferri and R. Haener, "Formation of two-dimensional supramolecular polymers by amphiphilic pyrene oligomers," *Angew. Chem. Int. Ed.,* vol. 52, p. 11488-11493, 2013.

[126] K. Nakata, T. Kobayashibcde and E. Tokunaga, "Electric field-controlled dissociation and association of porphyrin J-aggregates in aqueous solution," *Phys. Chem. Chem. Phys.,* vol. 13, pp. 17756-17767, 2011.

[127] F. C. Spano and C. Silva, "H- and J-aggregate behavior in polymeric semiconductors," *Annu. Rev. Phys. Chem.,* vol. 65, p. 477-500, 2014.

[128] S. B. Anantharaman, T. Stöferle, F. A. Nüesch, R. F. Mahrt and J. Heier, "Exciton dynamics and effects of structural order in morphology-controlled J-aggregate assemblies," *Adv. Funct. Mater.,* 1806997, 2018.

[129] S. Cherumukkil, B. Vedhanarayanan, G. Das, V. K. Praveen and A. Ajayaghosh, "Self-assembly of BODIPY-derived extended π-systems," *Bull. Chem. Soc. Jpn.,* vol. 91, pp. 100-120, 2018.

[130] W. Che, L. Zhang, Y. Li, D. Zhu, Z. Xie, G. Li, P. Zhang, Z. Su, C. Dou and B. Z. Tang, "Ultrafast and noninvasive long-term bioimaging with highly stable red aggregation-induced emission nanoparticles," *Anal. Chem.,* vol. 91, pp. 3467-3474, 2019.

[131] P. Maity, T. Gayathri, S. P. Singh and H. N. Ghosh, "Impact of FRET between molecular aggregates and quantum dots," *Chem. Asian J.,* vol. 14, pp. 597-605, 2019.

[132] E. Nikoloudakis, K. Karikis, J. Han, C. Kokotidou, A. Charisiadis, F. Folias, A. M. Douvas, A. Mitraki, G. Charalambidis, X. Yan and A. G. Coutsolelos, "A self-assembly study of PNA–porphyrin and PNA–BODIPY hybrids in mixed solvent systems," *Nanoscale,* vol. 11, pp. 3557-3566, 2019.

[133] L. Yang, G. Fan, X. Ren, L. Zhao, J. Wanga and Z. Chen, "Aqueous self-assembly of a charged BODIPY amphiphile via nucleation–growth mechanism," *Phys. Chem. Chem. Phys.,* vol. 17, pp. 9167-9172, 2015.

[134] D. Tleugabulova, Z. Zhang and J. D. Brennan, "Characterization of bodipy dimers formed in a molecularly confined environment," *J. Phys. Chem. B,* vol. 106, pp. 13133-13138, 2002.

[135] C. F. A. Gomez-Duran, R. Hu, G. Feng, T. Li, F. Bu, M. Arseneault, B. Liu, E. Peña-Cabrera and B. Z. Tang, "Effect of AIE substituents on the fluorescence of tetraphenylethene-containing BODIPY derivatives," *ACS Appl. Mater. Interfaces,* vol. 7, pp. 15168-15176, 2015.

[136] M. Castillo, S. L. Raut, S. Price, I. Bora, L. P. Jameson, C. Qiu, K. A. Schug, Z. Gryczynski and S. V. Dzyuba, "Spectroscopic differentiation between monomeric and aggregated forms of BODIPY dyes: effect of 1,1-dichloroethane," *RSC Adv.,* vol. 6, pp. 68705-68708, 2016.

[137] M. K. Kuimova, G. Yahioglu, J. A. Levitt and K. Suhling, "Molecular rotor measures viscosity of live cells via fluorescence lifetime imaging," *J. Am. Chem. Soc.,* vol. 130, pp. 6672-6673, 2008.

[138] S. Raut, J. Kimball, R. Fudala, H. Doan, B. Maliwal, N. Sabnis, A. Lacko, I. Gryczynski, S. V. Dzyuba and Z. Gryczynski, "A homodimeric BODIPY rotor as a fluorescent viscosity sensor for membrane-mimicking and cellular environments," *Phys. Chem. Chem. Phys.,* vol. 16, pp. 27037-27042, 2014.

[139] J. D. Kimball, S. Raut, L. P. Jameson, N. W. Smith, Z. Gryczynski and S. V. Dzyuba, "BODIPY–BODIPY dyad: assessing the potential as a viscometer for molecular and ionic liquids," *RSC Adv.,* vol. 5, pp. 19508-19511, 2015.

[140] K. A. Schug, I. Sawicki, D. D. Carlton, H. Fan, H. M. McNair, J. P. Nimmo, P. Kroll, J. Smuts, P. Walsh and D. Harrison, "Vacuum ultraviolet detector for gas chromatography," *Anal. Chem.,* vol. 86, pp. 8329-8335, 2014.

[141] S. L. Murov, "Properties of Solvents Used in Organic Chemistry," 2018. [Online]. Available: http://murov.info/orgsolvents.htm.

[142] S. Singh, V. Venugopalanac and K. Krishnamoorthy, "Organic soluble and uniform film forming oligoethylene glycol substituted BODIPY small molecules with improved hole mobility," *Phys. Chem. Chem. Phys.,* vol. 16, pp. 13376-13382, 2014.

[143] T. Ueno, T. Urano, H. Kojima and T. Nagano, "Mechanism-based molecular design of highly selective fluorescence probes for nitrative stress," *J. Am. Chem. Soc.,* vol. 128, pp. 10640-10641, 2006.

[144] S. M. Crawford and A. Thompson, "Conversion of 4,4-difluoro-4-bora-3a,4a-diaza-s-indacenes (F-BODIPYs) to dipyrrins with a microwave-promoted deprotection strategy," *Org. Lett.,* vol. 12, pp. 1424-1427, 2010.

[145] S. L. Raut, J. D. Kimball, R. Fudala, I. Bora, R. Chib, H. Jaafari, M. K. Castillo, N. W. Smith, I. Gryczynski, S. V. Dzyuba and Z. Gryczynski, "A triazine-based BODIPY trimer as a molecular viscometer," *Phys. Chem. Chem. Phys.,* vol. 18, pp. 4535-4540, 2016.

[146] S. Requena, O. Ponomarchuk, M. Castillo, J. Rebik, E. Brochiero, E. Borejdo, I. Gryczynski, S. V. Dzyuba, Z. Gryczynski, R. Grygorczyk and R. Fudala, "Imaging viscosity of intragranular mucin matrix in cystic fibrosis cells," *Sci. Rep.,* vol. 7, pp. 16761, 2017.

[147] M. A. Haidekkera and E. A. Theodorakis, "Molecular rotors-fluorescent biosensors for viscosity and flow," *Org. Biomol. Chem.,* vol. 5, pp. 1669-1678, 2007.

[148] M. L. Viriot, M. C. Carré, C. Geoffroy-Chapotot, A. Brembilla, S. Muller and J. F. Stoltz, "Molecular rotors as fluorescent probes for biological studies," *Clin. Hemorheol. Microcirc.,* vol. 19, pp. 151-160, 1998.

[149] Y. N. Andrade, J. Fernandes, E. Vázquez, J. M. Fernández-Fernández, M. Arniges, T. M. Sánchez, M. Villalón and M. A. Valverde, "TRPV4 channel is involved in the coupling of fluid viscosity changes to epithelial ciliary activity," *J. Cell Biol.,* vol. 168, p. 869-874, 2005.

[150] S. Howell, M. Dakanali, E. A. Theodorakis and M. A. Haidekker, "Intrinsic and Extrinsic Temperature-dependency of viscosity-sensitive fluorescent molecular rotors," *J. Fluoresc.* vol. 22, pp. 457-465, 2012.

[151] Z. R. Grabowski and K. Rotkiewicz, "Structural changes accompanying intramolecular electron transfer: focus on twisted intramolecular charge-transfer states and structures," *Chem. Rev.,* vol. 103, pp. 3899-4031, 2003.

[152] L. P. Jameson, J. D. Kimball, Z. Gryczynski, M. Balaz and S. V. Dzyuba, "Effect of ionic liquids on the conformation of a porphyrin-based viscometer," *RSC Adv.,* vol. 3, pp. 18300-18304, 2013.

[153] L. A. Levitt, M. K. Kuimova, G. Yahioglu, P. Chung, K. Suhling and D. Phillips, "Membrane-bound molecular rotors measure viscosity in live cells via fluorescence lifetime imaging," *J. Phys. Chem. C,* vol. 113, pp. 11634-11642, 2009.

[154] M. A. Alamiry, A. C. Benniston, G. Copley, K. J. Elliott, A. Harriman, B. Stewart and Y. Zhi, "A molecular rotor based on an unhindered boron dipyrromethene (BODIPY) dye," *Chem. Mater.,* vol. 20, pp. 4024-4032, 2008.

[155] Y. Wu, M. Štefl, A. Olzyńska, M. Hof, G. Yahioglu, P. Yip, D. R. Casey, O. Ces, J. Humpolíčková and M. K. Kuimova, "Molecular rheometry: direct determination of viscosity in Lo and Ld lipid phases via fluorescence lifetime imaging," *Phys. Chem. Chem. Phys.,* vol. 15, pp. 14986-14993, 2013.

[156] E. Bahaidarah, A. Harriman, P. Stachelek, S. Rihn, E. Heyer, R. Ziessel "Fluorescent molecular rotors based on the BODIPY motif: effect of remote substituents" *Photochem. Photobiol. Sci.,* vol. 13, pp. 1397-1401, 2014.

[157] D. Bai, A. C. Benniston, V. L. Whittle, H. Lemmetyinen and N. V. Tkachenko, "ROFRET: a molecular-scale fluorescent probe displaying viscosity-enhanced intramolecular fçrster energy transfer," *Chem. Phys. Chem.,* vol. 15, pp. 3089-3096, 2014.

[158] M. K. Kuimova, S. W. Botchway, A. W. Parker, M. Balaz, H. A. Collins, H. L. . Anderson, K. Suhling and P. R. Ogilby, "Imaging intracellular viscosity of a single cell during photoinduced cell death," *Nat. Chem.,* vol. 1, pp. 69-73, 2009.

[159] K. Venkataraman and D. R. Wagle, "Cyanuric chloride: a useful reagent for converting carboxylic acids into chlorides, esters, amides and peptides," *Tetrahedron Lett.,* vol. 20, pp. 3037-3040, 1979.

[160] S. Braese, "The virtue of the multifunctional triazene linkers in the efficient solid-phase synthesis of heterocycle libraries," *Acc. Chem. Res.,* vol. 37, pp. 805-816, 2004.

[161] K. Navamani and K. Senthilkumar, "Effect of structural fluctuations on charge carrier dynamics in triazene based octupolar molecules," *J. Phys. Chem. C ,* vol. 118, pp. 27754-27762, 2014.

[162] S. Liu, P. Y. Zavalij, Y. F. Lam and L. Isaacs, "Refolding foldamers: triazene-arylene oligomers that change shape with chemical stimuli," *J. Am. Chem. Soc.,* vol. 129, pp. 11232-11241, 2007.

[163] T. Foster and G. Hoffmann, "Effect of viscosity on the fluorescence quantum yield of a dye system," *Phys. Chem.,* vol. 75, pp. 63-76, 1971.

[164] J. S. Elborn, "Cystic fibrosis," *Lancet,* vol. 388, pp. 2519-2531, 2016.

[165] R. Bansil, E. Stanley and J. T. LaMont, "Mucin biophysics," *Annu. Rev. Physiol.,* vol. 57, pp. 635-657, 1995.

[166] X. X. Tang, L. S. Ostedgaard, M. J. Hoegger, T. O. Moninger, P. H. Karp, J. D. McMenimen, B. Choudhury, A. Varki, D. A. Stoltz and M. J. Welsh, "Acidic pH increases airway surface liquid viscosity in cystic fibrosis," *J. Clin. Invest.,* vol. 126, pp. 879-891, 2016.

[167] A. S. Klymchenko, "Solvatochromic and fluorogenic dyes as environment-sensitive probes: design and biological applications," *Acc. Chem. Res.,* vol. 50, pp. 366-375, 2017.

[168] W. Becker, "Fluorescence lifetime imaging – techniques and applications," *J. Microscopy,* vol. 247, pp. 119-136, 2012.

[169] P. Sarder, D. Maji and S. Achilefu, "Molecular probes for fluorescence lifetime imaging," *Bioconjugate Chem.,* vol. 26, pp. 963-974, 2015.

[170] L. E. Shimolina, M. A. Izquierdo, B. J. A. Lopez-Duarte Ismael, M. V. Shrimanova, L. G. Klapshina, E. V. Zagaynova and M. K. Kuimova, "Imaging tumor microscopic viscosity in vivo using molecular rotors," *Sci. Rep.,* vol. 7, pp. 41097, 2017.

[171] H. A. Collins, M. Khurana, E. H. Moriyama, A. Mariampillai, E. Dahlstedt, M. Balaz, M. K. Kuimova, M. Drobizhev, V. X. D. Yang, D. Phillips, A. Rebane, B. C. Wilson and H. L. Anderson, "Blood-vessel closure using photosensitizers engineered for two-photon excitation," *Nat. Photonics.,* vol. 2, pp. 420-424, 2008.

[172] A. Vysniauskas, M. Balaz, H. L. Anderson and M. K. Kuimova, "Dual mode quantitative imaging of microscopic viscosity using a conjugated porphyrin dimer," *Phys. Chem. Chem. Phys.,* vol. 17, pp. 7548-7554, 2015.

[173] L. P. Jameson, M. Balaz, S. V. Dzyuba and N. Kamiya, "Conformational preference of a porphyrin rotor in confined environments," *RSC Adv.,* vol. 4, pp. 705-708, 2014.

[174] H. Doan, S. L. Raut, D. Yale, M. Balaz, S. V. Dzyuba and Z. Gryczynski, "Mechanothermally induced conformational switch of a porphyrin dimer in a polymer film," *Chem. Commun.,* vol. 52, pp. 9510-9513, 2016.

[175] S. Kozaka, R. Wakabayashi, O. Annunziata, M. Balaz, M. Goto, N. Kamiya and S. V. Dzyuba, "Effect of macromolecular crowding on the conformational behaviour of a porphyrin rotor," *J. Photochem. Photobiol. A,* vol. 369, pp. 115-118, 2019.

[176] M. D. Peeks, P. Neuhaus and H. L. Anderson, " Experimental and computational evaluation of the barrier to torsional rotation in a butadiyne-linked porphyrin dimer" *Phys. Chem. Chem. Phys.,* vol. 18, pp. 5264-5274, 2016.

[177] P. Terech and R. G. Weiss, "Low molecular mass gelators of organic liquids and the properties of their gels" *Chem. Rev.,* vol. 97, pp. 3133-3160, 1997.

[178] S. Panettieri, J. R. Silverman, R. Nifosí, G. Signore, R. Bizzarri and G. John, "Unique photophysical behavior of coumarin-based viscosity probes during molecular self-assembly," *ACS Omega,* vol. 4, pp. 4785-4792, 2019.

[179] K. Hanabusa, K. Hiratsuka, M. Kimura and H. Shirai, "Easy preparation and useful character of organogel electrolytes based on low molecular weight gelator," *Chem. Mater.,* vol. 11, pp. 649-655, 1999.

[180] N. W. Smith, J. Knowles, J. G. Albright and S. V. Dzyuba, "Ionic liquid-assisted gelation of an organic solvent," *J. Mol. Liq.,* vol. 157, pp. 83-87, 2010.

[181] M. D. Peeks, P. Neuhausa and H. L. Anderson, "Experimental and computational evaluation of the barrier to torsional rotation in a butadiyne-linked porphyrin dimer," *Phys. Chem. Chem. Phys.,* vol. 18, pp. 5264-5274, 2016.

[182] A. Vysniauskas, D. Ding, M. Qurashi, I. Boczarow, M. Balaz, H. L. Anderson and M. K. Kuimova, "Tuning the sensitivity of fluorescent porphyrin dimers to viscosity and temperature," *Chem. Eur. J.,* vol. 23, pp. 11001-11010, 2017.

VITA

Marlius Castillo Rodriguez

EDUCATION

Ph.D. in Chemistry, specialization: Organic Chemistry and Spectroscopy
Texas Christian University, Fort Worth, TX, May 2019.
Advisor: Sergei V. Dzyuba
GPA: 3.94

B. S. in Chemistry
University of Carabobo, Valencia, Venezuela, 2008.

GRADUATE APPOINTMENTS

Research assistant, Texas Christian University, Fall 2014–present.
Teaching assistant, Organic Chemistry Laboratory, Texas Christian University, Fall 2014-Spring 2016.

PUBLICATIONS

1. **M. Castillo**, S. L. Raut, S. Price, I. Bora, L. P. Jameson, C. Qiu, K. A. Schug, Z Gryczynski, S. V. Dzyuba, "Spectroscopic differentiation between monomeric and aggregated forms of BODIPY dyes: effect of 1,1-dichloroethane." *RSC Adv.*, **2016**, *6*, 68705–68708.
2. S. L. Raut, J. D. Kimball, R. Fudala, I. Bora, R. Chib, H. Jaafari, **M. K. Castillo**, N. W. Smith, I. Gryczynski, S. V. Dzyuba, Z. Gryczynski, "A triazine-based BODIPY trimer as a molecular viscometer." *Phys. Chem. Chem. Phys.*, **2016**, *18*, 4535–4540.
3. H. Doan, **M. Castillo**, M. Bejjani, Z. Nurekeyev, S. Dzyuba, I. Gryczynski, Z. Gryczynski, S. Raut, "Solvatochromic dye LDS798 as microviscosity and pH probe." *Phys. Chem. Chem. Phys.*, **2017**, *19*, 29934–29939.
4. S. Requena, O. Ponomarchuk, **M. Castillo**, J. Rebik, E. Brochiero, J. Borejdo, I. Gryczynski, S. V. Dzyuba, Z. Gryczynski, R. Grygorczyk, R. Fudala, "Imaging viscosity of intragranular mucin matrix in cystic fibrosis cells." *Sci. Rep.*, **2017**, *7*, 16761–16766.
5. **M. Castillo**, C. Pho, A. V. Naumov, S. V. Dzyuba. "Modulating chirality-selective photoluminescence of single-walled carbon nanotubes by ionic liquids." *J. Phys. Chem. Lett.*, **2018**, *9*, 6689–6694.

6. **M. Castillo**, Z. Nukureyev, E. Sizemore, A. V. Naumov, Z. Gryczynski, M. Balaz, S. V. Dzyuba, "Conformational behavior of a porphyrin rotor in organogels." *to be submitted.*

PRESENTATIONS

ACS 50th Annual Meeting-in-Miniature: Organic/Biochemistry; Texas Christian University. Oral presentation: "Small molecule fluorophores as environmental probes." Spring-2017.

The Michael and Sally McCracken annual Student Research Symposium: Texas Christian University. Poster presentation: Ratiometric molecular probes for evaluation of soft materials." Spring-2019

AWARDS

SERC graduate research grant, Texas Christian University; "Ratiometric molecular rotors for determining phase-transitions of gels, waxes, and polymer films." Fall2018–Spring2019.

Outstanding TA Award, ACS (TCU Chemistry Club Members); Spring, 2016.

ABSTRACT

STUDIES ON FLUORESCENT MOLECULAR ROTORS AS ENVIRONMENT-SENSITIVE PROBES

by

Marlius Castillo

Department of Chemistry and Biochemistry

Texas Christian University

Dissertation Advisor: Sergei V. Dzyuba

Fluorescence small molecules or so-called environmental probes that could change their photophysical characteristics in response to physicochemical changes, have been widely used in various areas of sciences, engineering and medicine. In this work, the characterization and properties of BODIPY-based probes is studied, where it was found that the presence of 1,1-dichloroethane induces spectroscopic differentiation between aggregated and monomeric forms of BODIPY dyes (Chapter 2). A trimeric BODIPY rotor with a high extinction coefficients was developed and the fluorescence measurements established that the trimer could be used as a viscometer for molecular solvents, membrane-like environments and cancer cell lines (Chapter 3.1). Also, the use of a structural simple BODIPY-based rotor to map the viscosity of intragranular mucin matrices in bronchial epithelial cells using fluorescence lifetime imaging microscopy was demonstrated (Chapter 3.2). Finally, porphyrin rotor in organogels was evaluated in a temperature dependent manner (Chapter 4). Overall, BODIPY and prophyrin molecular rotors were studied as chemical probes in diverse systems. The results indicated an intricate complexity of the environmental factors on the conformation integrity of molecular rotors, which often are used as molecular viscometers.